

Statistics of continuous weak linear measurement

Franquet González, Albert

10.4233/uuid:473c2508-4f3c-49f8-9204-53aed4b4eeee

Publication date

Document Version Final published version

Citation (APA)

Franquet González, A. (2018). Statistics of continuous weak linear measurement. [Dissertation (TU Delft), Delft University of Technology]. https://doi.org/10.4233/uuid:473c2508-4f3c-49f8-9204-53aed4b4eeee

Important note

To cite this publication, please use the final published version (if applicable). Please check the document version above.

Copyright

Other than for strictly personal use, it is not permitted to download, forward or distribute the text or part of it, without the consent of the author(s) and/or copyright holder(s), unless the work is under an open content license such as Creative Commons.

Please contact us and provide details if you believe this document breaches copyrights. We will remove access to the work immediately and investigate your claim.

STATISTICS OF CONTINUOUS WEAK LINEAR MEASUREMENT



STATISTICS OF CONTINUOUS WEAK LINEAR MEASUREMENT

Dissertation

for the purpose of obtaining the degree of doctor at the Delft University of Technology, by the authority of the Rector Magnificus, Prof. dr. ir. T.H.J.J. van der Hagen, chair of the Board of Doctorates, to be defended publicly on Monday 17th of December 2018 at 12:30 o'clock

by

Albert Franquet González

Master of Science in Photonics, UPC Barcelona School of Telecommunications Engineering, Spain born in Barcelona, Spain. This dissertation has been approved by the promotor.

Composition of the doctoral committee:

Rector Magnificus, chairperson

Prof. dr. Y. V. Nazarov, Technische Universiteit Delft, promotor

Independent members:

Prof. dr. Y. M. Blanter, Technische Universiteit Delft Prof. dr. L. DiCarlo, Technische Universiteit Delft

Prof. dr. ir. T. H. Oosterkamp,

Universiteit Leiden

Prof. dr. B. Huard, Ecole Normale Supérieure de Lyon, France

Prof. dr. W. Belzig, Universität Konstanz, Germany

Prof. dr. C. J. M. Schoutens,

Universiteit van Amsterdam

Prof. dr. L. Kuipers, Technische Universiteit Delft, reserve member



Printed by: GILDEPRINT

Copyright © 2018 by A. Franquet González

Casimir PhD Series, Delft-Leiden 2018-50

ISBN/EAN 978-90-8593-379-3

An electronic version of this dissertation is available at

http://repository.tudelft.nl/.

CONTENTS

Summary						
Sa	men	vatting		хi		
1	Introduction					
	1.1	Prefac	ce	2		
	1.2	Quan	tum Measurement	2		
		1.2.1	Projective measurements	3		
		1.2.2	General measurements	3		
		1.2.3	POVM measurements	4		
		1.2.4	How do they fit together?	4		
	1.3	Conti	nuous weak linear measurement	5		
		1.3.1	The need for a more detailed physical description	5		
		1.3.2	CWLM description	6		
		1.3.3	Result of a CWLM	8		
		1.3.4	The state of the measured system	9		
		1.3.5	Other methods	11		
	1.4	Coun	ting Statistics method	12		
	1.5	Struct	ture of this Thesis	14		
		1.5.1	Chapter 2: Probability distributions of continuous measurement			
			results for conditioned quantum evolution	14		
		1.5.2	Chapter 3: Probability distributions of continuous measurement			
			results for two non-commuting variables subject to conditioned			
			quantum evolution	14		
		1.5.3	Chapter 4: Statistics of continuous weak quantum measurement of			
			an arbitrary quantum system with multiple detectors	15		
		1.5.4	Chapter 5: Conditioned outputs, distribution of decision times and			
			measurement-based feedback scheme for continuous weak linear			
	D (measurement of a simple quantum system	15		
	Refe	erences	8	16		
2	Pro	babilit	y distributions of continuous measurement results for conditioned			
	qua	ntum (evolution	19		
	2.1	Introd	duction	20		
	2.2	Metho	od	22		
	2.3	Half-o	quantization: a straightforward case	27		
	2.4		en jump: a simple consideration	31		
	2.5	Nume	erical results: long time scales	34		
	2.6	Nume	erical results: short time scales.	38		

vi Contents

		Conclusion						
3 Probability distributions of continuous measurement results for two no								
	commuting variables and conditioned quantum evolution							
	3.1	Introduction	46					
	3.2	Method	48					
	3.3	Quasi-distribution of shifts						
	3.4	Short time intervals and zero overlap	55					
	3.5	Numerical results: Short time scales	58					
	3.6	Numerical results: Longer time scales	61					
	3.7	Positivity of the distribution	69					
	3.8	Conclusion	72					
	Refe	erences	73					
4	Statistics of continuous weak quantum measurement of an arbitrary quan-							
	tum	n system with multiple detectors	77					
	4.1	Introduction	78					
	4.2	FCS derivation	79					
	4.3	Drift-diffusion equation	84					
	4.4	Lindblad construction derivation	85					
	4.5	Output rescaling and separation	88					
	4.6	Discrete update	88					
	4.7	Stochastic trajectories	89					
		4.7.1 Oscillator update	90					
		4.7.2 Qubit update	91					
	4.8	Conclusions	91					
	Refe	erences	92					
5	Con	nditioned outputs, distribution of decision times and measurement-based						
feedback scheme for continuous weak linear measurement of a simple quan								
		n system	95					
		Introduction						
	5.2	The simulation tool						
		5.2.1 Qubit as a linear detector						
	5.3	The simple measurement setup: simulation results						
		5.3.1 Quantum trajectories						
		5.3.2 Simulation of the detector signal						
		5.3.3 Results for conditioned output						
		5.3.4 Decision time distribution						
	5.4	Results on the feedback scheme						
		5.4.1 Analytics						
		5.4.2 Numerical results						
	5.5	Conclusion						
	References							

CONTENTS	vii
Curriculum Vitæ	115
List of Publications	117



SUMMARY

One of the pillars of the scientific method is the fact that all scientific predictions and explanations of phenomena in the universe are testable. Testing in the context of physics involves the action of measuring. Thus, the measurement process plays an important role in physics.

While classically we all understand the idea of measurement in a very straightforward fashion, in quantum mechanics the concept of measurement departs from our everyday experience in physics. In fact, although the quantum measurement obeys rather simple rules, its interpretation has been a subject of discussion since the beginning of the 20th century.

Some of the physics involved in the process of a quantum measurement have no classical analogues, challenging in this way our intuition: the famous paradox of a cat in a box is a clear example of this.

In recent years, with the boom of quantum information and computing, it has become evident that the ability to control a quantum system is of crucial technological importance. For that, a sufficiently general description of the measurement process is needed. The theory of continuous weak linear measurement (CWLM) provides such description. In contrast with the usual descriptions, a sufficiently weak coupling between the quantum system and multiple degrees of freedom of a detector mediates their entanglement and results in a conversion of discrete quantum information into continuous time-dependent readings of the detector. It provides a description that involves the requirement of a measurement time and a continuous set of measurement outcomes; two important characteristics missing in other generally used descriptions.

In this thesis we put forward a framework to compute the statistics of CWLM. In Chapter 2, we reveal and investigate two signatures of the measurement statistics during conditioned quantum evolution related to purely quantum interference effects. We concentrate on a relevant case of conditioned evolution where the information of the state before (preparation) and after (post-selection) a measurement can lead to drastically different statistics than the unconditioned case. The first signature is that of *half-quantization*; where either peaks or dips at half-quantized values of the measurement output appear in the probability distribution of measurement outcomes. The second signature, we term *sudden-jump* of the integrated output; where in the case of zero overlap between pre and post-selected states, a jump of integrated output appears at small time scales, revealing unconventionally large values of the average output.

Chapter 3 extents these results to the case of the measurement of two non-commuting variables. In this way we investigate the interplay of extra decoherence due to the simultaneous measurement of non-commuting variables with the goal of revealing the signatures of quantum interference in conditioned evolution in the statistics of measurement

x Summary

outcomes.

We generalise the theoretical framework for the description of continuous quantum measurements and the statistics of the measurement results in Chapter 4. We present various approaches to the problem and show their equivalence. These include the use of a full counting statistics evolution equation for a pseudo-density matrix, a drift-diffusion equation for a density matrix in the space of detector outcomes and discrete stochastic updates. We also provide the derivation of the underlying equations and stablish the necessary conditions on the phenomenological parameters that guarantee the physical interpretation of these results.

Finally, in Chapter 5, we take a closer look at the idea of stochastic updates. Using this idea, we show a scheme to numerically simulate a CWLM. This allows us to generate single quantum trajectories of the measured system and the integrated measurement signal. Using a simple example of a qubit non-demolition measurement we numerically investigate a rather counter-intuitive fact: the average output of a measurement conditioned on the final state does not depend on time.

Next, we consider how fast a decisive CWLM can be. We conclude by showing how this method can be extended to engineer and simulate simple measurement feedback schemes. In these schemes, the information collected from the statistics of the measurement output can be used in real time to condition the qubit evolution. Thus, moving from the more formal computation of measurement statistics to the direction of quantum control engineering.

SAMENVATTING

Eén van de bouwstenen van de wetenschappelijke methode is het feit dat alle wetenschappelijke voorspellingen en verklaringen van fenomenen in het universum testbaar zijn. In natuurkundige context is testen gerelateerd aan de actie van het meten. Daarom speelt het meetproces een belangrijke rol in de natuurkunde.

Terwijl we allemaal op een eenvoudige manier het idee van een klassieke meting kunnen begrijpen, wijkt het concept van een meting in de kwantummechanica af van onze dagelijkse ervaring in de natuurkunde. Ondanks dat de kwantummeting betrekkelijk eenvoudige regels volgt, is de interpretatie ervan het onderwerp van discussie sinds het begin van de twintigste eeuw.

Een deel van de natuurkunde met betrekking tot het proces van een kwantummeting heeft geen klassieke analoog, waardoor het onze intuïtie uitdaagt: het beroemde voorbeeld van de kat in de doos is daarvan een duidelijk voorbeeld.

Door de snelle ontwikkelingen in de kwantuminformatie en -berekening van de afgelopen jaren is het duidelijk geworden dat het vermogen om een kwantumsysteem te controleren van cruciaal technologisch belang is. Daarvoor is een voldoende algemene beschrijving van het meetproces benodigd. De theorie van continue zwakke lineaire meting (continuous weak linear measurement, CWLM) voorziet in zo'n beschrijving. In contrast met de gebruikelijke beschrijvingen geeft een voldoende zwakke koppeling tussen het kwantumsysteem en meerdere vrijheidsgraden van een detector verstrengeling door en resulteert het in een conversie van discrete kwantuminformatie naar continue tijdafhankelijke aflezingen van de detector. Het voorziet in een beschrijving dat betrekking heeft tot de voorwaarde van een meettijd en een continue verzameling van meetuitkomsten, twee belangrijke karakteristieken die missen in andere algemeen gebruikte beschrijvingen.

In deze thesis presenteren we een kader om de statistieken van CWLM te berekenen. In Hoofdstuk 2 onthullen en onderzoeken we twee kenmerken van de meetstatistieken gedurende geconditioneerde kwantumevolutie, gerelateerd aan pure kwantuminterferentieeffecten. We concentreren op een relevant geval van geconditioneerde evolutie, waarin de informatie van de toestand vóór (preparatie) en na (post-selectie) een meting kan leiden tot drastisch verschillende statistieken vergeleken met het ongeconditioneerde geval. Het eerste kenmerk is dat van *half-kwantisatie*, waarbij pieken of dalen op halfgekwantiseerde waarden van de meetuitkomst verschijnen in de waarschijnlijkheidsverdeling van meetuitkomsten. Het tweede kenmerk noemen we de *plotse sprong* van de geïntegreerde output, waar in het geval van nul overlap tussen pre- en post-geselecteerde toestanden een sprong in de geïntegreerde output verschijnt op korte tijdschalen, waarbij het onconventioneel grote waarden van de gemiddelde output onthuldt.

Hoofdstuk 3 breidt deze resultaten uit naar het geval van de meting van twee niet-commuterende

xii Samenvatting

variabelen. Op deze manier onderzoeken we het samenspel van extra decoherentie veroorzaakt door de gelijktijdige meting van niet-commuterende variabelen, met als doel het ontdekken van kenmerken van kwantuminterferentie in geconditioneerde evolutie in de statistiek van meetuitkomsten.

We generaliseren het theoretisch kader voor de beschrijving van continue kwantummetingen en hun resulterende statistieken in Hoofdstuk 4. We presenteren verschillende benaderingen van het probleem en tonen hun equivalentie. Deze benaderingen bevatten het gebruik van een evolutievergelijking voor volledige tellingstatistiek van een pseudo-dichtheidsmatrix, een drift-diffusievergelijking voor een dichtheidsmatrix in de ruimte van detectoruitkomsten en discrete stochastische updates. We geven ook de afleiding van de onderliggende vergelijkingen en we stellen de benodigde voorwaarden vast voor de fenomenologische parameters die de fysische interpretatie van deze resultaten garanderen.

Als laatste bekijken we in Hoofdstuk 5 het idee van stochastische updates. Gebruikmakend van dit idee presenteren we een schema om een CWLM numeriek te simuleren. Dit geeft ons de mogelijkheid om enkele quantumpaden van het gemeten systeem en het geïngegreerde meetsignaal te genereren. Door een eenvoudig voorbeeld van een niet-verstorende qubitmeting te gebruiken onderzoeken we numeriek een zeer tegenintuïtief feit: de gemiddelde output van een meting geconditioneerd op de uiteindelijke toestand is onafhankelijk van de tijd.

Daarna beschouwen we hoe snel een beslissende CWLM kan zijn. Tenslotte tonen we te tonen hoe deze methode kan worden uitgebreid om eenvoudige meting-terugkoppelingschema's te construeren en te simuleren. In deze schema's kan de informatie verzameld vanuit de statistieken van de meetoutput onmiddelijk gebruikt worden om de qubitevolutie te conditioneren. Hiermee bewegen we ons van de meer formele berekening van meetstatistieken in de richting van kwantumcontrole-ontwikkeling.

Introduction

2 Introduction

1.1. Preface

Almost a century after the advent of quantum mechanics and despite its success in explaining phenomena observed in the physical world, the abstract status of the theory is still discussed to understand it deeper [1]. The discussion is commonly centered around two main areas depicted by two famous paradoxes: the Schrödinger's cat paradox [2] and the Einstein-Podolsky-Rosen paradox [3]. This thesis relates to the first, which is often known as the quantum measurement problem.

Measurement is the abstract promoter of the wave function collapse which, in 1927, Werner Heisenberg contemplated as a way of describing the measurement process [4]. In this same work he presented his famous uncertainty principle and used it as a physical explanation of quantum uncertainty.

The following discussions concerning the topic gave rise to different interpretations of quantum mechanics, as it would seem nature was fundamentally stochastic, a property people found difficult to accept. Half a century later, the idea of quantum decoherence is consolidated and mainstream, and used to understand the quantum measurement problem in the framework of interaction of various quantum systems [5].

From a pragmatical point of view, any observation in an experimental setup requires at least a minimal understanding of the measurement process. In that spirit, far away from starting yet another debate on the interpretation of the measurement process or trying to explain the measurement problem, this thesis aims at providing a new theoretical framework that incorporates all the needed ingredients for a physically relevant description of a quantum measurement.

For that, this introduction will follow a pedagogical approach in building this framework. Pedagogical in the sense that it will be built from the bottom up, starting with the most basic mathematical description of a quantum measurement usually provided in any introductory course of quantum mechanics. Recalling the main problems of this description from a physical point of view, we will introduce the concept of a continuous weak measurement.

Finally, we will shift the focus of attention to not only the measured system, but also the detector and the classical outcomes of the measurement process. With this, I will provide a mathematical framework in the paradigm of continuous weak linear measurement (CWLM).

1.2. QUANTUM MEASUREMENT

In most undergraduate courses in quantum mechanics, the theory is introduced starting with its mathematical structure. For that, it is usual to mention the postulates of quantum mechanics or directly the Dirac-von Neumann axioms, introduced by Dirac (1930) [6] and von Neumann (1932) [7]. It is in postulate number 3 that the concept of measurement is first mentioned. Historically, this postulate is also known as Born's Rule [8]. Born's rule can be described by two simple statements: (1) Let the unit vectors $|b\rangle$ and $|a\rangle$ represent the states before and after the measurement, b and a, respectively. (2) If the state before the measurement is b, the probability of the measurement outcome

1

corresponding to the state a, is given by

$$P(a|b) = |\langle a|b\rangle|^2, \tag{1.1}$$

where $|\langle a|b\rangle|$ symbolize the absolute value of the inner product of the vectors $|b\rangle$ and $|a\rangle$.

What is not clear with this postulate is which property of the physical world explains why (1) and (2) lead to exceptional correspondence between experiments and theory. For more details see, e. g., [9].

Nowadays we have a more detailed mathematical description of postulate 3. Here I will adopt the basic definitions that appear in [10] and collect the essential concepts of this postulate in the reminder of this section.

1.2.1. PROJECTIVE MEASUREMENTS

The first class of measurements that are usually introduced are the so called projective measurements. A projective measurement is described by a physical observable \hat{M} . This observable has a spectral decomposition $\hat{M} = \sum_m \hat{P}_m$, where \hat{P}_m is the projector on to the eigenspace of \hat{M} with eigenvalue m.

The possible outcomes of the measurement correspond to the eigenvalues, m, of the observable. If the state of the system is $|\Psi\rangle$ immediately before the measurement then the probability that result m occurs is given by

$$P(m) = \langle \Psi | \hat{P}_m | \Psi \rangle. \tag{1.2}$$

Given that the outcome m occurs, the state of the measured system immediately after the measurement is

$$\frac{\hat{P}_m |\Psi\rangle}{\sqrt{P(m)}}.\tag{1.3}$$

Projective measurements are a special case of a broader class of measurements (a special case of postulate 3). Upon being measured the system is successfully projected to a specific eigenspace of the observable measured. They are also called *von Neumann* measurements.

1.2.2. GENERAL MEASUREMENTS

It is worth noting that, for a large number of physical experiments, the notion of projective measurements is enough to describe the experiment with high accuracy. However, postulate 3 can be introduced in a more general fashion.

In this definition, quantum measurements are described by a collection $\{\hat{M}_m\}$ of measurement operators. The index m labels the measurement outcomes that may occur in the experiment. If the state of the system is $|\Psi\rangle$ immediately before the measurement then the probability that result m occurs is given by

$$P(m) = \langle \Psi | \hat{M}_{m}^{\dagger} \hat{M}_{m} | \Psi \rangle, \qquad (1.4)$$

4 Introduction

and the state of the system after the measurement is

$$\frac{\hat{M}_m |\Psi\rangle}{\sqrt{\langle \Psi | \hat{M}_m^{\dagger} \hat{M}_m |\Psi\rangle}}.$$
 (1.5)

These measurement operators satisfy a completeness relation,

$$\sum_{m} \hat{M}_{m}^{\dagger} \hat{M}_{m} = \hat{1}, \tag{1.6}$$

which expresses the fact that probabilities sum to one.

1.2.3. POVM MEASUREMENTS

Another special case of this more general version of postulate 3 are the so called *POVM* measurements. The acronym stands for "Positive Operator-Valued Measure".

This special case is naturally used in situations where the post-measurement state of the system is of little interest, with the main item of interest being the probabilities of the respective measurement outcomes.

Suppose we define

$$\hat{E}_m \equiv \hat{M}_m^{\dagger} \hat{M}_m \tag{1.7}$$

for the same measurement situation described above. The set of operators \hat{E}_m are sufficient to determine the probabilities of the different measurement outcomes. These are known as the *POVM elements* associated with the measurement, with the complete set $\{\hat{E}_m\}$ known as a *POVM*. Note that by this definition, \hat{E}_m is a positive operator that completes the identity.

This formalism is a simple consequence of the general measurements description introduced previously. However, POVM measurements are an elegant and widely used theory, that deserves a separate mention.

1.2.4. How do they fit together?

Most introductory courses on quantum mechanics give only one description of postulate 3 in the form of projective measurements. The idea of general measurements or the POVM formalism are consequently unfamiliar to many physicists. Given the historical controversy around the subject of quantum measurement it is surprising that this is in fact the case. The main reason for it is that in most physical scenarios measurements can only be performed in a very harsh manner.

More general and detailed descriptions only start to be relevant when one aims for a high level of control of the measurements to be done. This is precisely why in the last 30 years more general and precise descriptions of quantum measurement appeared; rapid technological progress has made the fields of quantum information, computation and simulation flourish quickly.

1

5

Interestingly enough, one may argue that given the formalism of projective measurements and augmenting it with unitary operations it is possible to find a description equivalent to general measurements. However, there are several reasons why general measurements are a better starting point to describe the measurement process.

First, general measurements are simpler than projective measurements in that they involve fewer restrictions on the measurement operators. Which gives rise to useful properties for general measurements that projective measurements do not possess. Second, important problems in the fields of quantum information and computation - such as the the optimal way to distinguish a set of quantum states - involve the use of general measurements, rather than projective measurements.

A third reason is related to the *repeatability* of projective measurements. If we perform a projective measurement and obtain the outcome m, repeating the measurement will give the outcome m each time without changing the state of the measured system. Although it seems a desirable quality for a physical measurement in terms of trust, as a formalism it lacks the ability to correctly describe many physical measurements that are not repeatable (usually measurements where the measured system is destroyed).

But why are then POVMs a special case that should be mentioned? POVMs are best viewed as a mathematical tool, providing the simplest means by which general measurement statistics can be described, without necessarily knowing the post-measurement state. They are, in fact, a mathematically convenient way to study quantum measurement that sometimes can give extra insights into quantum measurements.

1.3. CONTINUOUS WEAK LINEAR MEASUREMENT

1.3.1. THE NEED FOR A MORE DETAILED PHYSICAL DESCRIPTION

In the last subsection we made clear why general measurements are the way to go when describing a quantum measurement. However, several questions remain elusive when we want to describe a measurement in the context of an experiment.

So far we described the measurement process as an instantaneous event, which abruptly changes the wave function of the measured system and gives a discrete result. This description is notably not physical. The measurement process in an experiment is indeed neither instantaneous nor discrete. The statistics and measurement results take a finite time to accumulate and the measurement results form a continuous set, rather than a discrete one.

In addition, there is no description of the measuring device. The idea that the detector is a quantum system that may be substantially bigger than the measured system becomes relevant if one wants to describe the measurement process with experimentally relevant quantities like noises or susceptibilities.

Thus it is clear that there is a need for a larger class and framework of quantum measurement. Such description is provided by the theory of *Continuous Weak Linear Measurement* (CWLM) [11–16], where a sufficiently weak coupling between the quantum

1

system and multiple degrees of freedom of a detector mediates their entanglement and results in conversion of discrete quantum information into continuous time-dependent readings of the detector. The description follows from general linear response theory and gives an explicit connection between quantum measurement and quantum noise. [17–19]

It is worth noting that the same measurement paradigm can be achieved extending the general measurement theory introduced in the previous section by taking into account a quantum description of the detector system and a coupling between detector and measured system. In fact, Any CWLM can be described as a general quantum measurement, which involves a measured system and detector degrees of freedom.

Interestingly enough, although the name *von Neumann* is associated to projective measurements. His seminal work [7] introduced what is known as the *von Neumann measurement scheme* which already described measurements by taking into account the measuring apparatus as a quantum object, thus paving the way for concepts like quantum decoherence.

1.3.2. CWLM DESCRIPTION

Consider the simplest measurement scenario in which a quantum system with dynamics described by a Hamiltonian \hat{H}_s is being measured using another quantum system (the detector), with its dynamics described by \hat{H}_d .

For the detector to have some information about the measured system, a coupling interaction is introduced. The complete dynamics of this scenario can then be described by a total Hamiltonian

$$\hat{H} = \hat{H}_s + \hat{H}_d + \hat{H}_c, \tag{1.8}$$

where $\hat{H}_c = \hat{\mathcal{O}} \hat{Q}$ is the coupling Hamiltonian. With $\hat{\mathcal{O}}$ acting on the space of the measured system and the detector's *input* variable \hat{Q} acting on the detector's space.

As mentioned, it is an important feature of CWLM that the information is transferred from the measured system to the measuring apparatus. Thus, the measurement outcome is represented by the detector degrees of freedom. These detector degrees of freedom are continuous variables, in contrast to the discrete result of a projective measurement. Additionally these variables might be subject to noise, and this noise can affect the measured system too.

In comparison with the previously introduced measurement schemes, the CWLM takes time to both accumulate information and to distort the measured system. The time t_a required to obtain a result with sufficient accuracy is called *measurement time* or *acquisition time* and is characteristic of a CWLM setup.

It is another characteristic of CWLM that the dynamics of these detector variables are linear. Thus in general the form of \hat{H}_d is that of a boson bath. The input and output of the detector are given by the *input* and *output* variables \hat{Q} and \hat{V} respectively. Arbitrary linear dynamics are reproduced if these variables are linear combinations of the boson creation/annihilation operators.

In the spirit of linear response theory [20–22] and of the Caldeira-Legget approach [23], all the information of the measurement can be expressed in terms of the two point correlators of the detector *input* and *output* variables:

The noises

$$S_{QQ} = \frac{1}{2} \int_{-\infty}^{t} dt' \left\langle \left\langle \hat{Q}(t)\hat{Q}(t') + \hat{Q}(t')\hat{Q}(t) \right\rangle \right\rangle, \tag{1.9a}$$

$$S_{QV} = \frac{1}{2} \int_{-\infty}^{t} dt' \left\langle \left\langle \hat{Q}(t) \hat{V}(t') + \hat{V}(t') \hat{Q}(t) \right\rangle \right\rangle, \tag{1.9b}$$

$$S_{VV} = \frac{1}{2} \int_{-\infty}^{t} dt' \left\langle \left\langle \hat{V}(t)\hat{V}(t') + \hat{V}(t')\hat{V}(t) \right\rangle \right\rangle, \tag{1.9c}$$

where $\langle \langle \hat{A}\hat{B} \rangle \rangle = \langle (\hat{A} - \langle \hat{A} \rangle) \rangle \langle (\hat{B} - \langle \hat{B} \rangle) \rangle$. And the response functions,

$$a_{QQ} = -\frac{i}{\hbar} \int_{-\infty}^{t} dt' \left\langle [\hat{Q}(t), \hat{Q}(t')] \right\rangle, \tag{1.10a}$$

$$a_{QV} = -\frac{i}{\hbar} \int_{-\infty}^{t} dt' \left\langle [\hat{Q}(t), \hat{V}(t')] \right\rangle, \tag{1.10b}$$

$$a_{VQ} = -\frac{i}{\hbar} \int_{-\infty}^{t} dt' \langle [\hat{V}(t), \hat{Q}(t')] \rangle, \qquad (1.10c)$$

$$a_{VV} = -\frac{i}{\hbar} \int_{-\infty}^{t} dt' \left\langle [\hat{V}(t), \hat{V}(t')] \right\rangle, \tag{1.10d}$$

as given by linear response theory and the Kubo formula [24]. In contrast to general approaches, thermodynamic equilibrium is not assumed. In fact, in most practical detectors this assumption is wrong, as signal amplification cannot take place in thermal equilibrium. To guarantee the linear dynamics of the detector variables we require that Wick's theorem holds for the boson operators involved. This is sufficient for the CWLM to be a Gaussian process, meaning that these two-point correlators are enough to completely define the measurement process.

The usefulness of this approach becomes clear when understanding the physical meaning of these detector correlation functions. Let us note that the two point correlators in Eq. (1.9) are nothing more than quantum noises [17] of different detector variables. S_{QQ} is the noise of the input variable. It is responsible for the inevitable measurement back action and associated decoherence of the qubit. S_{VV} is the output variable noise: it determines the time required to measure the detector outcome with a given accuracy. The cross noise S_{QV} quantifies possible correlations of these two noises. The response function a_{VQ} determines the detector gain: it is the susceptibility relating the detector output to the qubit variable measured, $\langle \hat{V} \rangle = a_{VQ} \langle \hat{\mathcal{O}} \rangle$. The response function a_{QV} is correspondingly the reverse gain of the detector: it gives the change of the qubit variable proportional to the detector reading. Other response functions a_{QQ} , a_{VV} are, respectively, related to the input and output impedances and are not of immediate interest for us. Conforming to the assumption of slow qubit dynamics, the noises are white and responses are instant.

These correlators are constrained by a Cauchy-Schwartz inequality:

8 Introduction

$$S_{QQ}S_{VV} - |S_{QV}|^2 \ge \frac{\hbar^2}{4} |a_{VQ} - a_{QV}|^2.$$
 (1.11)

With this, one can define and relate the dephasing rate $\gamma = S_{QQ}/\hbar^2$ and the acquisition time $t_a \equiv 4S_{VV}/\left|a_{VQ}\right|^2$ required to measure the variable with $\mathscr O$ with a relative accuracy $\simeq 1$. If one further assumes the direct gain to be much larger than the reverse gain, $a_{VO} \gg a_{OV}$, it is implied that

$$\gamma t_a \ge 1 \tag{1.12}$$

This figure of merit shows that one cannot measure a quantum system without dephasing it.

1.3.3. RESULT OF A CWLM

The output of a linear detector is a continuous number defined for a continuous time interval, \mathcal{T} , that is the duration of the measurement. It has a spectrum defined by S_{VV} and the instant output value has an infinite variance so an actual experimental reading gives the output integrated over the measurement time $V \equiv \frac{1}{\mathcal{T}} \int_t^{t+\mathcal{T}} d\tau \hat{V}(\tau)$. Thus, the result of a CWLM has a finite variance S_{VV}/\mathcal{T} .

For each state of the measured system $\hat{\rho}$, the probability of getting the result V for a CWLM of duration \mathcal{T} can be described by the Gaussian distribution

$$P_{\rho}(V) = \sqrt{\frac{\mathcal{F}}{2\pi S_{VV}}} \exp\left(-\frac{\left(V - a_{VQ} \langle \hat{\mathcal{O}} \rangle_{\rho}\right)^{2} \mathcal{F}}{2S_{VV}}\right), \tag{1.13}$$

with $\langle \mathcal{O} \rangle_{\rho} = \text{Tr} \left[\hat{\rho} \hat{\mathcal{O}} \right]$. So the statistics of such measurement are described by the probability distribution of measurement outcomes:

$$P(V) = \sqrt{\frac{\mathcal{F}}{2\pi S_{VV}}} \sum_{i} \rho_{i} \exp\left(-\frac{\left(V - a_{VQ}\mathcal{O}_{i}\right)^{2} \mathcal{F}}{2S_{VV}}\right), \tag{1.14}$$

where the state $\hat{\rho}$ of the measured system has been expressed in the eigenbasis of the measured variable $\hat{\mathcal{O}}$. Meaning $\hat{\rho} = \sum_i \rho_i |i\rangle \langle i|$ where $\hat{\mathcal{O}} |i\rangle = \mathcal{O}_i |i\rangle$.

Several characteristics of CWLM are depicted by this distribution. First, let us consider the duration of measurement \mathcal{T} . The separation of the means of the distributions for two different eigenstates $i \neq j$ grows linearly with the measurement duration, while the width of the distributions diminishes as $\sqrt{\mathcal{T}}$. At small measurement durations the distribution covers all possible measurement results while at infinitely long measurement durations the distribution converges to a delta distribution peaked at the mean value $\langle \hat{V} \rangle = a_{VQ} \langle \hat{\mathcal{O}} \rangle$.

This shows how a CWLM converges to a projective measurement for infinite measurement times $\mathcal{T} \to \infty$. And how at infinitely small measurement durations $\mathcal{T} \to 0$, the

measurement result contains no information about the measured system.

To exemplify this a bit further, let us consider the simple scenario of a qubit measurement. Imagine a measurement of the $\hat{\sigma}_z$ variable of a qubit system in the state $\hat{\rho} = \frac{\hat{1} + \hat{\sigma}_x}{2}$. In this case we can write the distribution in Eq. (1.14) as,

$$P(\nu) = \sqrt{\frac{t}{2\pi}} \left(\frac{1}{2} \exp\left(-\frac{(\nu - 1)^2 t}{2}\right) + \frac{1}{2} \exp\left(-\frac{(\nu + 1)^2 t}{2}\right) \right),\tag{1.15}$$

Where we normalized the output $v = V/a_{VQ}$ and the time scale $t = \mathcal{T}a_{VQ}^2/S_{VV}$. With this the average output corresponds with the measured variable $\langle v \rangle = \langle \hat{\sigma}_z \rangle$.

This distribution is now composed of two Gaussian distributions, centred at the two possible outcomes ± 1 of the projective measurement of the qubit variable. It is shown in Fig. 1.1 for different measurement times t. For small times $t \ll 1$ the width of the two Gaussian distributions is so big that one cannot distinguish one from another and the measurement is completely noise dominated. At this time scale it is impossible to resolve in which state the measured system is. At the time $\mathcal{T}=t_a$, i.e., t=4, the two peaks are sufficiently narrow such that one can resolve them with accuracy ~ 1 .

Finally, in the limit $t \to \infty$ the distribution becomes two delta peaks at the position of the two eigenvalues ± 1 , and with certainty one of the two results is obtained with probability 1/2. This is what we expect for the projective measurement of $\hat{\sigma}_z$ of a qubit initially in the state $\hat{\rho} = \frac{\hat{1} + \hat{\sigma}_x}{2}$.

1.3.4. THE STATE OF THE MEASURED SYSTEM

So far we have explored the physics of a CWLM in terms of the detector statistics and seen that it is sufficient to define the two-point correlation functions in Eq. (1.9) and (1.10) of the detector variables to have a complete description of the measurement process.

However, in all the previously introduced classes of measurements, the state of the system after the measurement is defined. What happens then to the measured system during a CWLM?

Let us go back to the total Hamiltonian of the system and detector in Eq. (1.8). If we do not consider any other interaction, the dynamics of the complete system are defined by this Hamiltonian.

Assuming that the coupling between system and measurement apparatus turns on at a definite time such that both systems are initially separate, i.e., on a product state $\hat{R}(0) = \hat{\rho} \otimes \hat{\rho}_d$. With $\hat{\rho}$ being the initial state of the measured system and $\hat{\rho}_d$ the initial state of the detector. Then the dynamics of the total system can be computed as

$$\frac{\partial \hat{R}}{\partial t} = \frac{i}{\hbar} [\hat{H}, \hat{R}]. \tag{1.16}$$

Solving this equation is in general a difficult task. In most cases it is more practical to concentrate on one of the two systems. This can be done by tracing out the degrees of

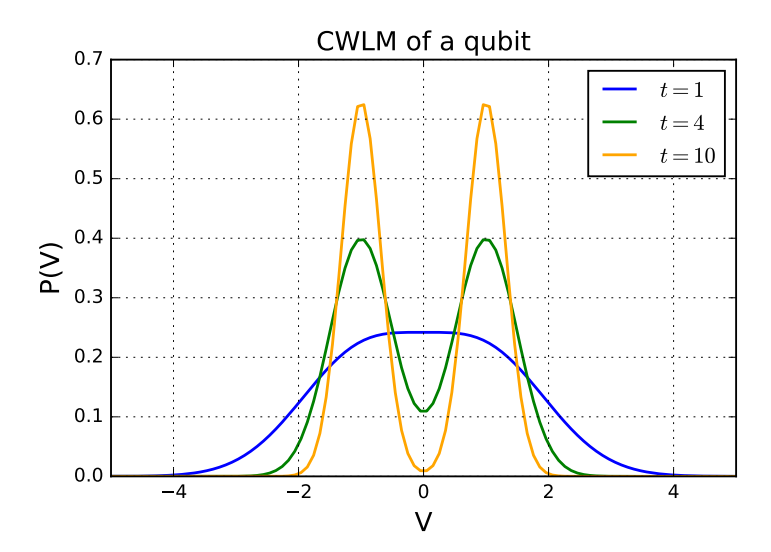


Figure 1.1: Distribution of measurement results, P(V), for a CWLM of the $\hat{\sigma}_Z$ variable of a qubit initially in the state $\hat{\rho} = \frac{\hat{1} + \hat{\sigma}_X}{2}$. For small measurement times (blue curve) the two qubit states cannot be resolved and the measurement is noise dominated. For a measurement duration $\mathcal{F} = t_a$ (green curve), the two eigenvalues ± 1 corresponding to the two qubit eigenstates can be resolved with an accuracy ~ 1 . Finally, for relatively long measurement times (orange curve), the CWLM statistics become close to those of a projective measurement. Showing two peaks at the two eigenvalues with a width that decreases as $1/\sqrt{t}$.

freedom of the other system and obtaining an equation for the system of interest alone. In the case of quantum measurement, in most practical scenarios we will be interested in the dynamics of the measured system.

Here, we assume that the coupling between the measured system and the detector is weak enough that the detector's state is negligibly affected by the interaction on the time scale of the evolution of the measured system. This is a usual assumption in open quantum system dynamics. The assumption of a weak coupling is in fact responsible for the terminology of *weak measurement*.

A time-dependent perturbation theory seems appropriate to tackle this problem. Thus, one could compute the dynamics of the measured system as

$$\frac{\partial \hat{\rho}}{\partial t} = -\frac{i}{\hbar} [\hat{H}_s, \hat{\rho}] - \frac{1}{\hbar^2} \int_{-\infty}^t \text{Tr}_d \Big\{ [\hat{H}_c(t), [\hat{H}_c(t'), \hat{R}(t')]] \Big\} dt', \tag{1.17}$$

where ${\rm Tr}_d$ corresponds to the partial trace over the detector degrees of freedom. Note that the first order contribution vanishes by construction as $\langle \hat{Q} \rangle = \langle \hat{V} \rangle = 0$.

This resembles the Nakajima–Zwanzig equation that describes the time evolution of the density matrix $\hat{\rho}$. Note that this equation is not local in time, and the state at time t depends on the state at previous times t'. The effect of the detector relates these two times and it is hidden in a memory kernel, the form of which can be explicitly written:

$$\frac{\partial \hat{\rho}}{\partial t} - \frac{i}{\hbar} [\hat{H}_{\mathcal{S}}, \hat{\rho}] - \frac{1}{\hbar^2} \int_{-\infty}^{t} dt' \bigg\{ \langle \hat{Q}(t) \hat{Q}(t') \rangle [\hat{\mathcal{O}}(t), \hat{\mathcal{O}}(t') \hat{\rho}(t')] + \langle \hat{Q}(t') \hat{Q}(t) \rangle [\hat{\rho}(t') \hat{\mathcal{O}}(t'), \hat{\mathcal{O}}(t)] \bigg\}. \tag{1.18}$$

It is clear from this expression that the state of the measured system can also be completely described by the two-point correlators in Eq. (1.9).

Although this equation can describe almost any physical situation, the fact that it is not local in time makes it very difficult to work with. However, it can be modified to a master equation that is local in time and still be valid in most experimentally relevant scenarios.

At this point, the so called Markov approximation is used. When the time scale associated with the reservoir (in this case, the detector) correlations is much smaller than the time scale over which the density matrix of the measured system varies appreciably. Then one can approximate $\hat{\rho}(t') \approx \hat{\rho}(t)$. This is true for a "memory-less" bath.

Another way of stating it is that the large size of the detector system (the proximity of its energy levels) ensures that from one moment to the next the system effectively interacts with a different part of the environment. With this, one obtains a Bloch-Redfield type of master equation. All these steps are often called the "Born-Markov" approximation.

It is worth mentioning that although this Bloch-Redfield equation is trace preserving and correctly reproduces a physical state for asymptotic propagation, it does not guarantee the positivity of the density matrix $\hat{\rho}$. This equation approaches the correct dynamics only for sufficiently weak couplings.

With one more approximation one can ensure the positivity of the density matrix. The equation is then called Lindblad equation [25], and it is the most common form describing the dynamics of open quantum systems.

This last approximation involves averaging over rapidly oscillating terms in the Bloch-Redfield equation. In general, a preferred choice of the spectral properties of the bath (detector) correlation functions is enough to ensure this. In particular, assuming fast correlation decay (i.e., instant detector responses and white, frequency-independent, noises) is enough to guarantee this form:

$$\frac{\partial \hat{\rho}}{\partial t} = -\frac{i}{\hbar} [\hat{H}_{s}, \hat{\rho}] - \frac{S_{QQ}}{\hbar^{2}} \mathcal{D}[\hat{\mathcal{O}}] \hat{\rho}, \tag{1.19}$$

with $\mathcal{D}[\hat{A}]\hat{\rho} \equiv (\frac{1}{2}[\hat{A}^{\dagger}\hat{A},\hat{\rho}]_{+} - \hat{A}\hat{\rho}\hat{A}^{\dagger}).$

1.3.5. OTHER METHODS

We chose a very particular method to introduce CWLM in order to highlight its simplicity and the similarity to experimental research with respect to the relevant physical quantities. However, a description of CWLM can be achieved by several methods. In simple situations like non-demolition measurements [12] one can use the quantum filtering equation [26]. More sophisticated approaches include the effective action method [11, 15], path integral formulation [14, 27] and past states formalism [28].

Some methods rely on the general measurement definition introduced by postulate 3 of the previous section. For example, a powerful numerical method of experimental significance is the stochastic update equation [29] which allows to monitor the density matrix taking into account the measurement results. In this method, the distribution of outcomes is obtained numerically by collecting statistics of the realizations of "quantum trajectories".

Continuous measurement and monitoring of quantum systems, and even the information about single quantum trajectories [30–36] have been recently achieved in experiments thanks to recent technological advances. Thus, making the stochastic update equation or "quantum trajectories" an important description of CWLM.

In contrast to these methods, the method of Ref. [27] permits the direct computation of the generating function of the probability distribution of detector outcomes. It unifies the full system and detector statistics in a single equation. In the following section we will introduce this method by extending the density matrix of the measured system to incorporate the detector statistics.

1.4. COUNTING STATISTICS METHOD

Consider again the simple example of a system being measured by a single detector. The detector is characterised by linear dynamics of its input and output variables \hat{Q} and \hat{V} respectively.

The density matrix evolution during a CWLM can be described using the noises and response functions in Eq. (1.9) and (1.10), but what about the statistics of the measurement outcome? Conforming to the linear dynamics of the detector, a Normal probability distribution is expected (Eq. (1.14)). However, so far it seems like direct computation of the statistics of measurement outcomes cannot be achieved from the Hamiltonian dynamics. It would be fundamentally interesting to do this in the same fashion as we did for the measured system statistics.

To achieve this, one starts again with the Hamiltonian in Eq. (1.8). The statistics of the detector variable \hat{V} can be evaluated by introducing a counting field $\chi(t)$ coupled to the output variable \hat{V} . This field plays the role of the parameter in the generating function $C(\chi(t))$ of the probability distribution of the detector readings V(t).

This generating function is computed in the extended Keldysh scheme [19] where the evolution of the "ket" and "bra" wave functions is governed by different Hamiltonians, \hat{H}^+ and \hat{H}^- respectively. The extra term describing the interaction with the counting field reads $\hat{H}^\pm = \hat{H} \pm \hbar \chi(t) \hat{V}(t)/2$. This method was first employed in Ref. [37].

This generating function then has the form

$$C(\{\chi(t)\}) = \operatorname{Tr}_{s}\left(\hat{\rho}(\{\chi(t)\})\right),\tag{1.20}$$

 $\hat{\rho}$ being now a quasi-density matrix of the system after the evolution,

$$\hat{\rho}(\chi;t) = \operatorname{Tr}_d\left(\overrightarrow{T}e^{-i/\hbar\int dt \hat{H}^-}\hat{R}(0)\overleftarrow{T}e^{+i/\hbar\int dt \hat{H}^+}\right). \tag{1.21}$$

Here, $\operatorname{Tr}_s(\cdots)$ and $\operatorname{Tr}_d(\cdots)$ denote the trace over system and detector variables, respec-

tively, and $\overrightarrow{T}(\overleftarrow{T})$ denotes time (reversed) ordering in evolution exponents. $\hat{R}(0)$ is the initial density matrix for both measured and detector systems.

Assuming white noises and instant responses, one can derive a Bloch-master equation for the quasi-density matrix that is local in time. This is done in the same spirit as one derives Eq. (1.19).

$$\frac{\partial \hat{\rho}}{\partial t} = -\frac{i}{\hbar} [\hat{H}_q, \hat{\rho}] - \frac{S_{QQ}}{\hbar^2} \mathscr{D}[\hat{\mathcal{O}}] \hat{\rho} - \frac{\chi^2(t)}{2} S_{VV} \hat{\rho}
- \frac{S_{QV}}{\hbar} \chi(t) [\hat{\rho}, \hat{\mathcal{O}}] + \frac{i a_{VQ} \chi(t)}{2} [\hat{\rho}, \hat{\mathcal{O}}]_+.$$
(1.22)

Here, $[\cdot,\cdot]$ and $[\cdot,\cdot]_+$ refer to commutator and anti-commutator operations respectively and we have also assumed $a_{VQ} \gg a_{QV}$, a general condition for a good amplifier.

Imagine a single measurement over a time interval $(0,\mathcal{T})$. To define the output of such measurement, one accumulates the time-dependent detector output during this time interval and normalizes it by the same interval: $V \equiv \frac{1}{\mathcal{F}} \int_0^{\mathcal{F}} V(t') dt'$. The counting field $\chi(t)$ corresponding to this output is conveniently constant , $\chi(t) \equiv \chi$, on the time interval $(0,\mathcal{F})$ and 0 otherwise. The probability distribution of the detector outcomes can be computed from the generating function defined by Eq. (1.20),

$$P(V) = \frac{\mathcal{T}}{2\pi} \int d\chi e^{-i\chi V \mathcal{T}} C(\chi; \mathcal{T}). \tag{1.23}$$

The joint statistics are extracted from the quasi-density matrix $\hat{\rho}(\chi;\mathcal{F})$ at time \mathcal{F} .

In this thesis we will formulate the theory of CWLM using this latter method, as it has several advantages over other formulations:

Firstly, the statistics of the measured system and the statistics of the measurement results are computed in an equal footing. Computing the statistics of the classical measurement outputs via a generating function method allows us to use all the statistical machinery developed for characteristic functions. This means that concrete and special distributions can be accessed easily: The equilibrium distributions of measurement outcomes, distributions at specific measurement times under conditions of specific measurement outputs at other times, even distribution of measurement outcomes conditioned on specific quantum states of the measured system or detectors at specific times [38, 39] can be computed and studied in an elegant manner.

Secondly, it's equivalence to other methods can be shown from microscopical, phenomenological or interaction and numerical approaches [40]. It is thus a good foundation for a general framework for describing CWLM.

14 Introduction

1.5. STRUCTURE OF THIS THESIS

1.5.1. CHAPTER 2: PROBABILITY DISTRIBUTIONS OF CONTINUOUS MEA-SUREMENT RESULTS FOR CONDITIONED QUANTUM EVOLUTION

For a conditioned evolution, both the initial and final states of the system are fixed: the latter is achieved by post-selection in the end of the evolution. The statistics may drastically differ from the nonconditioned case, and the interference between initial and final states can be observed in the probability distributions of measurement outcomes, as well as in the average values exceeding the conventional range of nonconditioned averages. We develop a proper formalism to compute the distributions of measurement outcomes, and evaluate and discuss the distributions in experimentally relevant setups. We demonstrate the manifestations of the interference between initial and final states in various regimes. We consider analytically simple examples of nontrivial probability distributions. We reveal peaks (or dips) at half-quantized values of the measurement outputs. We discuss in detail the case of zero overlap between initial and final states demonstrating anomalously big average outputs and sudden jump in time-integrated output. We present and discuss the numerical evaluation of the probability distribution aiming at extending the analytical results and describing a realistic experimental situation of a qubit in the regime of resonant fluorescence.

1.5.2. CHAPTER 3: PROBABILITY DISTRIBUTIONS OF CONTINUOUS MEA-SUREMENT RESULTS FOR TWO NON-COMMUTING VARIABLES SUB-JECT TO CONDITIONED QUANTUM EVOLUTION

Both conditioned quantum measurement and that of two non-commuting variables differ drastically for either classical or quantum projective measurement. In this chapter we explore the peculiarities brought by the combination of the two.

We put forward a proper formalism for the evaluation of the distributions of measurement outcomes. We compute and discuss the statistics in idealized and experimentally relevant setups. We demonstrate the visibility and manifestations of the interference between initial and final states in the statistics of measurement outcomes for both variables in various regimes.

We analytically predict the peculiarities at the circle $\mathcal{O}_1^2 + \mathcal{O}_2^2 = 1$ in the distribution of measurement outcomes in the limit of short measurement times and confirm this by numerical calculation at longer measurement times. We analytically demonstrate anomalously large values of the time-integrated output cumulants in the limit of short measurement times (sudden jump) and zero overlap between initial and final states, and give detailed distributions. Finally, we present the numerical evaluation of the probability distributions for experimentally relevant parameters in several regimes and demonstrate that interference effects in the conditioned measurement can be accurately predicted even if they are small.

1

1.5.3. CHAPTER 4: STATISTICS OF CONTINUOUS WEAK QUANTUM MEASURE-MENT OF AN ARBITRARY QUANTUM SYSTEM WITH MULTIPLE DETEC-TORS

In this chapter, we establish a general theoretical framework for the description of continuous quantum measurements and the statistics of the results of such measurements. The framework concerns the measurement of an arbitrary quantum system with an arbitrary number of detectors under the realistic assumption of instant detector reactions and white noise sources. We present various approaches to the problem, showing their equivalence. The approaches include the full counting statistics (FCS) evolution equation for the pseudo-density matrix, the drift-diffusion equation for a density matrix in the space of integrated outputs, and discrete stochastic updates. We provide the derivation of the underlying equations from a microscopic approach based on full counting statistics, a phenomenological approach based on the Lindblad construction, and interaction with auxiliary quantum systems representing the detectors. We establish the necessary conditions on the phenomenological susceptibilities and noises that guarantee the unambiguous interpretation of the measurement results and the positivity of the density matrix. Our results can easily be extended to describe various quantum feedback schemes where the manipulation decision is based on the values of detector outputs.

1.5.4. CHAPTER 5: CONDITIONED OUTPUTS, DISTRIBUTION OF DECISION TIMES AND MEASUREMENT-BASED FEEDBACK SCHEME FOR CONTIN-UOUS WEAK LINEAR MEASUREMENT OF A SIMPLE QUANTUM SYSTEM

We address the peculiarities of the quantum measurement process in the course of a continuous weak linear measurement (CWLM). As a tool, we implement an efficient numerical simulation scheme that allows us to generate single quantum trajectories of the measured system state, as well as the recorded detector signal, and study statistics of these trajectories with and without post-selection. In this scheme, a linear detector is modelled with a qubit that is weakly coupled to the measured quantum system and is subject to projective measurement and re-initialization after a time interval at each simulation step. We explain the conditions under which the scheme provides an accurate description of CWLM.

We restrict ourselves to a simple but generic situation of a qubit non-demolition measurement. The qubit is initially in an equal-weight superposition of two quantum states. Over time, the detector signal is accumulated and the superposition is destroyed. It is known that the times required to resolve the quantum states and to destroy the superposition are of the same order. We prove numerically a rather counter-intuitive fact: the average detector output conditioned on the final state does not depend on time. It seems like the qubit knows its final state from the very beginning. We study statistics of decision times, i.e. the time required for the density matrix along a certain trajectory to reach a threshold where it is close to one of the resulting states. This is useful to estimate how fast a decisive CWLM can be.

Based on this, we devise and study a simple feedback scheme that attempts to keep the

16 References

1

qubit in the equal-weight superposition. The detector readings are used to decide in which state the qubit is, and which correction rotation to apply to bring it back to the superposition. We show how to optimize the feedback parameters and move towards more efficient feedback schemes.

REFERENCES

- [1] A. J. Leggett, The quantum measurement problem, Science 307, 871 (2005).
- [2] E. Schrödinger, *Die gegenwärtige situation in der quantenmechanik*, Naturwissenschaften **23**, 807 (1935).
- [3] A. Einstein, B. Podolsky, and N. Rosen, *Can quantum-mechanical description of physical reality be considered complete?* Phys. Rev. **47**, 777 (1935).
- [4] W. Heisenberg, Über den anschaulichen inhalt der quantentheoretischen kinematik und mechanik, Zeitschrift für Physik 43, 172 (1927).
- [5] M. Schlosshauer, *Decoherence, the measurement problem, and interpretations of quantum mechanics*, Rev. Mod. Phys. **76**, 1267 (2005).
- [6] P. A. M. Dirac, The Principles of Quantum Mechanics (Clarendon Press, 1930).
- [7] J. von Neumann, *Mathematische Grundlagen der Quantenmechanik. (German) [Mathematical Foundations of Quantum Mechanics]* (Springer-Verlag, Berlin, Germany / Heidelberg, Germany / London, UK / etc., 1932) reprinted: Dover Publications (1943); Presses Universitaires de France (1947); Madrid, Institute de Matematicas "Jorge Juan" (1949). Translated from German by Robert T. Beyer, Princeton University Press (1955).
- [8] M. Born, Zur quantenmechanik der stoßvorgänge, Zeitschrift für Physik 37, 863 (1926).
- [9] A. Cabello, A simple explanation of born's rule, arXiv:1801.06347 [quant-ph] (2018).
- [10] M. Nielsen and I. Chuang, *Quantum Computation and Quantum Information* (Cambridge University Press, 2000).
- [11] M. B. Mensky, *The action uncertainty principle in continuous quantum measurements*, Physics Letters A 155, 229 (1991).
- [12] A. N. Korotkov, *Continuous quantum measurement of a double dot*, Phys. Rev. B **60**, 5737 (1999).
- [13] A. Jordan and M. Buttiker, *Continuous quantum measurement with independent detector cross correlations*, Phys. Rev. Lett. **95**, 220401 (2005).
- [14] A. Chantasri and A. N. Jordan, *Stochastic path-integral formalism for continuous quantum measurement*, Phys. Rev. A **92**, 032125 (2015).

- [15] A. Chantasri, J. Dressel, and A. N. Jordan, Action principle for continuous quantum measurement, Phys. Rev. A 88, 042110 (2013).
- [16] K. Jacobs and D. A. Steck, *A straightforward introduction to continuous quantum measurement*, Contemporary Physics **47**, 279 (2006), http://dx.doi.org/10.1080/00107510601101934.
- [17] A. A. Clerk, M. H. Devoret, S. M. Girvin, F. Marquardt, and R. J. Schoelkopf, *Introduction to quantum noise, measurement, and amplification*, Rev. Mod. Phys. **82**, 1155 (2010).
- [18] Y. V. Nazarov and J. Danon, *Advanced Quantum Mechanics: A practical guide* (Cambridge University Press, 2013).
- [19] Y. V. Nazarov and Y. M. Blanter, *Quantum Transport: Introduction to Nanoscience* (Cambridge University Press, 2009).
- [20] S. Pilgram and M. Büttiker, *Efficiency of mesoscopic detectors*, Phys. Rev. Lett. **89**, 200401 (2002).
- [21] A. A. Clerk, S. M. Girvin, and A. D. Stone, *Quantum-limited measurement and information in mesoscopic detectors*, Phys. Rev. B **67**, 165324 (2003).
- [22] A. N. Korotkov and D. V. Averin, *Continuous weak measurement of quantum coherent oscillations*, Phys. Rev. B **64**, 165310 (2001).
- [23] A. O. Caldeira and A. J. Leggett, *Quantum tunnelling in a dissipative system*, Annals of Physics **149**, 374 (1983).
- [24] R. Kubo, *The fluctuation-dissipation theorem*, Reports on Progress in Physics **29**, 255 (1966).
- [25] G. Lindblad, *On the generators of quantum dynamical semigroups*, Communications in Mathematical Physics **48**, 119 (1976).
- [26] V. Belavkin, *A new wave equation for a continuous nondemolition measurement,* Physics Letters A **140**, 355 (1989).
- [27] H. Wei and Y. V. Nazarov, Statistics of measurement of noncommuting quantum variables: Monitoring and purification of a qubit, Phys. Rev. B 78, 045308 (2008).
- [28] S. Gammelmark, B. Julsgaard, and K. Mølmer, *Past quantum states of a monitored system*, Phys. Rev. Lett. 111, 160401 (2013).
- [29] H. Wiseman and G. Milburn, *Quantum theory of optical feedback via homodyne detection*, Phys.Rev. Lett. **70**, 548 (1993).
- [30] M. Hatridge, S. Shankar, M. Mirrahimi, F. Schackert, K. Geerlings, T. Brecht, K. M. Sliwa, B. Abdo, L. Frunzio, S. M. Girvin, R. J. Schoelkopf, and M. H. Devoret, *Quantum back-action of an individual variable-strength measurement*, Science 339, 178 (2013).

18 References

[31] K. W. Murch, S. J. Weber, C. Macklin, and I. Siddiqi, *Observing single quantum trajectories of a superconducting quantum bit*, Nature **502**, 211 (2013).

- [32] N. Roch, M. E. Schwartz, F. Motzoi, C. Macklin, R. Vijay, A. W. Eddins, A. N. Korotkov, K. B. Whaley, M. Sarovar, and I. Siddiqi, Observation of measurement-induced entanglement and quantum trajectories of remote superconducting qubits, Phys. Rev. Lett. 112, 170501 (2014).
- [33] P. Campagne-Ibarcq, L. Bretheau, E. Flurin, A. Auffèves, F. Mallet, and B. Huard, *Observing interferences between past and future quantum states in resonance fluo-rescence*, Phys. Rev. Lett. **112**, 180402 (2014).
- [34] J. P. Groen, D. Ristè, L. Tornberg, J. Cramer, P. C. de Groot, T. Picot, G. Johansson, and L. DiCarlo, *Partial-measurement backaction and nonclassical weak values in a superconducting circuit*, Phys. Rev. Lett. 111, 090506 (2013).
- [35] S. J. Weber, A. Chantasri, J. Dressel, A. N. Jordan, K. W. Murch, and I. Siddiqi, *Mapping the optimal route between two quantum states*, Nature **511**, 570 (2014).
- [36] D. Tan, S. J. Weber, I. Siddiqi, K. Mølmer, and K. W. Murch, *Prediction and retrodiction for a continuously monitored superconducting qubit*, Phys. Rev. Lett. 114, 090403 (2015).
- [37] Y. V. Nazarov and M. Kindermann, *Full counting statistics of a general quantum mechanical variable*, The European Physical Journal B Condensed Matter and Complex Systems **35**, 413 (2003).
- [38] A. Franquet and Y. V. Nazarov, *Probability distributions of continuous measurement results for conditioned quantum evolution*, Phys. Rev. B **95**, 085427 (2017).
- [39] A. Franquet and Y. V. Nazarov, *Probability distributions of continuous measure-ment results for two non-commuting variables and conditioned quantum evolution*, arXiv:1708.05662 [quant-ph] (2017).
- [40] A. Franquet, Y. V. Nazarov, and H. Wei, *Statistics of continuous weak quantum measurement of an arbitrary quantum system with multiple detectors*, arXiv:1804.07639 [quant-ph] (2018).

1

PROBABILITY DISTRIBUTIONS OF CONTINUOUS MEASUREMENT RESULTS FOR CONDITIONED QUANTUM EVOLUTION

2.1. Introduction

The concept of measurement is one of the most important, characteristic, and controversial parts of quantum mechanics. Due to the intrinsically probabilistic nature of the measurement and associated paradoxes, [1] it continues to attract research attention and stimulate new experiments. The ability to control a quantum system that is of increasing importance in the context of quantum information processing, requires an adequate yet sufficiently general description of the measurement process. Such description is provided by the theory of continuous weak linear measurement (CWLM), where a sufficiently weak coupling between the quantum system and multiple degrees of freedom of a detector mediates their entanglement and results in conversion of discrete quantum information into continuous time-dependent readings of the detector. [2–8] The description follows from the general linear response theory and gives an explicit connection between quantum measurement and quantum noise. [9]

Recent experimental advances have made possible the efficient continuous measurement and monitoring of elementary quantum systems (qubits) giving the information on individual quantum trajectories. [10-12] The individual traces of quantum evolution can be post-selected by a projective measurement at the end of evolution, thus enabling the experimental investigation of conditioned quantum evolution where both initial and final states are known. [13-16]

For experimentally relevant illustrations, we concentrate in this paper on a setup of resonance fluorescence. [13] In this setup, a transmon qubit with ground state $|g\rangle$ and excited state $|e\rangle$ is enclosed in a non-resonant three-dimensional (3D) superconducting cavity connected to two transmission lines. A resonant field drives the qubit via the weakly coupled line, while most of the fluorescence signal exits via the other line which is coupled strongly. The amplitude of the signal is proportional to σ_- , the average of the lowering operator $\hat{\sigma}_- = |g\rangle\langle e|$ of the qubit, and oscillates with the Rabi frequency Ω set by the resonant drive.

A heterodyne detection setup is used to measure this signal. The measurement proceeds in many runs of equal time duration. At each run, the qubit is prepared in a state $|e\rangle$ or $|g\rangle$ and the signal is monitored at the time interval $0 < t < \mathcal{T}$. At the end of the interval, $t = \mathcal{T}$, one can projectively measure the qubit to find it either in the state $|e\rangle$ or $|g\rangle$ with high fidelity using a microwave tone at the bare cavity frequency. With such a setup, the fluorescence signal can be interpreted as a result of a weak continuous measurement, that can be conditioned not only on an initial state but also on a final state by post-selecting with the result of the projective measurement. The authors have concentrated on the conditioned signal at a given moment of time that is averaged over many runs. Its time traces reveal interference patterns interpreted in terms of weak values [17] and associated with the interference of initial and final quantum states in this context. [18, 19]

The concept of weak values has been introduced in [17] to describe the average result of a weak measurement subject to post-selection in a simplified setup. The authors have shown that the average measurement results may be paradoxically large as compared to the outputs of corresponding projective measurements. Since that, the concept has been extended in various directions, e.g. to account for the intermediate measurement strength, the Hamiltonian evolution of the quantum states during the measurement, see

2.1. Introduction 21

[20, 21] for review. In [18], the average measurement outputs have been investigated in the context of continuous weak measurement, this has been further elaborated in [22–24]. As to the detailed statistics of the measurement outcomes, in this context it has been considered only for simplified meter setups that correspond to measuring the light intensities in quantum optics. [20, 21] There is a tendency to term "weak value" a result of any weak measurement that involves post-selection. This may be confusing in general. For instance, the duration of a weak measurement can exceed the relaxation time of the system measured. The averaged measurement output in this case is not affected by post-selection and equals to the expectation value of the operator measured with the equilibrium density matrix. This is very far from the original definition of weak values [17]. We prefer to stick to the original definition.

We notice that the experiment discussed gives access not only to the conditioned averages, but also to the conditioned statistics of the measurement results. For instance, at each run one can accumulate the output signal on a time interval that is $(0,\mathcal{T})$ or a part of it and record the results. After many runs, one makes a histogram of the records that depends on the initial as well as on the final state of the qubit.

This article elaborates on the method to evaluate the distribution of the accumulated signal and gives the detailed theoretical predictions of the conditioned statistics for examples close to the actual experimental situation, and in a wide range of parameters.

In this Article, we put forward and investigate two signatures of the conditioned statistics. First is the *half-quantized* measurement values. A non-conditioned CWLM distribution under favourable circumstances peaks at the values corresponding to quantized values of the measured operator, in full correspondence with a text-book projective measurement. We demonstrate that a conditioned distribution function displays peculiarities — that are either peaks or dips — at *half-sums* of the quantized values.

Second signature pertains the case of zero or small overlap between initial and final state and time intervals that are so short as the wave function of the system does not significantly change. In this case, we reveal unexpectedly large values of the cumulants of the distribution function of time-integrated outputs for such short intervals, that we term *sudden jump*. For the average value of the output, the fact that it may by far exceed the values of typical outcome of a projective measurement, can be understood from the weak value theory [17]. We extend these results to the distributions of the output and reveal the role of decoherence at small time intervals.

We stress that the signatures by itself present no new phenomenon. Rather, the basic quantum phenomena like interference manifest themselves in these signatures in the context of CWLM statistics. As such, we permit a re-interpretation of these phenomena in the context considered.

Our approach to the CWLM statistics is based on the theory of full counting statistics in the extended Keldysh formalism. [25] The statistics of measurements of $\int dt \hat{V}(t)$, V(t) being a quantum mechanical variable representing linear degrees of freedom of the environment, are generated via a characteristic function method and the use of counting field technique. It provides the required description of the whole system consisting of the measured system, the environment and detectors.

Here we develop this formalism first introduced in, [6, 26] to include the conditioned

evolution. We focus on the pre- and post-selected measurements. In this case, a quantum system is initially prepared in a specific state. After that, it is subject of CWML during a time interval \mathcal{T} . The post-selection in a specific state takes place in the end of the procedure. We show that the evolution of a qubit whose past and future states are known can be inferred and understood from the measured statistics of measurement outcomes. The measurement of the statistics can reveal purely quantum features in experimentally relevant regimes.

We show how interference arises even at relatively small time scales and how the information about the initial qubit state is lost during the time evolution making the interference to vanish at sufficiently long time scales. We exemplify how different features in the distributions can be understood as the manifestations of the qubit evolution during the measurement. And we numerically study various parameter regimes of interest in the case of a measurement of a single observable.

Actually, we show with our results that one can have very detailed theoretical predictions of CWLM distributions that can account for every detail of the experiment. This enables investigation and characterization of quantum effects even if the choice of parameters is far from the optimal one and these effects are small.

The structure of the article is as follows. We develop the necessary formalism in Section 2.2, starting from a Bloch-master equation for the qubit evolution that is augmented with counting fields to describe the detector statistics, and explain how the postselection is introduced in this scheme. The scheme can be applied to various experimental scenarios, in particular we focus on the setup described in [13]. It is important to illustrate how the Cauchy-Schwartz inequalities impose restrictions on the parameters entering the Bloch-master equations, this resulting in several different time scales. In Section 2.3 we examine a measurement of a general observable and explain how the half-quantized peculiarities arise in the distributions of measurement outcomes depending on the initial and final state. In Section 2.4 we concentrate on the case of zero overlap and take the Hamiltonian dynamics into account to arrive at essentially non-Gaussian probability distributions. In these Sections, we mostly concentrate on a simple limit where the time interval \mathcal{T} is much smaller than the typical time scales of qubit evolution, this gives the opportunity for analytical results. Next, we extend our study to longer time intervals. In the Section 2.5 we present numerical simulations at the scale of decoherence time for three relevant cases: the case of an ideal detector, and the experimentally relevant case with and without detuning. In Section 2.6, we concentrate on the time scales of Hamiltonian dynamics and experimentally relevant parameters. We conclude in the Section 2.7.

2.2. METHOD

The description of CWLM can be achieved by several methods, all of them taking into account the stochastic nature of the measurement process. In simplest situations like non-demolition measurements [3] one can use the quantum filtering equation [27]. More sophisticated approaches include effective action method [2, 8], path integral formulation [6, 7], past states formalism [19]. A powerful numerical method of experimental significance is the stochastic update equation [28] that allows to monitor density matrix

taking into account the measurement results. In this method, the distribution of outcomes is obtained numerically by collecting statistics of the realizations of "quantum trajectories". In contrast to this, the method of [6] permits the direct computation of the generating function of the probability distribution.

The present goal is to formulate a method to compute probability distributions of a continuous measurement in the course of a conditioned quantum evolution. We will extend the method presented in [6] where the central object is a Bloch-master equation for the evolution of the measured quantum system that is augmented with the counting fields. Evaluating the trace of the extended density matrix from this equation as a function of the counting fields provides the generating function for the probability distribution of the detector output. To outline the formalism, we will focus first on the simplest setup where a single detector measures a single qubit variable $\hat{\mathcal{O}}$. In the end of the section we will give a generalization to the case of two variables.

In general, the dynamics of an isolated quantum system are governed by a Hamiltonian \hat{H}_q . For a realistic system, weak interaction with an environment representing the outside world will generate decoherence and relaxation . In the CWLM paradigm, the quantum system is embedded in a linear environment described in the same manner by a Hamiltonian \hat{H}_d . The quantum system interacts with the environment via a coupling Hamiltonian \hat{H}_c ,

$$\hat{H} = \hat{H}_q + \hat{H}_c + \hat{H}_d \tag{2.1}$$

with

$$\hat{H}_{c} = \hat{\mathcal{O}}\hat{Q},\tag{2.2}$$

 $\hat{\mathcal{O}}$ being an operator in the space of the quantum system, that value is to be measured. Since \hat{H}_d is a Hamiltonian of a linear system, it can generally be represented by a boson bath Hamiltonian. The input of the detector is characterized by an *input* variable \hat{Q} that is linear in boson fields. The output of the detector is represented by the *output* variable \hat{V} that is also linear in boson fields.

The dynamics and statistics of the measurement process are fully characterized by the two-time correlators of the operators $\hat{Q}(t)$, $\hat{V}(t)$. If we assume the qubit dynamics is slower than a typical time scale of the environment, the four relevant quantities correspond to zero-frequency values of the correlators,

$$S_{QQ} = \frac{1}{2} \int_{-\infty}^{t} dt' \left\langle \left\langle \hat{Q}(t)\hat{Q}(t') + \hat{Q}(t')\hat{Q}(t) \right\rangle \right\rangle, \tag{2.3a}$$

$$S_{QV} = \frac{1}{2} \int_{-\infty}^{t} dt' \left\langle \left\langle \hat{Q}(t)\hat{V}(t') + \hat{V}(t')\hat{Q}(t) \right\rangle \right\rangle, \tag{2.3b}$$

$$S_{VV} = \frac{1}{2} \int_{-\infty}^{t} dt' \left\langle \left\langle \hat{V}(t)\hat{V}(t') + \hat{V}(t')\hat{V}(t) \right\rangle \right\rangle, \tag{2.3c}$$

$$a_{VQ} = -\frac{i}{\hbar} \int_{-\infty}^{t} dt' \langle [\hat{V}(t), \hat{Q}(t')] \rangle, \qquad (2.3d)$$

$$a_{QV} = -\frac{i}{\hbar} \int_{-\infty}^{t} dt' \langle [\hat{Q}(t), \hat{V}(t')] \rangle. \tag{2.3e}$$

where $\langle \langle \hat{A}\hat{B} \rangle \rangle = \langle (\hat{A} - \langle \hat{A} \rangle) \rangle \langle (\hat{B} - \langle \hat{B} \rangle) \rangle$ for any pair of operators \hat{A}, \hat{B} .

These four quantities define the essential characteristics of the measurement process and have the following physical meaning. S_{QQ} is the noise of the input variable. It is responsible for the inevitable measurement back action and associated decoherence of the qubit. S_{VV} is the output variable noise: it determines the time required to measure the detector outcome with a given accuracy. The cross noise S_{QV} quantifies possible correlations of these two noises. The response function a_{VQ} determines the detector gain: it is the susceptibility relating the detector output to the qubit variable measured, $\langle \hat{V} \rangle = a_{VQ} \langle \hat{\mathcal{O}} \rangle$. The response function a_{QV} is correspondingly the reverse gain of the detector: it gives the change of the qubit variable proportional to the detector reading. Conforming to the assumption of slow qubit dynamics, the noises are white and responses are instant.

The values of these noises and responses are restricted by a Cauchy-Schwartz inequality, [9]

$$S_{QQ}S_{VV} - |S_{QV}|^2 \ge \frac{\hbar^2}{4} |a_{VQ} - a_{QV}|^2.$$
 (2.4)

For a simple system like a single qubit it is natural to make the measured operator dimensionless, with eigenvalues of the order of one, or, even better, ± 1 . With this, one can define and relate the dephasing rate $2\gamma = 2S_{QQ}/\hbar^2$ and the acquisition time $t_a \equiv 4S_{VV}/\left|a_{VQ}\right|^2$ required to measure the variable with $\mathscr O$ with a relative accuracy $\simeq 1$. If one further assumes the direct gain to be much larger than the reverse gain, $a_{VQ} \gg a_{QV}$, it is implied by the central equation of [9], Eq. (2.8),

$$\gamma t_a \ge 1 \tag{2.5}$$

This figure of merit shows that one cannot measure a quantum system without dephasing it.

The statistics of the detector variable \hat{V} can be evaluated with introducing a counting field $\chi(t)$ coupled to the output variable \hat{V} . This field plays the role of the parameter in the generating function $C(\chi(t))$ of the probability distribution of the detector readings V(t).

This generating function is computed in the extended Keldysh scheme [25] where the evolution of the "ket" and "bra" wave functions is governed by different Hamiltonians, \hat{H}^+ and \hat{H}^- respectively. The extra term describing interaction with the counting field reads $\hat{H}^{\pm} = \hat{H} \pm \hbar \chi(t) \hat{V}(t)/2$. The generating function has then the form

$$C(\{\chi(t)\}) = \operatorname{Tr}_q(\hat{\rho}(\{\chi(t)\})), \tag{2.6}$$

 $\hat{\rho}$ being a quasi-density matrix of the qubit in the end of evolution,

$$\hat{\rho}(\chi;t) = \text{Tr}_d \left(\overrightarrow{T} e^{-i/\hbar \int dt \hat{H}^-} \hat{\rho}(0) \overleftarrow{T} e^{+i/\hbar \int dt \hat{H}^+} \right). \tag{2.7}$$

Here, $\operatorname{Tr}_q(\cdots)$ and $\operatorname{Tr}_d(\cdots)$ denote the trace over qubit and detector variables, respectively, and $\overrightarrow{T}(T)$ denotes time (reversed) ordering in evolution exponents. $\hat{\rho}(0)$ is the

initial density matrix for both qubit and detector systems.

Assuming white noises and instant responses, one can derive an evolution Blochmaster equation for the quasi-density matrix that is local in time, like Eq. (13) in [6]. For the simplest setup, under assumption of a single coupling operator $\hat{\mathcal{O}}$ it reads:

$$\frac{\partial \hat{\rho}}{\partial t} = -\frac{i}{\hbar} [\hat{H}_q, \hat{\rho}] - \frac{S_{QQ}}{\hbar^2} \mathscr{D}[\hat{\mathcal{O}}] \hat{\rho} - \frac{\chi^2(t)}{2} S_{VV} \hat{\rho}
- \frac{S_{QV}}{\hbar} \chi(t) [\hat{\rho}, \hat{\mathcal{O}}] + \frac{i a_{VQ} \chi(t)}{2} [\hat{\rho}, \hat{\mathcal{O}}]_+.$$
(2.8)

Here, [,] and [,]₊ refer to commutator and anti-commutator operations respectively and $\mathcal{D}[\hat{A}]\hat{\rho} \equiv \left(\frac{1}{2}[\hat{A}^{\dagger}\hat{A},\hat{\rho}]_{+} - \hat{A}\hat{\rho}\hat{A}^{\dagger}\right)$. Here we have also assumed $a_{VQ} \gg a_{QV}$, a general condition for a good amplifier. A single coupling operator is an idealization, in a more realistic situation, the quantum system is also coupled to the environment with other degrees of freedom not related to the equation, this is manifested as intrinsic relaxation and decoherence. This modifies the above equation.

We give the concrete form of this equation for the experimental situation of [13]. There is a qubit with two levels split in z-direction under conditions of strong resonant drive that compensates the splitting of the qubit levels. The effective Hamiltonian reads

$$\hat{H}_q = \frac{\hbar}{2} \Omega \hat{\sigma}_x + \frac{\hbar}{2} \Delta \hat{\sigma}_z, \tag{2.9}$$

 Ω being the Rabi frequency proportional to the amplitude of the resonant drive, and Δ being the detuning of the drive frequency from the qubit energy splitting. The interaction with the environment induces decoherence, excitation and relaxation of the qubit, with the rates $\gamma_d, \gamma_\uparrow, \gamma_\downarrow$ respectively. The measured quantity is the amplitude of the irradiation emitted from the qubit, so $\mathcal O$ is convenient to choose to be either σ_x or σ_y . With this, the equation reads

$$\frac{\partial \hat{\rho}}{\partial t} = -\frac{i}{\hbar} [\hat{H}_{q}, \hat{\rho}] - \gamma_{d} \mathcal{D}[\hat{\sigma}_{z}] \hat{\rho} - \gamma_{\uparrow} \mathcal{D}[\hat{\sigma}_{+}] \hat{\rho}
- \gamma_{\downarrow} \mathcal{D}[\hat{\sigma}_{-}] \hat{\rho} - \frac{S_{QV}}{\hbar} \chi(t) [\hat{\rho}, \hat{\mathcal{O}}]
+ \frac{i a_{VQ} \chi(t)}{2} [\hat{\rho}, \hat{\mathcal{O}}]_{+} - \frac{\chi^{2}(t)}{2} S_{VV} \hat{\rho},$$
(2.10)

 $\hat{\sigma}_+$ ($\hat{\sigma}_-$) being the rising and lowering operators of the qubit, and $\hat{\sigma}_z = |e\rangle\langle e| - |g\rangle\langle g|$ the standard Pauli operator.

The rates and noises are restricted by the following Cauchy-Schwartz inequality: $\frac{1}{4} \left(\gamma_{\uparrow} + \gamma_{\downarrow} \right) S_{VV} - \left| S_{QV} \right|^2 \ge \frac{\hbar^2}{4} \left| a_{VQ} \right|^2$. All the parameters entering the equation can be characterized from experimental measurements. We provide an example of concrete values in Section 2.5.

We will concentrate on a single measurement during a time interval $(0,\mathcal{T})$. To define an output of such measurement, we accumulate the time-dependent detector output during this time interval and normalize it by the same interval, $V = \frac{1}{\mathcal{T}} \int_0^{\mathcal{T}} V(t') dt'$. The counting field $\chi(t)$ corresponding to this output is conveniently constant, $\chi(t) = \chi$ on the

time interval and 0 otherwise. Our goal is to evaluate the probability distribution P(V) of the measurement results, conditioned to an initial qubit state given by $\hat{\rho}(0)$, and to a post-selection of the qubit in a specific state $|\Psi\rangle$ at the time moment \mathcal{F} . This involves the projection on the state $|\Psi\rangle$, represented by the projection operator $\hat{P}_{\Psi} = |\Psi\rangle \langle \Psi|$.

The probability distribution of the detector outcomes with no regard for the final qubit state can be computed from the generating function defined by Eq. (2.6),

$$P(V) = \frac{\mathcal{T}}{2\pi} \int d\chi e^{-i\chi V \mathcal{T}} C(\chi; \mathcal{T}). \tag{2.11}$$

The joint statistics are extracted from the quasi-density matrix $\hat{\rho}(\chi; \mathcal{F})$ at the end of the interval.

Upon the post-selection, the quasi-density matrix is projected on the final state measured, $\hat{P}_{\Psi}\hat{\rho}(\chi;\mathcal{F})$, so the conditioned generating function of the detector outcomes reads as

$$\tilde{C}(\chi;\mathcal{T}) = \frac{\operatorname{Tr}_{q}(\hat{P}_{\Psi}\hat{\rho}(\chi;\mathcal{T}))}{\operatorname{Tr}_{q}(\hat{P}_{\Psi}\hat{\rho}(\chi=0;\mathcal{T}))}.$$
(2.12)

where the proper normalization is included.

This is the second central equation in our method. Together with Eq. (2.8) it permits an efficient evaluation of the conditioned probability distributions as the Fourier transform of this generating function.

Sometimes it is convenient to normalize the time-integrated output introducing $\mathcal{O} = V/a_{VQ}$ that immediately corresponds to the eigenvalues of $\hat{\mathcal{O}}$ (We stress that \mathcal{O}) are coming from the averaging of an environmental operator rather than $\hat{\mathcal{O}}$.

In this Article, we will concentrate on the distributions of a single variable. For completeness, we mention that the approach can be extended to joint statistics of simultaneous measurement of two non-commuting observables, e.g. $\hat{\sigma}_x$ and $\hat{\sigma}_y$. For the case of identical but independent detectors with associated output variables \hat{V}_x , \hat{V}_y and counting fields $\chi_x(t)$, $\chi_y(t)$ the corresponding equation reads(i labels $\{x,y\}$)

$$\frac{\partial \hat{\rho}}{\partial t} = -\frac{i}{\hbar} [\hat{H}_q, \hat{\rho}] - \sum_i \frac{S_{QQ}(i)}{\hbar^2} \mathcal{D}[\hat{\sigma}_i] \hat{\rho}
- \sum_i \left(\frac{S_{QV}}{\hbar} \chi_i(t) [\hat{\rho}, \hat{\sigma}_i] + \frac{i a_{VQ} \chi_i(t)}{2} [\hat{\rho}, \hat{\sigma}_i]_+ - \frac{\chi_i^2(t)}{2} S_{VV} \hat{\rho} \right).$$
(2.13)

for the situation where the qubit decoherence is due to the detector back actions only. The parameters are restricted by inequalities similar to Eq. (2.4) for each set of noise and response functions corresponding to a given detector.

The form of this equation that can account for the realistic experimental situation [13] is similar to Eq. (2.10):

$$\frac{\hat{\sigma}\hat{\rho}}{\hat{\sigma}t} = -\frac{i}{\hbar}[\hat{H}_{q},\hat{\rho}] - \gamma_{d}\mathcal{D}[\hat{\sigma}_{z}]\hat{\rho} - \gamma_{\uparrow}\mathcal{D}[\hat{\sigma}_{+}]\hat{\rho}
- \gamma_{\downarrow}\mathcal{D}[\hat{\sigma}_{-}]\hat{\rho} - \sum_{i} \frac{S_{QV}^{(i)}}{\hbar} \chi_{i}(t)[\hat{\rho},\hat{\sigma}_{i}]
+ \sum_{i} \frac{ia_{VQ}^{(i)} \chi_{i}(t)}{2}[\hat{\rho},\hat{\sigma}_{i}]_{+} - \sum_{i} \frac{\chi_{i}^{2}(t)}{2} S_{VV}^{(i)}\hat{\rho},$$
(2.14)

where i = x, y and we account for detector-dependent noises and response functions. Two inequalities put restrictions on the parameters involved:

$$\frac{1}{4} \left(\gamma_{\uparrow} + \gamma_{\downarrow} \right) S_{VV}^{(x)} - \left| S_{QV}^{(x)} \right|^2 \ge \frac{\hbar^2}{4} \left| a_{VQ}^{(x)} \right|^2, \tag{2.15a}$$

$$\frac{1}{4} \left(\gamma_{\uparrow} + \gamma_{\downarrow} \right) S_{VV}^{(y)} - \left| S_{QV}^{(y)} \right|^2 \ge \frac{\hbar^2}{4} \left| a_{VQ}^{(y)} \right|^2. \tag{2.15b}$$

Here, we have assumed an ideal and fast post-selection so that the system measured is projected on a known pure state $|\Psi\rangle$. This is the case of the experimental setup [13]. In reality, there can be errors in the post-selection. We note that such errors can also be accounted for in the formalism outlined. To this end, one replaces the projection operator \hat{P}_{Ψ} with a density matrix-like Hermitian operator $\hat{\rho}_f$ satisfying $\text{Tr}[\hat{\rho}_f] = 1$. For instance, if after a faulty projection measurement with the result "1" the system is in a orthogonal state $|\Psi_2\rangle$ with probability p_e , the corresponding $\hat{\rho}_f$ reads

$$\hat{\rho}_f = (1 - p_e)|\Psi_1\rangle\langle\Psi_1| + p_e|\Psi_2\rangle\langle\Psi_2| \tag{2.16}$$

2.3. Half-quantization: a straightforward case

The outcomes of an ideal projective measurement of a quantum variable $\hat{\mathcal{O}}$ are confined to the eigenvalues \mathcal{O}_i of the corresponding operator. If a CWML approximates well this ideal situation, one expects the distribution of outcomes to peak near \mathcal{O}_i , and it is indeed so. In this Section, we argue that if the measurement outcomes are conditioned on a final state, the distribution also has peculiarities at half-sums $(\mathcal{O}_i + \mathcal{O}_j)/2$ of the eigenvalues. We prove first this counter-intuitive statement for a restricting limiting case where the measurement interval \mathcal{T} is much smaller than the typical time scales of the system dynamics. The results are summarized in Eq. 2.20. The resulting distributions may formally correspond to negative probabilities in the limit of vanishing overlap between initial and final state. To correct for this, and to extend the limits of validity to larger time intervals, we concentrate further on a specific but constructive case of non-demolition measurement. With this, we investigate the influence of decoherence on half-quantization. The results are given by Eq. 2.23.

To start, we take the measurement interval \mathcal{T} to be much smaller than typical time scales of the quantum system dynamics. This immediately implies that the accuracy of the measurement will be too low to make it practically useful. However, the resulting distribution comes out of a straightforward calculation, since the state of the quantum system does not have time to change significantly during the measurement.

In Eq. (2.8) we may then neglect all terms describing the dynamics and containing no $\chi(t)$ Let us also assume no correlation between the noises of the input and output variables of the detector, $S_{OV} = 0$.

With this, Eq. (2.8) can be simplified to the following form

$$\frac{\partial \hat{\rho}}{\partial t} = -\frac{\chi^2(t)}{2} S_{VV} \hat{\rho} + \frac{i a_{VQ} \chi(t)}{2} [\hat{\rho}, \hat{\mathcal{O}}]_+. \tag{2.17}$$

Let us concentrate on a piecewise-constant $\chi(t) \equiv \chi \Theta(t) \Theta(\mathcal{T} - t)$ corresponding to the accumulation of the signal during the measurement interval. We take $\hat{\rho}(\chi;0) = \hat{\rho}(0)$ as

the initial condition. After the time interval of the measurement \mathcal{F} , the quasi-density matrix becomes

$$\hat{\rho}(\chi;\mathcal{T}) = e^{-\frac{S_{VV}}{2}\chi^2\mathcal{T}} e^{i\frac{a_{VQ}}{2}\chi\mathcal{T}\hat{\mathcal{O}}} \hat{\rho}(0) e^{i\frac{a_{VQ}}{2}\chi\mathcal{T}\hat{\mathcal{O}}}.$$
 (2.18)

The generating function of the outcome distribution is given by Eq. (2.12) and involves the projection \hat{P}_{Ψ} on the final state $|\Psi\rangle$. The calculations are straightforward in the basis of the eigenstates of the operator $\hat{\mathcal{O}}$, $\hat{\mathcal{O}}|i\rangle=\mathcal{O}_i|i\rangle$. It is also convenient to normalize the output variable on the value of $\hat{\mathcal{O}}$ introducing a rescaled variable $\mathcal{O}\equiv V/a_{VQ}$. The resulting distribution is a linear superposition of shifted normal distributions

$$g(x) = \frac{1}{\sigma\sqrt{2\pi}} \exp\left(-\frac{x^2}{2\sigma^2}\right) \tag{2.19}$$

with the same variance $\sigma^2 = S_{VV}/(\mathcal{T}a_{VO}^2) = t_a/4\mathcal{T}$,

$$\tilde{P}(\mathcal{O}) = \sum_{i} W_{ii} g(\mathcal{O} - \mathcal{O}_i) +$$

$$\sum_{i \neq j} W_{ij} g\left(\mathcal{O} - \frac{\mathcal{O}_i + \mathcal{O}_j}{2}\right)$$
(2.20)

and the weights W_{ij} given by

$$W_{ij} = \frac{\Psi_j \Psi_i^* \rho_{ij}^{(0)}}{\langle \Psi | \rho^{(0)} | \Psi \rangle}; \sum_{i,j} W_{ij} = 1.$$
 (2.21)

Let us discuss this result. The terms of the first group are normal distributions centered at the eigenvalues of \mathcal{O}_i . The coefficients in front of these terms are proportional to the product of the initial probability to be in the state i, $\rho(0)_{ij}$, and the probability to be found in final state after being in the state i, $|\Psi_i|^2$. If there would be no quantum mechanics, the system on its way from initial to final state should definitely pass one of the eigenstates of $\widehat{\mathcal{O}}$ shifting the measurement output by the corresponding eigenvalue. The sum of the probabilities W_{ii} would be 1. In fact, it is not 1: owing to quantum interference, the system does not have to pass a definite state i. One can say that "bras" and "kets" may pass the different states, and this shifts the output by a half-sum of the corresponding eigenvalues. These interference contributions disappear if there is no postselection in the final state. Indeed, summing W_{ij} over a complete basis of possible final states $|\Psi\rangle$ gives zero. These coefficients also disappear in case of diagonal $\hat{\rho}^{(0)}$ Although the form (2.20) suggests that real values $W_{i,j} + W_{j,i}$ could be interpreted as "probabilities" of "half-quantized" outcomes, this does not work since these values can be negative as well as positive, and the contributions centered at half-quantized values can be peaks as well as dips. This is typical for an interference effect. The double peak structure of the distribution has been discussed earlier in the context of CWLM [3, 4, 6, 29] The interpretation in terms of half-quantization is an innovation of the present article.

A double-peak probability distribution has been predicted in the context of post-selected measurements [30, 31]. While this effect is also based on interference, it is

clearly distinct from the half-quantization considered here since it is observed for an operator with continuous spectrum and in fact, in distinction from the effect described here, permits a classical interpretation [31]. The half-quantization also does not bear any resemblance with the 3-box paradox [32] since the latter involves a third quantum state absent in our setup.

Nevertheless, the interference signatures can be revealed by a close inspection of the probability distribution of the outcomes of the conditioned measurement. We notice that the limit of small $\mathcal T$ we presently concentrate on is not favourable for such inspection since the peaks (or dips) are hardly separated, $\mathcal O_i \ll \sqrt{\sigma}$, so that $P(\mathcal O) \approx g(\mathcal O)$, that is, hardly depends on the quantum system measured. To enhance the effect, one would increase $\mathcal T$. However, at sufficiently large $\mathcal T$ the quantum system would relax to equilibrium, this suppresses the interference effects. Numerical calculations presented in Sections 2.5 and 2.6 show that the interference contributions become quite pronounced in the case of intermediate $\mathcal T$.

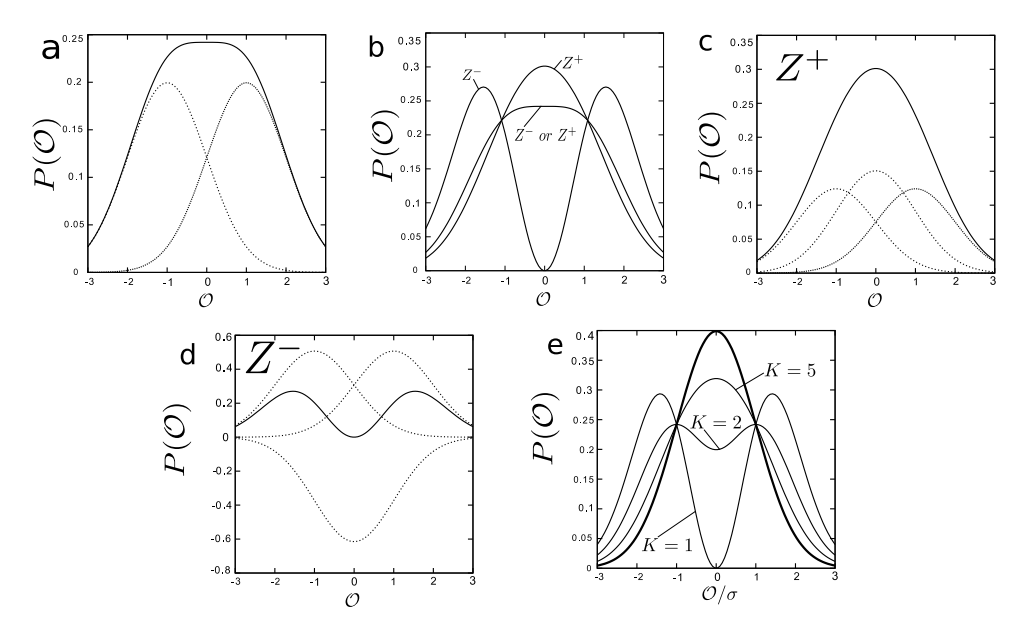


Figure 2.1: Probability distributions of CWLM outcomes of $\hat{\sigma}_x$ for relatively small duration $\mathcal{F}=0.5\Gamma_d$. The qubit is initialized in the Z^+ state. a. The distribution without post-selection consists of the two marginally separated Gaussian peaks shown by dotted lines. b. Conditioned distributions for Z^+ and Z^- and the distribution without post-selection. c.-d. Decomposition of the conditioned distributions into Gaussians (dotted curves). The Gaussians centered at 0 manifest the half-quantization. e. The conditioned distribution for zero overlap (Eq. 2.24) in the limit of small $\mathcal F$ for different K. K=1 corresponds to ideal detector.

In this Section, we mention a special case where the interference effects become enhanced and significant even in the limit $\mathcal{T} \to 0$. This is the case of a small overlap between the initial state $\hat{\rho}(0)$ and the post-selected final state, $|\Psi\rangle$, $\langle\Psi|\hat{\rho}(0)|\Psi\rangle \to 0$. The coefficients W_{ij} diverge upon approaching this limit, and Eq. 2.20 becomes invalid giving a negative probability density. To consider the case properly, we need to regularize Eq. 2.18 taking into account the dephasing which comes at least from the detector

back-action. The simplest way to provide such regularization is to include dephasing produced by interaction with the same operator $\hat{\mathcal{O}}$. The resulting equation reads

$$\frac{\partial \hat{\rho}}{\partial t} = -\frac{\chi^2(t)}{2} S_{VV} \hat{\rho} + \frac{i a_{VQ} \chi(t)}{2} [\hat{\rho}, \hat{\mathcal{O}}]_+ - \gamma \mathcal{D}[\hat{\mathcal{O}}] \hat{\rho}. \tag{2.22}$$

It looks we have disregarded the Hamiltonian dynamics in Eq. 2.22. This does not seem consistent since usually $H_q\gg\hbar\gamma$, this provides a common separation between the fast time-scales of Hamiltonian dynamics and longer time-scales of the decoherence and relaxation. We note that we do not have to disregard it in an important case of non-demolition measurement when \hat{H}_q and $\hat{\mathcal{O}}$ commute. In this case, the only effect of the Hamiltonian dynamics is to provide time-dependent phase factors for non-diagonal elements of the density matrix. These trivial phase factors can be compensated by a proper rotation of the final state and the Hamiltonian dynamics can be gauged away from Eq. 2.22. We address the relevant Hamiltonian dynamics in the next Section.

By virtue of the Cauchy-Schwartz inequality (2.4), $\gamma \geq a_{QV}^2/4S_{VV}$. Therefore it is convenient to characterize the dephasing rate γ with dimensionless $K \equiv 4\gamma S_{VV}/a_{QV}^2 = \gamma t_a$, $K \geq 1$, that characterizes the quality of the detector.

The equation is easily solved in the basis of eigenvalues of $\hat{\mathcal{O}}$. In comparison with Eq. 2.18, each non-diagonal element ρ_{ij} of the quasi-density matrix acquires an extra time-dependent suppression factor $\exp\left(-\gamma t \frac{(\mathcal{O}_i - \mathcal{O}_j)^2}{2}\right)$. With this, the probability distribution is given by Eq. 2.20 with modified coefficients $W_{ij} \to \tilde{W}_{ij}$,

$$\tilde{W}_{ij} \equiv \frac{\Psi_j \Psi_i^* \rho_{ij} e^{-\gamma \mathcal{F} \frac{(\theta_i - \theta_j)^2}{2}}}{\tilde{W}}; \qquad (2.23)$$

$$\tilde{W} \equiv \sum_{i,j} \Psi_j \Psi_i^* \rho_{ij} e^{-\gamma \mathcal{F} \frac{(\theta_i - \theta_j)^2}{2}}$$

At any non-zero overlap, $P(\mathcal{O}) \to g(\mathcal{O})$ in the limit of $\mathcal{T} \to 0$. Let us concentrate on a special case of zero overlap, $\langle \Psi | \hat{\rho}^{(0)} | \Psi \rangle = 0$, and let us note that this also implies $\hat{\rho}^{(0)} | \Psi \rangle = 0$ by virtue of positivity of the density matrix. In the limit of $\mathcal{T} \to 0$ the chance to find the system in the final state vanishes, $\tilde{W} \approx \gamma \mathcal{T} \langle \Psi | \hat{\mathcal{O}} \hat{\rho}^{(0)} \hat{\mathcal{O}} | \Psi \rangle$. This divergence should be compensated by the terms $\propto \mathcal{T}$ that come from expansion of $g(\mathcal{O} - (\mathcal{O}_i + \mathcal{O}_j)/2)$ up to the second order in \mathcal{O}_i as well as \tilde{W}_{ij} . The resulting distribution of the measurement outcomes for these rare events differs essentially from the normal one,

$$P(\mathcal{O}) = \left(1 + \frac{(\mathcal{O}/\sigma)^2 - 1}{K}\right) g(\mathcal{O}) \neq g(\mathcal{O})$$
 (2.24)

For an ideal detector, K = 1, the probability even vanishes at $\mathcal{O} = 0$. For bigger decoherence exceeding the minimal one, $K \gg 1$, the interference term vanishes and $P(\mathcal{O}) \approx g(\mathcal{O})$.

We illustrate the content of this Section with some simple plots (Fig. 2.1). We consider a qubit that is initially prepared in Z^+ state, $\hat{\sigma}_z|Z^+\rangle = |Z^+\rangle$. The measurement accesses the x-component of the qubit spin, $\mathcal{O} = \hat{\sigma}_x$. After the measurement, the qubit is post-selected in either Z^+ or Z^- state. As it follows from the preceding discussion,

we expect the probability distribution of the outputs to be composed of the Gaussians centered at ± 1 , and also at the half sum of the eigenvalues, that is, at 0.

For the first four plots, we choose a relatively big $\mathcal{T}=0.5\gamma^{-1}$. Although this choice is contrary to our assumptions, it permits an easy visual resolution of the Gaussian peaks. We assume ideal detector K=1 and use Eq. 2.22 to evaluate the distributions. The distribution of the outcomes with no post-selection (Fig. 2.1a.) is composed from two Gaussian peaks centered at ± 1 that are hardly separated. The post-selected distributions differ much from each other and the original one (Fig. 2.1b.) The distribution for Z^- gives well-separated peaks while a single peak is seen in the distribution for Z^+ . This is due to the negative or positive half-sum contribution as illustrated in Fig. 2.1c. and.

The Fig. 2.1e. demonstrates the essential change of the conditioned distribution function for zero overlap. The distribution for ideal detector reaches zero, and approaches normal distribution upon increasing K.

To investigate in more detail the manifestations of the interference effects at longer time intervals $\approx t_a$, γ^{-1} and in experimental conditions, in Section 2.5 we numerically solve the evolution equations and compute the conditioned probability distributions. For this work, we concentrate on a single qubit.

2.4. SUDDEN JUMP: A SIMPLE CONSIDERATION

Let us now change the situation and consider the measurement of a variable that does not commute with the Hamiltonian. To simplify, we consider very small $\mathcal T$ such that the change of density matrix due to Hamiltonian dynamics is small. This is a more severe limitation than that used in the previous Section where $\mathcal T$ was only supposed to be smaller than the decoherence rate. Generally, this time interval is too small to measure anything and we expect the distribution to be close to $g(\mathcal O)$ thus to have a large spread. There is, however, an exceptional situation of zero overlap where after the measurement the state is projected on $|\Psi\rangle$ that is precisely orthogonal to the initial state $|i\rangle$, $\langle\Psi|i\rangle=0$. Let us concentrate on this situation and demonstrate a peculiarity of the output distribution which is best described as a *sudden jump* of the integrated output.

To give a clear picture, we first treat the situation completely disregarding the decoherence/relaxation terms, and take into account the Hamiltonian dynamics only. This seems relevant at such small \mathcal{F} . The general result is given by Eq. 2.26 while a constructive case is given by 2.27. This gives a sudden jump of cumulants while the attempt to derive the distribution results in a negative probability in an interval of outputs that increases with decreasing \mathcal{F} . To improve on this, we will sophisticate the treatment by including the decoherence. We reveal that the decoherence becomes important at very small time intervals $\mathcal{F} \ll (\Omega^2 t_a)^{-1}$, that can be interpreted as a finite but small duration of the sudden jump. The resulting probability distribution is given by Eq. 2.34 and is positive at any \mathcal{F} .

To start with, we disregard relaxation/decoherence terms in the evolution equation which seems relevant for such small \mathcal{T} and owing to orthogonality, the projected $\rho(\chi)$ vanishes at $\mathcal{T} \to 0$ and is determined by the first-order corrections to bra- and ket wave functions.

$$\operatorname{Tr}(\hat{P}_{\Psi}\hat{\rho}(\chi)) = \hbar^{-2} \mathcal{F}^{2} \langle \Psi | \hat{H}_{a}^{+} | i \rangle \langle i | \hat{H}_{a}^{-} | \Psi \rangle e^{-\chi^{2} \mathcal{F} S_{VV}/2}$$
(2.25)

Here $H^{\pm} = H_q \pm \hbar \chi a_{VQ} \hat{\mathcal{O}}$.

The small factor \mathcal{T}^2 cancels upon normalization in Eq. 2.12 so that the generating function of the conditioned output reads

$$\tilde{C}(\chi;\mathcal{T}) = \frac{\langle \Psi | \hat{H}_q^+ | i \rangle \langle i | \hat{H}_q^- | \Psi \rangle}{|\langle \Psi | \hat{H}_q | i \rangle|^2} e^{-\chi^2 \mathcal{T} S_{VV}/2}$$
(2.26)

We note that $\tilde{C}(\chi;\mathcal{T}\to 0)\neq 1$. Since the derivatives of $\ln \tilde{C}$ at $\chi\to 0$ are related to the cumulants κ_n of the distribution of the integrated output $\int_0^{\mathcal{T}} dt \hat{V}(t)$. This implies that the cumulants of the distribution of the integrated output do not vanish in the limit of short time interval: rather, there is a *sudden jump* of the integrated output not depending on the duration of the measurement. The jump occurs for the averaged output as well as for all cumulants. This is very counter-intuitive for a CWLM situation. In this case, one may expect that the integrated output in this limit is dominated by the detector noise, so that $\int_0^{\mathcal{T}} dt \hat{V}(t) \simeq \mathcal{T}^{1/2}$, $\kappa_n \simeq \mathcal{T}^{n/2}$, and thus vanishes at $\mathcal{T}\to 0$.

To see this in more detail, let us turn to a concrete example. We consider a situation corresponding to [13]: a qubit with the Hamiltonian $\hat{H}_q = \frac{\hbar}{2}\Omega\hat{\sigma}_x$. The initial and projected states are Z^+ and Z^- , respectively, and we measure the projection of the qubit on Y-axis, $\hat{\mathcal{O}} = \hat{\sigma}_y$. In this case,

$$\tilde{C}(\chi;\mathcal{T}) = \left(1 - \frac{i\chi a_{VQ}}{\Omega}\right)^2 e^{-\chi^2 \mathcal{T} S_{VV}/2}$$
(2.27)

In the limit $\mathcal{T} \to 0$ we obtain for the cumulants:

$$\kappa_n = \frac{\partial^n}{\partial (i\chi)^n} \ln\left(1 - \frac{i\chi a_{VQ}}{\Omega}\right)^2 = 2(-1)^n \left(\frac{a_{VQ}}{\Omega}\right)^n (n-1)! \tag{2.28}$$

We see a sudden jump in the cumulants of the time-integrated output.

The average value of the output (κ_1) is given by

$$a_{VQ}^{-1} \int_{0}^{\mathcal{T}} dt \langle \hat{V}(t) \rangle = -\frac{2}{\Omega}; \bar{\mathcal{O}} = -\frac{2}{\Omega \mathcal{T}}.$$
 (2.29)

This corresponds to the time-averaged output $\propto \mathcal{F}^{-1}$ that can exceed by far the expected values of a projective measurement, ± 1 . Such anomalously big outputs are naturally associated with the weak values [17]. Indeed, one can relate the above result with weak value conform to the definition [17] if one takes into account the evolution of the quantum state during the measurement [33]. However, we need to stress that the full distribution of the outputs cannot be obtained with the traditional weak value formalism and so far has not been obtained with its extensions [22–24] for continuous measurement. The method outlined here does not explicitly evoke the notion of weak values and provides a more elaborated description of a realistic measurement process.

An attempt to derive from (2.27) the overall distribution of the time-averaged outputs yields

$$P(\mathcal{O}) = \left(1 + \frac{\partial_{\mathcal{O}}}{\Omega \mathcal{F}}\right)^{2} g(\mathcal{O}) = \left(\left(1 - \frac{4\mathcal{O}}{\Omega t_{a}}\right)^{2} - \frac{4}{\Omega^{2} \mathcal{F} t_{a}}\right) g(\mathcal{O}) \tag{2.30}$$

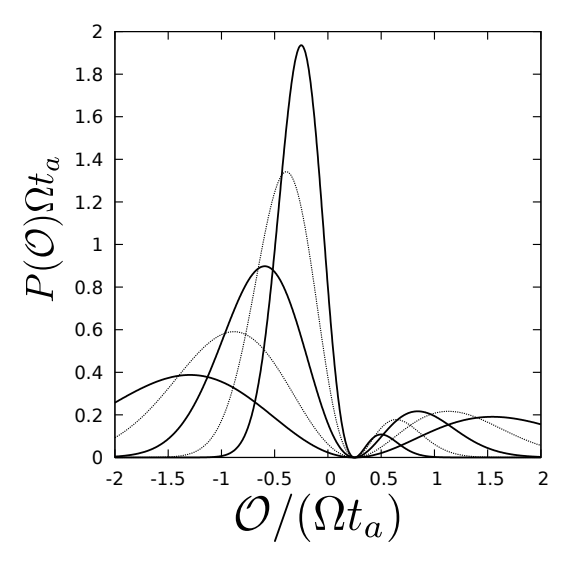


Figure 2.2: Probability distributions of outputs (Eq. 2.34) in the sudden jump regime in case of an ideal detector. The alternating solid-dotted curves correspond to different $\mathcal{F}=(0.25,0.5,1.0,2.0,4.0)(\Omega^2\,t_a)^{-1}$. Each curve consists of two peaks separated by a gap at $\mathcal{O}=\Omega t_a/4$. The curves with bigger \mathcal{F} are sharper, and the peaks become increasingly symmetric upon lowering \mathcal{F} .

There is a problem with this expression: it is negative in an interval of \mathcal{O} , and at sufficiently small $\mathcal{T} \lesssim (\Omega^2 t_a)^{-1}$ this interval encompasses the body of the "distribution". This signals that the current approach must be corrected. As we have seen in the previous Section, such correction most likely requires a proper account of the detector backaction that causes the decoherence of the qubit.

It is unusual to expect a decisive role of decoherence at such small time scales. However, if we take into account the decoherence (second term in the r.h.s. of Eq. $\,2.8$), we obtain

$$\operatorname{Tr}(\hat{P}_{\Psi}\hat{\rho}(\chi)) = \left(\gamma \mathcal{T} + \frac{\mathcal{T}^2}{4} \left(\Omega - i a_{QV} \chi\right)^2\right) e^{-\chi^2 \mathcal{T} S_{VV}/2} \tag{2.31}$$

Here, $\gamma \equiv S_{QQ}/\hbar^2$ is the corresponding decoherence rate. We see that the decoherence term may indeed compete with the term coming from Hamiltonian dynamics at short time intervals. The Physical reason for this is that a decoherence term of this sort induces the relaxation in Z-basis. The relaxation brings the qubit to Z^- faster than the Hamiltonian: The probability to find the system in Z^- is thus proportional to $\mathcal T$ in contrast to the probability $\propto \mathcal T^2$ induced by the Hamiltonian dynamics.

The resulting characteristic function reads

$$\tilde{C}(\chi) = \frac{4\gamma + \mathcal{F}\left(\Omega - i \, a_{QV} \chi\right)^2}{4\gamma + \mathcal{F}\Omega^2} e^{-\chi^2 \mathcal{F} S_{VV}/2}$$
(2.32)

and gives the average output

$$\bar{\mathcal{O}} = -\frac{2\Omega}{4\gamma + \mathcal{F}\Omega^2} \tag{2.33}$$

The value of the average output thus saturates at $-\Omega/2\gamma \ll -1$ in the limit of small $\mathcal{T} \ll \gamma/\Omega^2$. So if the decoherence is taken into account, the change of the output averages is not really sudden. One can regard the small time scale γ/Ω^2 of the saturation as a typical duration of the sudden jump of the time-integrated output.

The probability distribution valid at all time scales $\ll \Omega^{-1}$ is given by

$$P(\mathcal{O}) = \frac{K - 1 + (\mathcal{T}/4t_a)(\Omega t_a - 4\mathcal{O})^2}{K + \mathcal{T}t_a\Omega^2/4}g(\mathcal{O})$$
 (2.34)

where we again introduce the dimensionless $K = \gamma t_a \ge 1$ that characterizes the quality of the detector. The distribution is illustrated in Fig. 2.2 for an ideal detector K = 1 and various \mathcal{T} . In this case, the probability density is zero at $\mathcal{O} = \Omega t_a/4$.

If we compare the distributions (2.24) and (2.34), we see that the results of the previous Section are reproduced in the limit $\Omega \to 0$, as well as in the limit of $\mathcal{T} \ll (\Omega^2 t_a)^{-1}$ if we take $\sigma^2 = t_a/4\mathcal{T}$. The distribution (2.34) thus generalizes (2.24) to the case where the Hamiltonian dynamics are relevant.

To extend the results on larger time intervals $\simeq \Omega$ and on realistic conditions, we numerically solve the evolution equations in Section 2.6 and compute the corresponding conditioned probability distributions.

2.5. Numerical results: long time scales

In Section $\,2.3$, we have presented an analytical solution in the limit of small \mathcal{T} and shown that it remains qualitatively valid for bigger \mathcal{T} , at least in the case of ideal detectors. We will extend these results evaluating the conditioned distributions numerically. We concentrate on longer measurement times where the qubit dynamics become important. We will take into account the effects of decoherence and relaxation, as well as the effects of strong qubit drive or detuning, all being important in experimental situations.

In this Section, we address the distributions of the CWLM outcomes of a single variable at the time scales of the order of coherence/relaxation times and t_a . Generally, one can associate it with the qubit variable $\hat{\mathcal{O}} = \hat{\sigma}_x$. To start with, we assume zero detuning, that is, a qubit Hamiltonian of the form $\hat{H}_q = \frac{\hbar}{2}\Omega\hat{\sigma}_x$. In principle, we are now in the situation of a non-demolition measurement.

To start with, let us assume an idealized situation where all the decoherence is brought by the detector back action and its rate $\propto S_{QQ}$ assumes the minimum value permitted by the inequality ((2.4)). Since $\hat{H}_q = \frac{\hbar}{2}\Omega\hat{\sigma}_x$, the back-action does not interfere with free qubit dynamics causing transitions between the levels. In σ_x representation, the diagonal elements of the density matrix remain unchanged keeping the initial probability to be in X^\pm states while the non-diagonal ones oscillate with frequency Ω and decay with much slower rate $\Gamma_d \ll \Omega$.

If we keep the final state fixed to Z^{\pm} , the interference contribution to the conditioned distributions will exhibit fast oscillations as function of \mathcal{T} with a period $2\pi/\Omega$. It is proficient from both theoretical and experimental considerations to quench these rather trivial oscillations. We achieve this by projecting the qubit after the measurement on the

states $|\bar{Z}^{\pm}\rangle = e^{-i\hat{H}_q\mathcal{T}}|Z^{\pm}\rangle$ thereby correcting for the trivial qubit dynamics. In practice, such correction can be achieved by applying a short pulse rotating the qubit about x-axis right before the post-selection measurement. With this, the conditioned distribution of outcomes changes only at the time scale $t_a \simeq \Gamma_d^{-1}$, that is much longer than Ω^{-1} , and the dynamics are described by Eq. (2.22) with $\hat{\mathcal{O}} = \hat{\sigma}_x$.

In Fig. 2.3, we give the plots of the probability distributions conditioned on \bar{Z}^{\pm} for a series of measurement time intervals \mathcal{T} . We see that (different curves) are shown, for two cases in which the visibility of the interference feature is stronger, the case of equal preparation and post-selection, (a), and the case of orthogonal preparation and post-selection states, (b).

In this ideal situation, even for very small time intervals, the additional knowledge of the post-selection can lead to perfect resolution of the two eigenstates of the qubit variable (Fig. 2.3 (b)). While for small time intervals the middle peak results in less resolution for the opposite choice of post-selected qubit state (Fig. 2.3 (a)), at large time intervals, the detector back action has resulted in a complete decoherence of the qubit state and the interference signature disappears, making both distributions converge to two narrow peaks corresponding to either +X or -X. This exemplifies how the knowledge of the qubit preparation is lost in time due to decoherence.

The fact that we see no difference between the distributions in this limit is a result of a symmetric choice we made with respect to the projections. Indeed, if we project on $\pm X$ instead, the distributions would consist of a single peak positioned at the value of $\mathcal{O}=\pm 1$. Generally, for projections on arbitrary pair of orthogonal superpositions of X and Z, we expect in this limit different peak weights for two different projections. This difference, however, is of trivial origin and has nothing to do with the interference effects of interest. So we have made a symmetric choice to cancel it.

With this, the difference between the two distributions is due to interference only, that is, due to the half-quantized peak described in the previous Section. At smaller \mathcal{T} , the distributions take a very distinct shape: single-peak for that conditioned on +Z, and double-peak for that conditioned on -Z. The half-quantization is dumped on the scale of the decoherence time, so the difference is seen only for $\mathcal{T} < t_a$.

The separation of the distribution onto two peaks in the limit of $\mathcal{T}\gg t_a$ is a signature of the ideal situation of a quantum non-demolition measurement where neither measurement nor any other agent induces the relaxation rates causing the transitions between the qubit states. In this situation, the density matrix efficiently relaxes to its equilibrium value ρ_{eq} at time interval \mathcal{T} , and the distribution of the detector output tends to concentrate on the average value $\langle \mathcal{O} \rangle = \mathrm{Tr}[\hat{\mathcal{O}} \hat{\rho}_{eq}]$ with decreasing width $\simeq \sqrt{t_a/\mathcal{T}}$.

Let us now turn to the analysis of the experimental situation. We use the general evolution equation Eq. (2.10) to compute the distributions and substitute the parameters $\gamma_{\downarrow} = (22.5\mu \text{s})^{-1}$, $\gamma_{\uparrow} = (56\mu \text{s})^{-1}$, $\gamma_{d} = (15.6\mu \text{s})^{-1}$ given in [13]. The acquisition time comes from the measurement rate $2/t_a \approx (92\mu \text{s})^{-1}$. This rate in fluorescence experiments can be characterized by two different methods both based on the estimation of the probability distribution for the integrated homodyne signal conditioned on the state of the qubit, see Appendix F in the supplementary material of [9]. The quality of the measurement setup is thus rather far from ideal, $K = t_a \gamma_d \approx 12$. Nevertheless we predict some measurable interference effects in the outcome distributions.

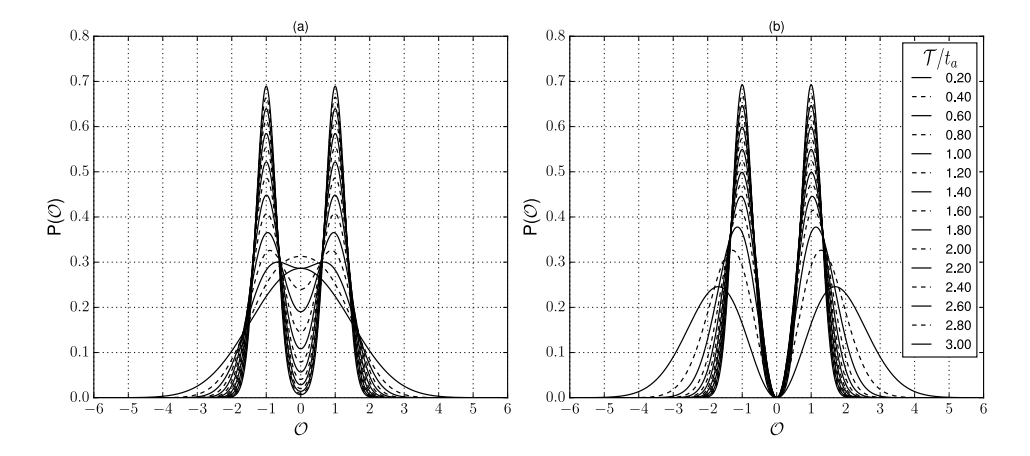


Figure 2.3: Probability distributions of a $\hat{\sigma}_X$ CWLM outcomes for the ideal measurement case for different ratios \mathcal{T}/t_a . The qubit is initially prepared in the +Z state and, after \mathcal{T} , is post-selected either in the +Z state (a) or -Z state (b).

We plot in Fig. 2.4 the results for zero detuning. There is no visible difference between the distributions, so in distinction from Fig. 2.3, we give only a single set of curves in Fig. 2.4. The curves for all $\mathcal T$ look dully Gaussian, no peak separation is visible. This is because of the low quality of the detector: the relaxation to the stationary density matrix $\hat 1/2$ mainly takes place at a time interval shorter than the acquisition time, so most of the time the detector measures this featureless state. As to short $\mathcal T$, the distribution is too wide to manifest the features of the density matrix.

However, there are still observable signatures of interference. To reveal those, we plot in Fig. 2.4 the difference of the probability densities for two projections. We see that at smallest $\mathcal{T}=0.2t_a$ the relative difference achieves 0.1 at $\mathcal{O}\approx 0$ and can be thus revealed from the statistics of several hundreds individual measurements. The shape of the difference suggests that the P_- is pushed on both positive and negative values of \mathcal{O} in comparison with P_+ , in agreement with the previous findings. The decoherence and relaxation quickly diminish the difference upon increasing \mathcal{T} .

At big values of \mathcal{O} , the difference quickly decreases together with the distributions. In this respect, it is instructive to inspect the difference normalized on the sum of the probability densities, $C(\mathcal{O}) \equiv (P_+(\mathcal{O}) - P_-(\mathcal{O}))/(P_+(\mathcal{O}) + P_-(\mathcal{O}))$. This quantity gives the certainty with which one can distinguish two distributions from each other given a reading \mathcal{O} . The values $C = \pm 1$ would imply that the measurement is *certainly* post-selected with $\pm Z$. As we see from Fig. 2.4, the certainty saturates with increasing \mathcal{O} , reaches relatively large values at short \mathcal{T} , and fades away upon increasing \mathcal{T} .

Let us inspect the distributions at non-zero detuning. In this case, there is no reason to expect the $\mathcal{O} \to -\mathcal{O}$ symmetry in the distribution. We illustrate the situation in Fig. 2.5 assuming relatively large detuning $\Delta = 1.7\Omega$. This value is chosen to maximize $\langle \mathcal{O} \rangle$ for the equilibrium density matrix. In the plots of Fig. 2.5a, we see a shift of the distribution maximum that tends to $\langle \mathcal{O} \rangle \approx -0.1$ at $\mathcal{T} \gg t_a$. The value of the shift does depend on \mathcal{T}

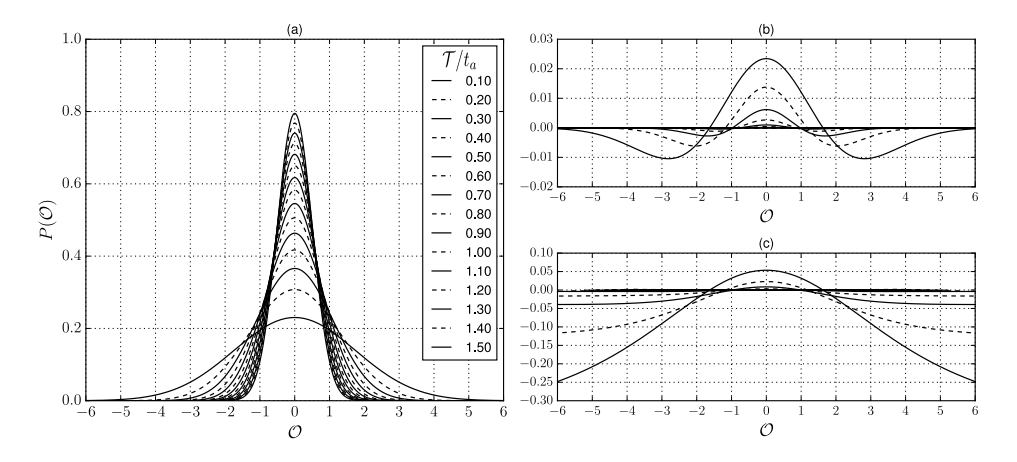


Figure 2.4: Probability distributions of the output $\hat{\sigma}_x$ CWLM for the experimental setup of [13] at various \mathcal{T} . Since the detection is far from ideal, the distributions conditioned on $\pm Z$ are not visually distinguishable, so we plot only one (a). However, the difference of the two distributions that is due to interference (b) is sufficiently large to detect: the relative difference is about 10% for small time intervals (top curve at $\mathcal{O}=0$ in (b))). In (c) we give the difference normalized to the sum of the probabilities. This quantity saturates at large \mathcal{O} .

as well as on the post-selection state.

If we concentrate on the difference of the probability distributions (Fig. 2.5b), we see the same order of magnitude as at zero detuning. However, the difference does not vanish in the limit of big \mathcal{T} . Rather, it is concentrated in an increasingly narrow interval of \mathcal{O} conform to the decreasing width of the distribution. As to the certainty (Fig. 2.5c), it rather quickly converges upon increasing \mathcal{T} to finite and rather big values in a wide interval of \mathcal{O} . This does not imply that the distributions P^{\pm} are different in this limit, since they become concentrated with divergent probability density, and the values of \mathcal{O} with high certainty occur with exponentially low probability, yet the finite limit of $P_+ - P_-$ is worth noting and deserves an explanation.

We can qualitatively explain these features assuming that in this limit the probability distributions are the Gaussians with a shift that depends on the post-selection state and the variance $\sigma^2 = t_a/4\mathcal{T}$, $P_{\pm} = g(\mathcal{O} \pm s_{\pm}(\mathcal{T}))$. In the limit of big \mathcal{T} we expect the difference of the shifts to be proportional $(\mathcal{T})^{-1}$, $s^{\pm} = \langle \mathcal{O} \rangle \pm S(t_a/\mathcal{T})$, $S \simeq 1$. This is because the effect of the post-selection is only felt during a time interval $\simeq \gamma^{-1}$ before the end of measurement, so that, at a fraction of the whole interval that is proportional to $(\mathcal{T})^{-1}$. With this, at $\mathcal{O} \simeq \sigma$ the difference of the probabilities approaches a limit not depending on \mathcal{T}

$$P_{+} - P_{-} = \frac{S}{2} \frac{(\mathcal{O} - \langle \mathcal{O} \rangle)}{\sigma \sqrt{2\pi}} \exp\left(-\frac{(\mathcal{O} - \langle \mathcal{O} \rangle)^{2}}{2\sigma^{2}}\right), \tag{2.35}$$

The maximum difference of probabilities $|P_+ - P_-|_{\text{max}} \approx 1.9S$ is thus achieved at $\mathcal{O} = \langle \mathcal{O} \rangle \pm \sigma$.

As to the certainty, it approaches an alternative limit at $\mathscr{O} \simeq 1 \gg \sigma$ that also does not

depend on \mathcal{T} at $\mathcal{T} \to \infty$

$$C(\mathcal{O}) = \frac{P_{+}(\mathcal{O}) - P_{-}(\mathcal{O})}{P_{+}(\mathcal{O}) + P_{-}(\mathcal{O})} = \tanh\left(4S(\mathcal{O} - \langle \mathcal{O} \rangle)\right)$$
(2.36)

As we see, the certainty reaches ± 1 in the limit of large (exponentially improbable) $|\mathcal{O}| \gg 1$.

The numerical results presented are satisfactory fitted by above expressions with $S \approx 0.04$. However, the fits are not mathematically exact since, for the sake of simplicity, the shifts s^{\pm} have been assumed not to depend on \mathcal{O} while in general they do.

Our results show that the difference of the conditioned distributions can be detected under realistic experimental circumstances.

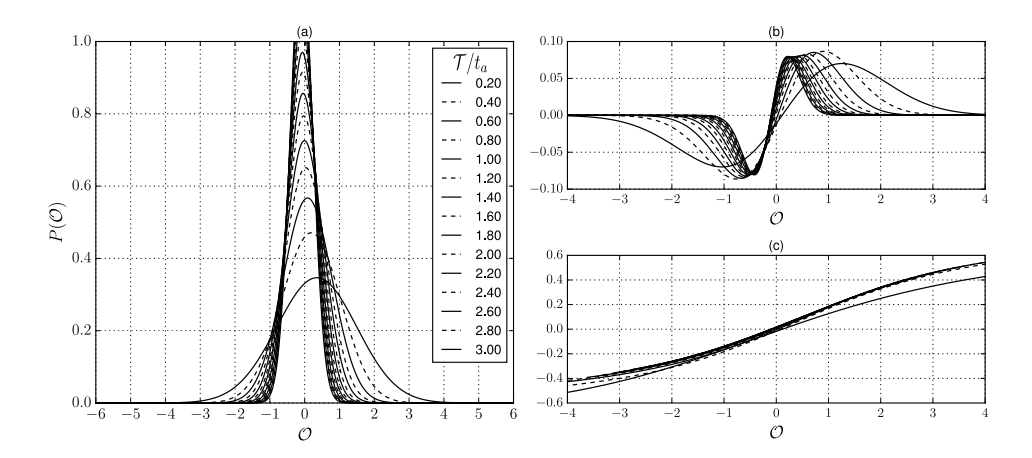


Figure 2.5: Probability distributions of a $\hat{\sigma}_X$ weak measurement for experimental rates. Here a relatively large detuning $\Delta \approx 1.7\Omega$ is introduced in the qubit Hamiltonian. The qubit is prepared in the +Z state and post-selected, after a specific time interval given by each curve, in the +Z state (a) or -Z state (not in the Figure). The difference of this two probabilities appears to remain at rather big time-scales while being remarkably large for small time intervals (wider curves in (b)) compared to the single distribution (a). Again, a good measure of this phenomena is the relative difference, here plotted in (c). Time in units of acquisition time t_a .

Although the interference signature seem to disappear for rather short \mathcal{T} in a realistic experimental regime, the actual measurements are done [13] for time intervals yet smaller than the time scale of qubit relaxation/decoherence. This correspond to the first several choices of short time intervals in Figures 2.3, 2.4, and 2.5 where the interference is still visible.

2.6. NUMERICAL RESULTS: SHORT TIME SCALES

In the previous Section, we have considered the statistics at time-scales $\mathcal{T} \simeq \gamma^{-1}$, t_a extending the analytical results of Section 2.5. In this Section, we will extend the analytical results of Section 2.4. We present numerical solutions for the probability distributions at a larger time-scale $\mathcal{T}\Omega \simeq 1$ of the Hamiltonian dynamics where the decoherence and

2

relaxation does not play an important role. We also consider smaller $\mathcal T$ where the *sudden jump* behaviour is manifested, and yet smaller $\mathcal T$ where the decoherence becomes important again and the time-averaged output saturates to the value $\simeq \Omega/\gamma \gg 1$. We restrict ourselves to the experimental circumstances and use for the computation the Eq. (2.10) with the parameters specified in Section 2.5.

We will concentrate on the conditioned measurement statistics of the variable $\hat{\sigma}_y$, that anticommutes with the qubit Hamiltonian $\hat{H}_q = \frac{\hbar}{2}\Omega\hat{\sigma}_x + \frac{\hbar}{2}\Delta\hat{\sigma}_z$. The qubit is initially prepared in Z^+ state and post-selected in either Z^+ or Z^- . In Fig. 2.6, the probability distributions of the integrated output \mathscr{O} are presented. The upper row plots (Figs. (a) and (b)) are for zero detuning ($\Delta=0$), while the lower row plots (Figs. (c) and (d)) show the corresponding distributions when at the detuning $\Delta\approx 1.7\Omega$ that maximizes $\langle\sigma_x\rangle$. Left and right figures correspond to post-selection in Z^+ and Z^- , respectively.

For unconditioned distributions, the average output is given by $Y(\mathcal{T}) = \frac{1}{\mathcal{T}} \int_0^{\mathcal{T}} dt \langle \Psi(t) | \sigma_y | \Psi(t) \rangle$, where $|\Psi(t)\rangle$ is obtained from Z^+ by Hamiltonian evolution. The function $Y(\mathcal{T})$ is plotted in the insets of the right plots with a solid curve. We would expect the distributions to be shifted with respect to the origin by a value $\mathcal{O} \simeq 1$. This shift would be clearly seen in the plots since the width of the distribution $\simeq \sqrt{t_a \simeq \mathcal{T}} \simeq \sqrt{t_a \Omega}$ is not very big at experimental values of $\Omega t_a \approx 200$. However, the plots on the left are perfectly centered at the origin at any \mathcal{T} . Indeed, the zero average of the distributions conditioned at Z^+ can be proven analytically in the limit of Hamiltonian dynamics. The averages of the distributions conditioned at Z^- (given by dashed curves in the insets of the plots) increase at small \mathcal{T} as \mathcal{T}^{-1} , in agreement with Eq. 2.29. The ratio of this average to conditioned average is just the inverse probability to be found in Z^- , $p_-(\mathcal{T}) = \sin^2(\sqrt{\Omega^2 + \Delta^2})\mathcal{T}/2)/(1 + (\Delta/\Omega)^2)$, $p_- \propto \mathcal{T}^2$ at small \mathcal{T} .

These averages are visually manifested as the shifts of the distributions that are largely Gaussian. We do not see anything resembling a gap in the distribution predicted for an ideal detector (Fig. 2.2). This is explained by relatively low detection efficiency (c.f. Eq. 2.34).

In a separate Fig. 2.7 we present the distributions conditioned on Z^- at yet smaller time-scales of the order of the sudden jump duration (see Eq. 2.33). In this regime, we see the saturation of the average $\bar{\mathcal{O}}$ at a value close to -11 in the limit $\mathcal{T} \to 0$. This gives the upper limit of anomalously big averages under experimental conditions of [13]. The distributions can be well approximated by shifted Gaussians, smaller \mathcal{T} corresponding to wider distributions.

2.7. CONCLUSION

Recent experimental progress has enabled the measurements in course of the conditioned quantum evolution. The average signals have been experimentally studied in [13, 14, 16]. The technical level of these experiments permits the characterization of the complete statistics of the measurement outputs.

In this work, we have developed a proper theoretical formalism based on full counting statistics approach [6, 26] to describe and evaluate these statistics. We illustrate it with several examples and prove that the interesting features in statistics can be seen in

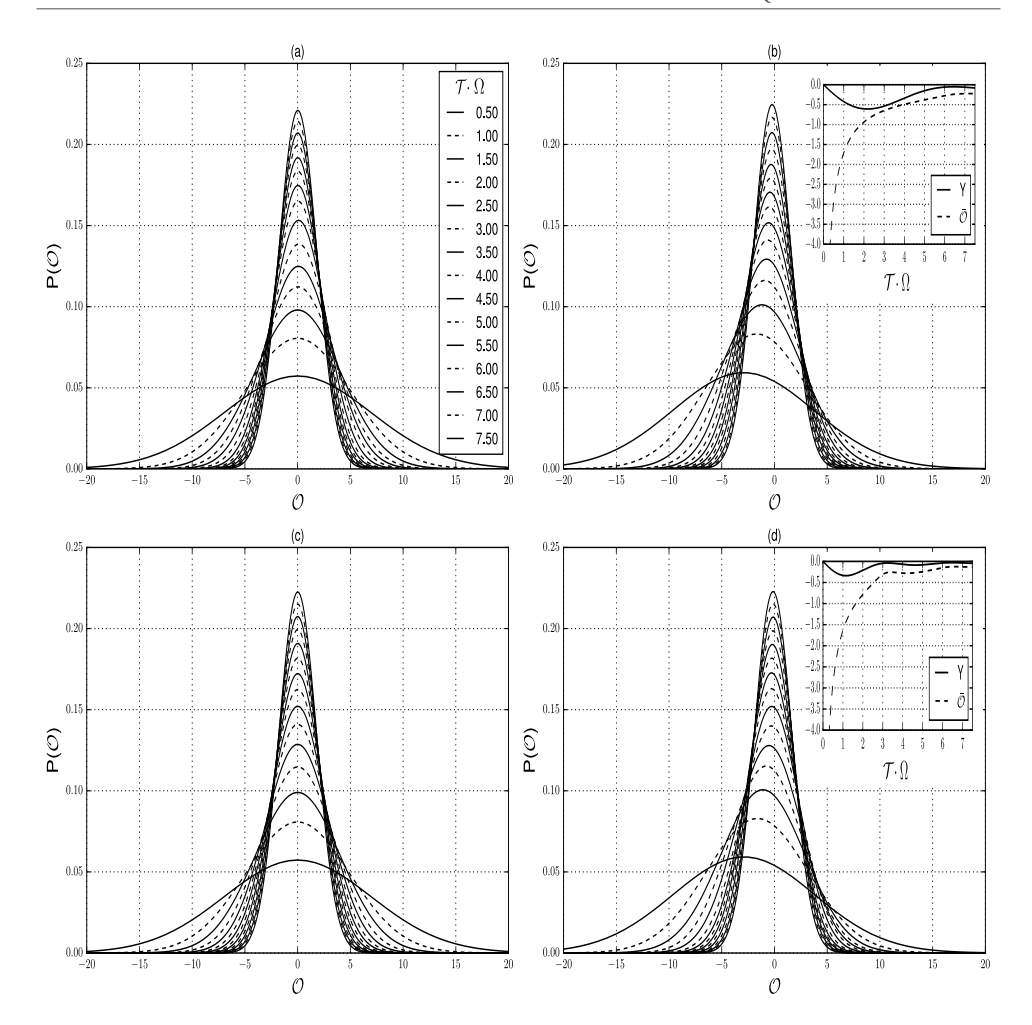


Figure 2.6: The output distributions for the $\hat{\sigma}_y$ measurements for a series of \mathcal{F} values at the scale of Ω^{-1} shown in the label of Figure (a). The qubit is initially prepared in the state Z^+ . Left column: the distributions conditioned on Z^+ . Right column: the distributions conditioned on Z^- . Upper row: $\Delta=0$. Lower row: $\Delta=1.7\Omega$. The insets in the right column plots present the unconditioned average (solid curves) and the average of the distribution conditioned on Z^- . The distributions conditioned on Z^+ are symmetric with zero average. The values of the parameters correspond to [13].

experimentally relevant regimes (Fig. 2.4 and 2.7), for both short and relatively long measurement time intervals.

We reveal and investigate analytically two signatures of the conditioned statistics that are related to quantum interference effects. First is the *half-quantized* measurement values. We demonstrate that the conditioned distribution function may display peculiarities — that are either peaks or dips — at *half-sums* of the quantized values.

Second signature pertains the case of zero overlap between initial and final state and

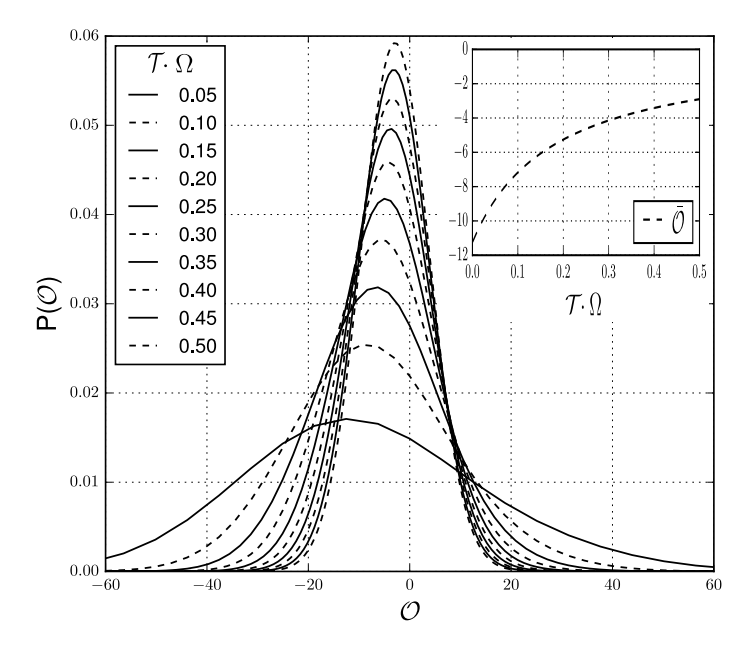


Figure 2.7: The probability distributions of outcomes of $\hat{\sigma}_y$ measurement for different $\mathcal{T}\ll\Omega^{-1}$. The values of the parameters correspond to [13]. The qubit is prepared in Z^+ and post-selected in an orthogonal state Z^- . The average output signal $\bar{\mathcal{O}}$ is shown in the inset. It exhibits anomalously large values and saturation in the limit $\mathcal{T}\to 0$.

time intervals that are so short as the wave function of the system does not significantly change by either Hamiltonian or dissipative dynamics.

We reveal unexpectedly large values of the time-integrated output cumulants for such short intervals, that we term *sudden jump*. We show that the account for decoherence leads to a finite duration of the jump at ultra-short time-scale $\gamma/(\Omega^2)$ and saturation of the anomalous eigenvalues at Ω/γ , Ω and γ being the frequency scales of the Hamiltonian and dissipative dynamics, respectively.

Actually, we have shown with our results that one can have very detailed theoretical predictions of CWLM distributions that can account for every detail of the experiment. This enables investigation and characterization of quantum effects even if the choice of parameters is far from the optimal one and these effects are small. We emphasize once again that the interference signature in the distributions that we predict in this Article can be seen in realistic experimental regimes and hope the effects can be experimentally observed soon. The efficient recording of time traces for a weak continuous monitoring of one, or several, qubit variables, is a key ingredient for accessing these statistics. It has been achieved in several articles and applied for observation of single quantum "trajectories" or real time feedback. [34] High fidelity preparation and post-selection of the qubit is also required for experiments with conditioned evolution, yet this is a general requirement in most qubit experiments. We thus believe that it is possible to extract the interesting statistics from the existing records.

42 References

2

REFERENCES

- [1] A. J. Leggett, The quantum measurement problem, Science 307, 871 (2005).
- [2] M. B. Mensky, *The action uncertainty principle in continuous quantum measurements*, Physics Letters A **155**, 229 (1991).
- [3] A. N. Korotkov, *Continuous quantum measurement of a double dot*, Phys. Rev. B **60**, 5737 (1999).
- [4] A. Jordan and M. Buttiker, *Continuous quantum measurement with independent detector cross correlations*, Phys. Rev. Lett. **95**, 220401 (2005).
- [5] K. Jacobs and D. A. Steck, *A straightforward introduction to continuous quantum measurement*, Contemporary Physics **47**, 279 (2006), http://dx.doi.org/10.1080/00107510601101934.
- [6] H. Wei and Y. V. Nazarov, *Statistics of measurement of noncommuting quantum variables: Monitoring and purification of a qubit*, Phys. Rev. B **78**, 045308 (2008).
- [7] A. Chantasri and A. N. Jordan, *Stochastic path-integral formalism for continuous quantum measurement*, Phys. Rev. A **92**, 032125 (2015).
- [8] A. Chantasri, J. Dressel, and A. N. Jordan, *Action principle for continuous quantum measurement*, Phys. Rev. A **88**, 042110 (2013).
- [9] A. A. Clerk, M. H. Devoret, S. M. Girvin, F. Marquardt, and R. J. Schoelkopf, *Introduction to quantum noise, measurement, and amplification*, Rev. Mod. Phys. **82**, 1155 (2010).
- [10] M. Hatridge, S. Shankar, M. Mirrahimi, F. Schackert, K. Geerlings, T. Brecht, K. M. Sliwa, B. Abdo, L. Frunzio, S. M. Girvin, R. J. Schoelkopf, and M. H. Devoret, *Quantum back-action of an individual variable-strength measurement*, Science **339**, 178 (2013).
- [11] K. W. Murch, S. J. Weber, C. Macklin, and I. Siddiqi, *Observing single quantum trajectories of a superconducting quantum bit*, Nature **502**, 211 (2013).
- [12] N. Roch, M. E. Schwartz, F. Motzoi, C. Macklin, R. Vijay, A. W. Eddins, A. N. Korotkov, K. B. Whaley, M. Sarovar, and I. Siddiqi, Observation of measurement-induced entanglement and quantum trajectories of remote superconducting qubits, Phys. Rev. Lett. 112, 170501 (2014).
- [13] P. Campagne-Ibarcq, L. Bretheau, E. Flurin, A. Auffèves, F. Mallet, and B. Huard, *Observing interferences between past and future quantum states in resonance fluo-rescence*, Phys. Rev. Lett. **112**, 180402 (2014).

43

- [14] J. P. Groen, D. Ristè, L. Tornberg, J. Cramer, P. C. de Groot, T. Picot, G. Johansson, and L. DiCarlo, *Partial-measurement backaction and nonclassical weak values in a superconducting circuit*, Phys. Rev. Lett. 111, 090506 (2013).
- [15] S. J. Weber, A. Chantasri, J. Dressel, A. N. Jordan, K. W. Murch, and I. Siddiqi, *Mapping the optimal route between two quantum states*, Nature **511**, 570 (2014).
- [16] D. Tan, S. J. Weber, I. Siddiqi, K. Mølmer, and K. W. Murch, *Prediction and retrodiction for a continuously monitored superconducting qubit*, Phys. Rev. Lett. 114, 090403 (2015).
- [17] Y. Aharonov, D. Z. Albert, and L. Vaidman, *How the result of a measurement of a component of the spin of a spin-1/2 particle can turn out to be 100*, Phys. Rev. Lett. **60**, 1351 (1988).
- [18] H. M. Wiseman, Weak values, quantum trajectories, and the cavity-qed experiment on wave-particle correlation, Phys. Rev. A 65, 032111 (2002).
- [19] S. Gammelmark, B. Julsgaard, and K. Mølmer, *Past quantum states of a monitored system*, Phys. Rev. Lett. 111, 160401 (2013).
- [20] A. G. Kofman, S. Ashhab, and F. Nori, *Nonperturbative theory of weak pre- and post-selected measurements*, Phys. Rep. **520**, 43 (2012).
- [21] J. Dressel, M. Malik, F. M. Miatto, A. N. Jordan, and R. W. Boyd, *Nonperturbative theory of weak pre- and post-selected measurements*, Rev. Mod. Phys. **86**, 307 (2014).
- [22] N. S. Williams and A. N. Jordan, *Weak values and the leggett-garg inequality in solid-state qubits*, Phys. Rev. Lett. **100**, 026804 (2008).
- [23] J. Dressel, S. Agarwal, and A. N. Jordan, *Contextual values of observables in quantum measurements*, Phys. Rev. Lett. **104**, 240401 (2010).
- [24] L. Qin, P. Liang, and X.-Q. Li, Weak values in continuous weak measurements of qubits, Phys. Rev. A 92, 012119 (2015).
- [25] Y. V. Nazarov and Y. M. Blanter, *Quantum Transport: Introduction to Nanoscience* (Cambridge University Press, 2009).
- [26] Y. V. Nazarov and M. Kindermann, Full counting statistics of a general quantum mechanical variable, The European Physical Journal B - Condensed Matter and Complex Systems 35, 413 (2003).
- [27] V. Belavkin, *A new wave equation for a continuous nondemolition measurement,* Physics Letters A **140**, 355 (1989).
- [28] H. Wiseman and G. Milburn, *Quantum theory of optical feedback via homodyne detection*, Phys.Rev. Lett. **70**, 548 (1993).
- [29] A. N. Korotkov and A. N. Jordan, *Undoing a weak quantum measurement of a solid-state qubit*, Phys. Rev. Lett. **97**, 166805 (2006).

44 REFERENCES

[30] S. Wu and Y. Li, *Weak measurements beyond the aharonov-albert-vaidman formalism*, Phys. Rev. A **83**, 052106 (2011).

- [31] D. J. Starling, P. B. Dixon, N. S. Williams, A. N. Jordan, and J. C. Howell, *Continuous phase amplification with a sagnac interferometer*, Phys. Rev. A **82**, 011802 (2010).
- [32] Y. Aharonov and L. Vaidman, *Complete description of a quantum system at a given time*, Journ. Phys. A **24**, 2315 (1991).
- [33] A. Di Lorenzo and J. C. Egues, *Weak measurement: Effect of the detector dynamics*, Phys. Rev. A **77**, 042108 (2008).
- [34] R. Vijay, C. Macklin, D. H. Slichter, S. J. Weber, K. W. Murch, R. Naik, A. N. Korotkov, and I. Siddiqi, *Stabilizing rabi oscillations in a superconducting qubit using quantum feedback*, Nature **490**, 77 (2012).

2

PROBABILITY DISTRIBUTIONS OF
CONTINUOUS MEASUREMENT
RESULTS FOR TWO
NON-COMMUTING VARIABLES AND
CONDITIONED QUANTUM
EVOLUTION

3.1. Introduction

Quantum computing and communication [1] are stimulating rapid progress in the understanding and control of small quantum systems. An important ingredient for advanced quantum control is the ability to realize continuous monitoring of a quantum system. Theories for continuous quantum measurement [2–8] and experiments [9–15] have enabled a detailed understanding of the realistic and practical measurement process in quantum mechanics.

A relevant case of quantum measurement is that of the measurement of non-commuting quantum variables. The fact that some observables *cannot* be measured together is one of the major differences between quantum and classical theory. Although it is possible to perform a simultaneous measurement of non-commuting variables, only recently [4, 6, 16–19] the dynamics of the qubit state has been studied under these conditions. It is important to note that the simultaneous measurement of non-commuting variables for a long time has been a topic of many experimental and theoretical studies in quantum optics [20]. The linearity of most optical measurements provides a perfect platform for experiments of this kind.

Another interesting and relevant kind of quantum measurement is the conditioned measurement. For a general conditioned evolution, both the initial and final states of the system can be regarded as fixed. This is achieved by the selection of the measurement results on the basis of the result of the concluding projective measurement. It has been shown that the statistics of such a conditioned measurement may drastically differ from the unconditioned case [5, 6]. In this context, the statistics of measurement results reveal purely quantum phenomena that can be interpreted in terms of weak values [21] and associated with the interference of initial and final states [22, 23] .

This paper elaborates on a combined case of quantum measurement of two non-commuting variables and for conditioned quantum evolution. The goal is to inspect the full statistics of the measurement results and its dependence on the dynamics of the system measured. For that purpose, we use the theory of continuous weak linear measurements (CWLM), where a sufficiently weak coupling between a quantum system and infinitely many degrees of freedom of a linear detector provides their entanglement and conversion of the (discrete) quantum information into continuous time-dependent readings of the detector [2–8]. Our approach to CWLM statistics was first introduced in [6, 24], and extended to include conditioned evolution in [25]. It is based on the theory of full counting statistics in the extended Keldysh formalism [26]. The statistics of measurements of $\int dt \hat{V}(t)$, V(t) being a quantum mechanical variable representing linear degrees of freedom that are measured, are evaluated with the characteristic functional method and the use of counting field technique. The method provides the necessary and compact description of the whole quantum system consisting of the measured system and multiple degrees of freedom describing general linear detectors.

The probability distributions for the measurement of a single variable have been extensively studied in our recent publication [25]. The motivation to address the two-variable case comes from the recent experiments [12] where a qubit has been measured in a resonance fluorescence setup. In the experiment, the transmon qubit enclosed in

47

a non-resonant three-dimensional (3D) superconducting cavity is resonantly driven at the Rabi frequency Ω and its fluorescence signal is recorded. The cavity is coupled to two transmission lines, the resonant driving field drives the qubit via a weakly coupled line, while most of the fluorescence signal exits via the other line which is coupled strongly. The complex amplitude of the the fluorescence signal is proportional to σ_- , the average of the lowering operator $\hat{\sigma}_- = |g\rangle \langle e|$ of the qubit, and oscillates with the Rabi frequency Ω . At each run, the qubit is prepared in either its ground $|g\rangle$ or excited $|e\rangle$ state and the signal is monitored during a time interval $(0,\mathcal{F})$. At time \mathcal{F} , the qubit is projectively measured using a strong pulse at the bare cavity frequency.

A heterodyne detection setup is used to measure this signal, and the fluorescence signal can be interpreted as a result of a weak continuous measurement. We notice that the experiment discussed can give access not only to the conditioned averages, but also to the conditioned statistics of the measurement results. Those are statistics of the continuous weak measurement of two non-commuting variables of the qubit, σ_x and σ_y that comprise $\hat{\sigma}_- = \hat{\sigma}_x - i\hat{\sigma}_y$.

The statistics of the conditioned measurement results reveal the signatures of interference between pre and post selected states. With the present work, we extend these signatures to the case of simultaneous measurement of non-commuting variables, and reveal the relation between the visibility of these signatures and the qubit dynamics in different parameter regimes.

Our results demonstrate that one can achieve very detailed theoretical predictions of the statistics of CWLM of two non-commuting variables, with account for every relevant experimental parameter. This allows for the study and characterization of quantum effects at any choice of parameters, even in the regime where the signatures are very weak.

Among other interesting results, we show that the joint distribution of measurement outcomes of two non-commuting quantum variables $P(\mathcal{O}_1, \mathcal{O}_2)$ has peculiarities located at the circle $\mathcal{O}_1^2 + \mathcal{O}_2^2 = 1$. This is the two-variable analog of the *half-quantized* measurement values for the single variable measurement case. We reveal these peculiarities by analytical calculation of the quasi-distribution of shifts in the limit of short measurement time, and demonstrate them in numerical results at larger measurement times. We demonstrate how the visibility of the circle is suppressed by the system dynamics, such that the joint distribution effectively becomes a product of two independent distributions $P(\mathcal{O}_1, \mathcal{O}_2) \approx P_1(\mathcal{O}_1)P_2(\mathcal{O}_2)$.

At measurement times that are so short that the wave function of the system does not change significantly, and in the case of zero or small overlap between initial and final states, we reveal anomalously large values of the cumulants of the distribution function of time integrated outputs that we previously nicknamed $sudden\ jump\ [25]$. In the case of simultaneous measurement of two non-commuting variables, we reveal simultaneous $sudden\ jump\$ of the two time integrated outputs $\mathcal{O}_1,\mathcal{O}_2$ with an appropriate choice of Hamiltonian. For the average value of the output, the big values are readily understood from the weak value theory [21]. We present both analytical and numerical results.

We also compute the distributions of the outputs under realistic experimental parameters of [12] concentrating on the quantum signatures of conditioned evolution and the non-commutativity of the variables.

3

The structure of the paper is as follows. We outline and develop the necessary formalism in Sec. 3.2, starting from a Bloch master equation for the qubit evolution that is augmented with counting fields to describe the statistics of detector readouts. This formalism has been elaborated in our previous work [25], we extend it here to the simultaneous measurement of two non-commuting variables. We reveal the role of various experimental parameters and formulate the relevant quantum noise inequalities for a general multiple detector setup. In Sec. 3.3 we concentrate on short \mathcal{T} and compute the quasi-distribution of the shifts of the joint distribution $P(\mathcal{O}_1,\mathcal{O}_2)$, revealing the circle shape discussed. In Sec. 3.4 we concentrate on the case of zero overlap between initial and final states and derive analytical expressions for the joint distribution $P(\mathcal{O}_1,\mathcal{O}_2)$ of measurement outcomes at short times. In this regime, the joint distribution is essentially non-Gaussian and manifests the *sudden jumps* in the integrated outputs.

In the next sections, we present numerical results at various times scales and in parameter regimes demonstrating the possibility of very detailed predictions of CWLM distributions. To start with, in Sec. 3.5 we present numerical simulations at time intervals that are much smaller than the typical time scales of all Hamiltonian dynamics focusing on three relevant cases: the case of ideal detectors, and the experimentally relevant case with and without detuning. In Sec. 3.6, we concentrate on time scales of the order of the decoherence time, inspecting the three cases for ideal detectors with and without drive, and for experimentally relevant setup. We conclude in Sec. 3.8.

3.2. METHOD

The description of CWLM in use was first introduced in [24], and later, extended in [25] to compute probability distributions of a continuous measurement for a conditioned quantum evolution.

In contrast to other methods such as path integral formulation [6, 7], effective action method [2, 8], past states formalism [23] or the stochastic update equation [27]; this description permits the direct evaluation of the generating function of the probability distribution of the measurement results.

The central object in this description is a Bloch-master equation for the evolution of the quasi-density matrix of the quantum system that is augmented with counting fields. Evaluating the trace of the augmented density matrix from this equation as a function of the counting fields provides the generating function for the probability distribution of the detector(s) output(s). We give the concrete expression of such equation for a simultaneous measurement of two variables $\mathcal{O}_1, \mathcal{O}_2$ of the quantum system. In an ideal measurement, where all decoherence is due to the coupling with $\mathcal{O}_1, \mathcal{O}_2$ and for the case of independent detectors, it reads,

$$\frac{\partial \hat{\rho}}{\partial t} = -\frac{i}{\hbar} [\hat{H}_{q}, \hat{\rho}] - \sum_{i} \frac{S_{QQ}^{(i,i)}}{\hbar^{2}} \mathcal{D}[\hat{\mathcal{O}}_{i}] \hat{\rho} - \frac{\chi_{i}^{2}(t)}{2} S_{VV}^{(i,i)} \hat{\rho}
- \frac{S_{QV}^{(i,i)}}{\hbar} \chi_{i}(t) [\hat{\rho}, \hat{\mathcal{O}}_{i}] + \frac{i a_{VQ}^{i,i} \chi_{i}(t)}{2} [\hat{\rho}, \hat{\mathcal{O}}_{i}]_{+}.$$
(3.1)

Here, [,] and [,]₊ refer to commutator and anti-commutator, respectively, $\mathcal{D}[\hat{A}]\hat{\rho} \equiv \left(\frac{1}{2}[\hat{A}^{\dagger}\hat{A},\hat{\rho}]_{+} - \hat{A}\hat{\rho}\hat{A}^{\dagger}\right)$ and i = 1,2.

For each output \mathcal{O}_i , there is a corresponding counting field $\chi_i(t)$ and a pair of input \hat{Q}_i - output \hat{V}_i operators of the corresponding detector. The parameters in the previous equation are the two-point correlators of these input-output operators, that give the set of noises and response functions in this linear measurement environment,

$$S_{QQ}^{(i,j)} = \frac{1}{2} \int_{-\infty}^{t} dt' \left\langle \left\langle \hat{Q}_{i}(t) \hat{Q}_{j}(t') + \hat{Q}_{j}(t') \hat{Q}_{i}(t) \right\rangle \right\rangle, \tag{3.2a}$$

$$S_{QV}^{(i,j)} = \frac{1}{2} \int_{-\infty}^{t} dt' \left\langle \left\langle \hat{Q}_{i}(t) \hat{V}_{j}(t') + \hat{V}_{j}(t') \hat{Q}_{i}(t) \right\rangle \right\rangle, \tag{3.2b}$$

$$S_{VV}^{(i,j)} = \frac{1}{2} \int_{-\infty}^{t} dt' \left\langle \left\langle \hat{V}_{i}(t)\hat{V}_{j}(t') + \hat{V}_{j}(t')\hat{V}_{i}(t) \right\rangle \right\rangle, \tag{3.2c}$$

$$a_{VQ}^{(i,j)} = -\frac{i}{\hbar} \int_{-\infty}^{t} dt' \langle [\hat{V}_i(t), \hat{Q}_j(t')] \rangle, \qquad (3.2d)$$

$$a_{QV}^{(i,j)} = -\frac{i}{\hbar} \int_{-\infty}^{t} dt' \langle [\hat{Q}_i(t), \hat{V}_j(t')] \rangle. \tag{3.2e}$$

This set of noise and response functions define completely the characteristics of the measurement process. Conforming to the assumption of slow qubit dynamics, the noises are white and the responses are instant, corresponding to zero-frequency correlators

The values of these noises and responses are restricted by a set of Cauchy-Schwartz inequalities of the form, [28]

$$S_{QQ}^{(i,i)}S_{VV}^{(j,j)} - \left|S_{QV}^{(i,j)}\right|^2 \ge \frac{\hbar^2}{4} \left|a_{VQ}^{(j,i)} - a_{QV}^{(i,j)}\right|^2, \tag{3.3}$$

for each pair of operators \hat{Q}_i , \hat{V}_i ; and not excluding inequalities for pairs of only input $(\hat{Q}$'s) or only output $(\hat{V}$'s) operators.

As discussed in [25], these inequalities impose the necessary conditions for the positivity of the probability distributions of measurement outputs. However, it is possible an necessary to derive a more restrictive set of inequalities that impose the conditions for this positivity. In two-detector case at hand, an extra restriction reads:

$$\begin{split} S_{QQ}^{(1,1)} + S_{QQ}^{(2,2)} &\geq \frac{\hbar^2}{4} \frac{\left| a_{VQ}^{(1,1)} - a_{QV}^{(1,1)} \right|^2}{S_{VV}^{(1,1)}} + \frac{\left| S_{QV}^{(1,1)} \right|^2}{S_{VV}^{(1,1)}} \\ &\quad + \frac{\hbar^2}{4} \frac{\left| a_{VQ}^{(2,2)} - a_{QV}^{(2,2)} \right|^2}{S_{VV}^{(2,2)}} + \frac{\left| S_{QV}^{(2,2)} \right|^2}{S_{VV}^{(2,2)}} \\ &\quad + \hbar \left| \frac{\left(a_{VQ}^{(1,1)} - a_{QV}^{(1,1)} \right) S_{QV}^{(2,1)}}{S_{VV}^{(1,1)}} - \frac{\left(a_{VQ}^{(2,2)} - a_{QV}^{(2,2)} \right) S_{QV}^{(1,2)}}{S_{VV}^{(2,2)}} \right| \\ &\quad + \frac{\left| S_{QV}^{(1,1)} \right|^2}{S_{VV}^{(1,1)}} + \frac{\left| S_{QV}^{(1,2)} \right|^2}{S_{VV}^{(2,2)}}. \end{split} \tag{3.4}$$

We demonstrate in Sec. 3.7 how to derive such inequalities from analytical expressions of the joint distribution of measurement outcomes. Those and more complex inequalities can be derived from the positivity of the matrix $S_{\beta\alpha} + i \frac{a_{\beta\alpha} - a_{\alpha\beta}}{2}$ where the indices α, β index the whole set of operators \hat{V}, \hat{Q} .

Let us focus in a experimental situation general to the one described in [12], a transmon qubit embedded in a 3D superconducting cavity with two levels split in z-direction under conditions of strong resonant drive that compensates the splitting of the qubit levels. The effective Hamiltonian reads

$$\hat{H}_q = \frac{\hbar}{2} \Omega \hat{\sigma}_x + \frac{\hbar}{2} \Delta \hat{\sigma}_z, \tag{3.5}$$

 Ω being the Rabi frequency proportional to the amplitude of the resonant drive, and Δ being the detuning of the drive frequency from the qubit energy splitting. The interaction with the environment induces decoherence, excitation and relaxation of the qubit, with the rates $\gamma_d, \gamma_\uparrow, \gamma_\downarrow$ respectively. The measured quantities are related to the fluorescence signal emitted from the qubit, so \mathcal{O}_1 and \mathcal{O}_2 are conveniently chosen to be σ_x and σ_y .

This is the case of heterodyne detection. The signal from $\sigma_{x,y}$ eventually oscillates at frequency Ω . The accumulating signal is obtained by the mixture of this signal with the resonant drive. As a result, it is in principle possible to measure both $\sigma_{x,y}$ signals with a single detector variable mixing it with sin and cos components of the resonant drive. Then Eq. 3.1 needs to be adjusted to the case of heterodyne detection. The symmetrized noises S_{VV} have to be taken at frequency Ω rather than on zero frequency. The same pertains the susceptibilities. The most important change concerns the second term in Eq. 3.1 that, for $\mathscr{O}_{1,2} = \sigma_{x,y}$ describes the decoherence and transitions between the states $\sigma_z | Z^{\pm} \rangle = \pm | Z^{\pm} \rangle$. In Eq. 3.1, the rates of these transitions are equal for both directions, $\gamma_{\downarrow} = \gamma_{\uparrow}$. For the case of heterodyne detection, they are not: there are two rates with gaining/loosing energy proportional to the quantum noise S_{QQ} at positive and negative

51

3

frequencies $\pm\Omega$. We also need to add the terms describing the decoherence of the states $|Z^{\pm}\rangle$.

With this, the equation reads, (i = 1, 2)

$$\frac{\partial \hat{\rho}}{\partial t} = -\frac{i}{\hbar} [\hat{H}_{q}, \hat{\rho}] - \gamma_{d} \mathcal{D}[\hat{\sigma}_{z}] \hat{\rho} - \gamma_{\uparrow} \mathcal{D}[\hat{\sigma}_{+}] \hat{\rho}
- \gamma_{\downarrow} \mathcal{D}[\hat{\sigma}_{-}] \hat{\rho} - \frac{S_{QV}}{\hbar} \sum_{i} \chi_{i}(t) [\hat{\rho}, \hat{\mathcal{O}}_{i}]
+ \frac{i a_{VQ}}{2} \sum_{i} \chi_{i}(t) [\hat{\rho}, \hat{\mathcal{O}}_{i}]_{+} - \sum_{i} \frac{\chi_{i}^{2}(t)}{2} S_{VV} \hat{\rho},$$
(3.6)

 $\hat{\sigma}_{+}(\hat{\sigma}_{-})$ being the rising and lowering operators of the qubit, and $\hat{\sigma}_{z} = |e\rangle\langle e| - |g\rangle\langle g|$ the standard Pauli operator.

All the parameters entering the equation can be characterized from experimental measurements. We provide an example of concrete values in Section 3.5.

For simplicity we inspect the case of identical but independent detectors. Meaning all cross noises and responses vanish and the behaviour of both detectors is physically the same. In that case, the rates and noises are restricted by the inequality,

$$S_{QQ}S_{VV} - \left|S_{QV}\right|^2 \ge \frac{\hbar^2}{4} \left|a_{VQ} - a_{QV}\right|^2.$$
 (3.7)

For a simple system like a single qubit it is natural to make the measured operator dimensionless, with eigenvalues of the order of one, or, even better, ± 1 . With this, one can define and relate the measurement induced dephasing rate $2\gamma = 2S_{QQ}/\hbar^2$ and the acquisition time $t_a = 4S_{VV}/|a_{VQ}|^2$ required to measure the variable $\mathcal{O}_{1,2}$ with a relative $accuracy \simeq 1.$

We concentrate on the simultaneous measurement of two variables of a qubit during a time interval $(0,\mathcal{F})$. During this time interval, one accumulates the time-dependent outputs of the detectors and normalize them by the same interval, $V_i \equiv \frac{1}{\pi} \int_0^{\mathcal{T}} V_i(t') dt'$ (i = 1,2). Our goal is to evaluate the joint probability distribution $P(V_1, V_2)$ of the measurement results, conditioned to an initial qubit state given by $\hat{\rho}(0)$, and to a post-selection of the qubit in a specific state $|\Psi\rangle$ at the time moment \mathcal{T} . This involves the projection on the state $|\Psi\rangle$, represented by the projection operator $\hat{P}_{\Psi} = |\Psi\rangle\langle\Psi|$. This works under assumption of an ideal and fast post-selection so that the system measured is projected on a known pure state $|\Psi\rangle$. This is the case of the experimental setup [12]. In reality, there can be errors in the post-selection. Such errors can also be accounted for in the formalism outlined. To this end, one replaces the projection operator \hat{P}_{Ψ} with a density matrix-like Hermitian operator $\hat{\rho}_f$ satisfying $\text{Tr}[\hat{\rho}_f] = 1$. For instance, if after a faulty projection measurement with the result "1" the system is in a orthogonal state $|\Psi_2\rangle$ with probability p_e , the corresponding $\hat{\rho}_f$ reads

$$\hat{\rho}_f = (1 - p_e)|\Psi_1\rangle\langle\Psi_1| + p_e|\Psi_2\rangle\langle\Psi_2| \tag{3.8}$$

The probability distribution of the detector outcomes can be computed from the generating function according to

$$P(V_1, V_2) = \frac{\mathcal{F}}{2\pi} \int \int d\chi_1 d\chi_2 e^{-i\chi_1 V_1 \mathcal{F}} e^{-i\chi_2 V_2 \mathcal{F}} C(\chi_1, \chi_2; \mathcal{F}). \tag{3.9}$$

The joint statistics are extracted from the quasi-density matrix $\hat{\rho}(\chi_1, \chi_2; \mathcal{F})$ at the end of the interval calculated using Eq. (3.1). With the post-selection, the quasi-density matrix is projected on the final state measured $|\Psi\rangle$, and the conditioned generating function of the detector outcomes reads [25]

$$\tilde{C}(\chi_1, \chi_2; \mathcal{T}) = \frac{\operatorname{Tr}_q(\hat{P}_{\Psi}\hat{\rho}(\chi_1, \chi_2; \mathcal{T}))}{\operatorname{Tr}_q(\hat{P}_{\Psi}\hat{\rho}(\chi_1 = 0, \chi_2 = 0; \mathcal{T}))}.$$
(3.10)

Here, Tr_a denotes the trace over qubit variables.

Sometimes it is convenient to normalize the time-integrated outputs introducing $\mathcal{O}_i = V_i/a_{VQ}^{(i,i)}$ that immediately corresponds to the eigenvalues of $\hat{\mathcal{O}}_i$ (We stress that \mathcal{O}_i are coming from the averaging of an environmental operator rather than $\hat{\mathcal{O}}_i$).

3.3. QUASI-DISTRIBUTION OF SHIFTS

For a sufficiently long measurement, the distribution of the measurement results is a shifted Gaussian with the value of the shift proportional to the averaged value of the operator measured. In this case, the spread of the Gaussian is much smaller than the shift. In this Section, we will attempt to understand the shifts in the limit of short measurement times \mathcal{T} . In principle, any distribution of a vector variable $P(\vec{\mathcal{O}})$ can be presented as a convolution of a Gaussian distribution P_G and a quasi-distribution of the shifts,

$$P(\vec{\mathcal{O}}) = \int d\vec{s} C(\vec{s}) P_G(\vec{\mathcal{O}} - \vec{s}) \tag{3.11}$$

One should only not to be confused with the fact that *C* is a quasi-distribution and should not be ever positively defined.

The convolution of such kind is especially natural since the solution of Eq. (3.1) is proportional to the characteristic function of the Gaussian distribution. If we neglect the cross-noises, and the Hamiltonian dynamics, the solution at short $\mathcal T$ can be represented as

$$\hat{\rho}(\mathcal{F}) = \exp\left(-\frac{\mathcal{F}\chi_i^2(t)}{2}S_{VV}^{(i,i)}\right)\hat{U}\hat{\rho}(0)\hat{U}$$
(3.12)

with $\hat{U}=\exp\left(\frac{ia_{VQ}^{i,l}\chi_{l}\mathcal{T}}{2}\right)$ The first factor here is the characteristic function of the Gaussian distribution generated by the detector noises. From the second factor, assuming the initial density matrix $\hat{\rho}_{i}$ and the post-selection described by $\hat{\rho}_{f}$, we obtain the generating function of the shift quasi-distribution

$$C(\vec{\chi}) = \frac{\text{Tr}[\hat{\rho}_f \hat{U} \hat{\rho}_i \hat{U}]}{\text{Tr}[\hat{\rho}_f \hat{\rho}_i]}.$$
(3.13)

We illustrate the quasi-distribution of the shifts for the case of a qubit. Although in this paper we concentrate on two-detector setups, it is much more instructive to consider now *three* detectors measuring all three Pauli matrices $\vec{\sigma} = (\sigma_x, \sigma_y, \sigma_z)$. We normalize the detector outputs on ± 1 of Pauli matrix eigenvalues and rescale the corresponding counting fields $\vec{\chi}$, accordingly. With this, the matrix \hat{U} becomes nicely symmetric

$$\hat{U} = \exp\left(-i(\vec{\chi}, \vec{\sigma})/2\right) \tag{3.14}$$

The final and initial density matrices for a qubit are represented as

$$\hat{\rho}_{i,f} = \frac{1}{2} (1 + (\vec{P}_{i,f}, \vec{\sigma})) \tag{3.15}$$

with polarization vectors $|\vec{P}_{i,f}| < 1$. The generation function for smaller number of detectors is obtained by setting some components of $\vec{\chi}$ to 0. For instance, setting $\chi_{z,y} = 0$ gives

$$C(\chi_x) = \left(1 + (\vec{P}_i, \vec{P}_f)\right)^{-1} \left(((\vec{P}_i, \vec{P}_f) - P_i^z P_f^z) + (1 + P_i^z P_f^z) \cos \chi_x + (P_i^z + P_f^z) \sin \chi \right)$$
(3.16)

which corresponds to the following quasi-distribution of the shifts

$$C(s_x) = \delta(s_x - 1) + \delta(s_x) + \delta(s_x + 1)$$
(3.17)

This quasi-distribution, as discussed in [25], is located on a compact support of half-sums of the eigenvalues ± 1 of the operator σ_x . The half-quantized value $s_x = 0$ is manifested only in the case of conditioned measurements.

Multiplying the matrices and taking the trace, we obtain the answer for three detectors. It can be naturally separated into scalar, vector, and tensor part $(\chi \equiv |\vec{\chi}|)$,

$$C_s(\vec{\chi}) = \cos \chi + (\vec{P}_i, \vec{P}_f) \tag{3.18}$$

$$C_{\nu}(\vec{\chi}) = i(\vec{P}_i + \vec{P}_f, \chi) \frac{\sin \xi}{\xi}$$
(3.19)

$$C_t(\vec{\chi}) = -(\vec{P}_i, \vec{\chi})(\vec{P}_f, \vec{\chi}) \frac{2\sin^2(\chi/2)}{\chi^2}$$
 (3.20)

$$C = \frac{C_s + C_v + C_t}{1 + (\vec{P}_i, \vec{P}_f)}. (3.21)$$

Let us now compute the quasi-distribution of the shifts the inverse Fourier transform of C,

$$C(\vec{s}) = \int \frac{d\vec{s}}{(2\pi)^3} C(\vec{\chi}) \exp\left(-i(\vec{s}, \vec{\chi})\right)$$
(3.22)

Eventually, the integral is rather involved. The best way to perform the integration is to try the direct transform. We note that

$$\frac{\sin(\chi A)}{\chi} \equiv z(A) = \int d\vec{s} \frac{\delta(s-A)}{4\pi A} \exp(i(\vec{s}, \vec{\chi}))$$
 (3.23)

at any A and

$$\frac{\sin(\chi)}{\gamma},\cos(\xi) = \lim_{A \to 1} z(A), \frac{d}{dA}z; \tag{3.24}$$

$$\frac{2\sin^2(\chi/2)}{\chi^2} = \int_0^1 dA z(A)$$
 (3.25)

With using this we arrive at the quasi-distribution of the form

$$C_s(\vec{s}) = -\frac{1}{4\pi} (\delta(s-1) + \delta'(s-1)) + (\vec{P}_i, \vec{P}_f) \delta(\vec{n})$$
 (3.26)

$$C_{\nu}(\vec{n}) = -(\vec{P}_i + \vec{P}_f, \frac{\partial}{\partial \vec{s}})\delta(s-1)$$
(3.27)

$$C_{t}(\vec{n}) = (\vec{P}_{i}, \frac{\partial}{\partial \vec{s}})(\vec{P}_{f}, \frac{\partial}{\partial \vec{s}}) \frac{\Theta(1-s)}{s}$$
(3.28)

$$C = \frac{C_s + C_v + C_t}{1 + (\vec{P}_i, \vec{P}_f)} \tag{3.29}$$

We observe that the vector and tensor contributions provide a quasi-distribution located on a compact support s=0 or s=1. The latter is rather surprising: it invokes a notion of a 'classical' qubit spin, a classical unit vector pointing in an arbitrary direction. While for such classical spin the quasi-distribution would have been positive, this is not the case of actual quantum mechanical expression: the quasi-distribution is made of δ -function and its derivatives. We do not find it instructive to plot the resulting quasi-distribution. The tensor part also contains terms located on this support. In addition, there are terms $\propto (\vec{P}_f, \vec{s})(\vec{P}_i, \vec{s})/s^5$ located within the sphere s < 1. The tensor part persists only for the case of conditional measurement $\vec{P}_f \neq 0$.

To obtain the distribution of 2 outputs, we integrate it over s_z making use of

$$\int ds_z \ z(A) = \frac{2}{\sqrt{A^2 - s_\perp^2}}; \ s_\perp \equiv \sqrt{s_x^2 + s_y^2}$$
 (3.30)

The resulting quasi-distribution reads (here, the indices a, b = x, y)

$$C_s(\vec{s}) = -\frac{1}{2\pi} \frac{1}{(1 - s_\perp^2)^{3/2}} + (\vec{P}_i, \vec{P}_f) \delta(s_x) \delta(s_y)$$
 (3.31)

$$C_{v}(\vec{s}) = -(P_{i}^{a} + P_{f}^{a}, \frac{\partial}{\partial n^{a}})\delta(s-1)$$
(3.32)

$$C_t(\vec{s}) = P_i^a \frac{\partial}{\partial s^a} P_f^b \frac{\partial}{\partial s^b} \operatorname{arccosh}(s_{\perp}^{-1})$$
 (3.33)

$$C = \frac{C_s + C_v + C_t}{1 + (\vec{P}_i, \vec{P}_f)} \tag{3.34}$$

We see that this quasi-distribution is located at the compact support $s_x^2 + s_y^2 = 1$, $s_x^2 + s_y^2 = 0$ as well as inside the circle $s_x^2 + s_y^2 < 1$. This gives us an expectation that the actual

3

distribution of the measurement results should exhibit some peculiarities at $s_x^2 + s_y^2 = 1$, an expectation that is confirmed by numerical results of subsequent Sections.

It is worth noting that the generalized functions involved in the quasi-distributions presented in the Eqs. (3.34) and (3.29) are rather involved and should be dealt with carefully. In particular, a direct attempt to integrate Eq.(3.34) over n_y does not immediately reproduce Eq. (3.17) as it should. Rather, the integration diverges near $s_x^2 + s_y^2 = 1$. To resolve this apparent paradox, one requires a regularization of the generalized functions involved. Such regularization can be provided by replacing

$$\delta(s-A) \to \pi^{-1} \operatorname{Im} \frac{1}{A+i\xi}$$
 (3.35)

at small but finite ξ . With this, the divergence at the circle edge is eliminated and Eq. (3.17) is reproduced.

3.4. SHORT TIME INTERVALS AND ZERO OVERLAP

In this Section, we consider again very short \mathcal{T} such that the change of the density matrix due to Hamiltonian and dissipative dynamics is small. Since the measuring time is too short to resolve the signal with sufficient accuracy, we expect the distribution to be close to the Gaussian one

$$P_G(\mathcal{O}_1, \mathcal{O}_2) = \prod_{i=1,2} \frac{1}{\sigma_i \sqrt{2\pi}} \exp\left(-\frac{\mathcal{O}_i^2}{2\sigma_i^2}\right),\tag{3.36}$$

with $\sigma_i^2 = S_{VV}^{(i,i)}/(\mathcal{T}\left|a_{VQ}^{(i,i)}\right|^2)$. The spread of \mathscr{O} is much larger than their eigenvalues. However, the distribution can become quite different if the overlap between the initial state, $|i\rangle$, and the final state of the projective measurement, $|\Psi\rangle$, vanishes: $\langle i|\Psi\rangle=0$. The latter implies that such output of the projective measurement is very improbable, but it can be singled out and its statistics are worth studying.

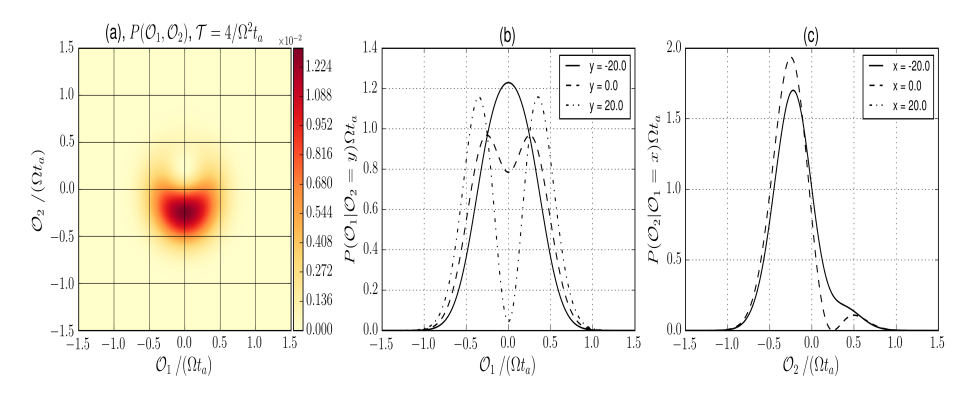


Figure 3.1: (a): Probability distribution of outputs [Eq. (3.39)] in the sudden jump regime in case of an ideal detector ($K \equiv \gamma t_a = 1$). The figures (b) and (c) present conditioned distributions. In (b), we plot the probability distribution of \mathcal{O}_1 output given a $\mathcal{O}_2 = y$ result for the other output. (c) gives the probability distribution of \mathcal{O}_2 output given a $\mathcal{O}_1 = x$ result for the other output. All distributions are evaluated at $\mathcal{T} = 4/(\Omega^2 t_a)$.

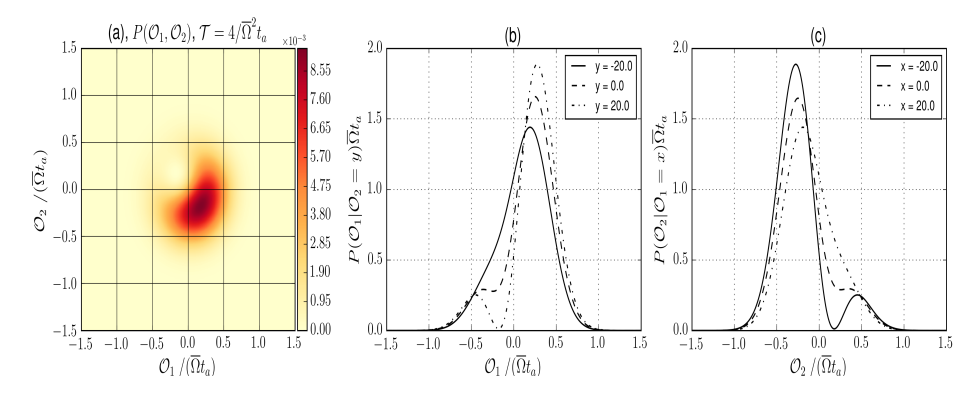


Figure 3.2: (a): Probability distribution of outputs [Eq. (3.42)] in the sudden jump regime in case of an ideal detector ($K \equiv \gamma t_a = 1$). Both figures (b) and (c) present conditioned distributions. (b) gives the probability distribution of \mathcal{O}_1 output given a $\mathcal{O}_2 = y$ result for the other output. (c) gives the probability distribution of \mathcal{O}_2 output given a $\mathcal{O}_1 = x$ result for the other output. All the distributions are evaluated at $\mathcal{F} = 4/(\bar{\Omega}^2 t_a)$. We set $\Omega_X = \Omega_Y$, this explains the symmetry.

A peculiarity termed a *sudden jump* of the integrated output, is characteristic for this situation. It can be explained from the concept of weak values [21] as far as average outputs are concerned. For the whole statistics of the outputs, the sudden jump was studied for a single variable measurement [25]. Here we demonstrate that the sudden jump is still seen in the statistics of simultaneous measurement of two variables. A proper choice of Hamiltonian permits for a simultaneous sudden jump in both integrated outputs. The signature of sudden jump is enhanced in the distribution where the distribution of one output is conditioned on a specific value of another one.

To this end, let us focus first at the experimental situation in $\[12]$. In this case, the two measured variables are conveniently chosen to be $\hat{\sigma}_x$ and $\hat{\sigma}_y$ and the qubit is driven by a Hamiltonian $\hat{H}_q = \hbar \frac{\Omega}{2} \hat{\sigma}_x$. In the simplest case where the two detectors are independent and no cross noises are present, and with the assumptions of short \mathcal{T} and zero overlap $\langle i|\Psi\rangle=0$ (the qubit is prepared in $|Z^+\rangle$ and post-selected in $|Z^-\rangle$), one obtains the following joint characteristic function of the distribution of detector outputs:

$$C(\chi, \mathcal{F}) = \frac{4\gamma + \mathcal{F}\left(\left(\Omega - i a_{VQ}^{(2,2)} \chi_2\right)^2 - \left(a_{VQ}^{(1,1)} \chi_1\right)^2\right)}{4\gamma + \mathcal{F}\Omega^2} e^{-\frac{1}{2}\sum_i S_{VV}^{(i,i)} \chi_i^2 \mathcal{F}}.$$
 (3.37)

 $\gamma=S_{QQ}^{(1,1)}/\hbar^2+S_{QQ}^{(2,2)}/\hbar^2$ being the decoherence rate. This gives the average outputs

$$\bar{\mathcal{O}}_1 = 0, \qquad \bar{\mathcal{O}}_2 = -\frac{2\Omega}{4\gamma + \mathcal{T}\Omega^2}; \qquad (3.38)$$

and the joint distribution

$$P(\mathcal{O}_1, \mathcal{O}_2) = \frac{1}{4\gamma + \mathcal{T}\Omega^2} \left(4\gamma + \mathcal{T} \left[\left(\Omega - \frac{4\mathcal{O}_2}{t_{a2}} \right)^2 - \frac{4}{\mathcal{T}t_{a2}} + \frac{4}{t_{a1}} \left(\frac{4\mathcal{O}_1^2}{t_{a1}} - \frac{1}{\mathcal{T}} \right) \right] \right) P_G(\mathcal{O}_1, \mathcal{O}_2)$$
(3.39)

The value of average output $\bar{\mathcal{O}}_2$ thus saturates at $-\Omega/2\gamma\ll-1$ in the limit of short $\mathcal{T}\ll\gamma/\Omega^2$. Note that this sudden jump behaviour, at a time scale of γ/Ω^2 now is only visible at the time-integrated output of the variable \mathcal{O}_2 not commuting with the Hamiltonian. Thus, to achieve a simultaneous sudden jump for both time-integrated outputs, we need to require that the Hamiltonian does not commute with both variables .

Let us modify the Hamiltonian to $\hat{H}_q = \hbar \frac{\Omega_x}{2} \hat{\sigma}_x + \hbar \frac{\Omega_y}{2} \hat{\sigma}_y$. The joint characteristic function can be written as

$$C(\chi,\mathcal{T}) = \frac{4\gamma + \mathcal{T}\left((\Omega_x - ia_{VQ}^{(2,2)}\chi_2)^2 - (i\Omega_y - a_{VQ}^{(1,1)}\chi_1)^2\right)}{4\gamma + \mathcal{T}\bar{\Omega}^2} e^{-\frac{1}{2}\sum_i S_{VV}^{(i,i)}\chi_i^2 \mathcal{T}}, \tag{3.40}$$

where $\bar{\Omega}^2 = \left(\Omega_x^2 + \Omega_y^2\right)$. This gives the average outputs

$$\bar{\mathcal{O}}_1 = \frac{2\Omega_y}{4\gamma + \mathcal{T}\bar{\Omega}^2}; \quad \bar{\mathcal{O}}_2 = -\frac{2\Omega_x}{4\gamma + \mathcal{T}\bar{\Omega}^2}.$$
 (3.41)

Therefore, both time-integrated outputs exhibit a sudden jump at a time scale of $\gamma/\bar{\Omega}^2$. The joint probability distribution of measurement outcomes can then be computed by Fourier transformation of the joint characteristic function (3.40), and is given by

$$P(\mathcal{O}_1, \mathcal{O}_2) = \frac{1}{4\gamma + \mathcal{T}\bar{\Omega}^2} \left(4\gamma + \mathcal{T} \left[\left(\Omega_x - \frac{4\mathcal{O}_2}{t_{a2}} \right)^2 + \left(\Omega_y + \frac{4\mathcal{O}_1}{t_{a1}} \right)^2 - \frac{4}{\mathcal{T}t_{a2}} - \frac{4}{\mathcal{T}t_{a1}} \right] \right) P_G(\mathcal{O}_1, \mathcal{O}_2). \tag{3.42}$$

Here, $t_{ai} \equiv 4S_{VV}^{(i,i)}/\left|a_{VQ}^{i,i}\right|^2$ are the acquisition times corresponding to each detector. For the simplest case of identical but independent detectors, $t_{a1} = t_{a2}$, this distribution is positive as long as $K \equiv \gamma t_a \ge 1$ (K = 1 corresponding to an ideal detector), which is always guaranteed by the corresponding Cauchy-Schwartz inequality (3.7).

It is instructive to inspect the forms of the distributions (3.39) and (3.42) to understand the main characteristics of such a measurement scenario. We do that by plotting the joint distributions and several cross sections of these joint distributions as the distribution of one integrated output given a specific result for the other integrated output. In Figures 3.1 and 3.2 we present this two distributions for a measurement time $\mathcal{T}=4/\Omega^2\,t_a$ and $\mathcal{T}=4/\bar{\Omega}^2\,t_a$ respectively. The first plot, (a) presents the joint distribution covering a huge range of detector outcomes due to the short measurement time \mathcal{T} . The sudden jump behaviour of the integrated output is visible at this time scale. The position of the peaks and the average integrated outputs in the $(\mathcal{O}_1,\mathcal{O}_2)$ plane for these distributions depend only on the choice of the Hamiltonian dynamics, as can be seen by comparing Figures 3.1 and 3.2.

In Fig. 3.1 (b) and (c) we present cross sections of the joint distribution (3.39). First, due to the asymmetry of the Hamiltonian with respect to the two detector outputs, the distributions for \mathcal{O}_1 (plot (a)) are intrinsically different than the distributions for \mathcal{O}_2 (plot (b)). While the average value of the integrated output \mathcal{O}_1 corresponding to the measurement of $\hat{\mathcal{O}}_1 = \hat{\sigma}_x$ is zero, the average integrated output of the second variable $\hat{\mathcal{O}}_2 = \hat{\sigma}_y$ can reach anomalously big values as explained by theory of weak values [21]. Figure (b) also shows how conditioning on results of the second integrated output, can be used to drastically change the distribution of the first integrated output, going from a noise-dominated distribution (full line curve for $\mathcal{O}_2 = -20$) to a well-resolved measurement (dashed-dotted curve for $\mathcal{O}_2 = 20$).

As noted above, with a proper choice of Hamiltonian, one can achieve anomalously large average integrated outputs in both variables. Thus, now using $\hat{H}_q = \hbar \frac{\Omega_x}{2} \hat{\sigma}_x + \hbar \frac{\Omega_y}{2} \hat{\sigma}_y$, in Fig. 3.2 (b) and (c) we present cross sections of the joint distribution (3.42). Here, the asymmetry between the two distributions (a) and (b) disappears and the maximum and minimum values are the same due to our choice of parameters ($\Omega_x = \Omega_y$).

In Sec. 3.7, we use the analytical results for the distribution in the limit of short time and zero overlap to check the positivity of the distribution of measurement outcomes for a more general set of detector noises and responses. We show that the positivity of the distribution is guaranteed provided the restriction (3.4).

3.5. Numerical results: Short time scales

In this section, we are going to numerically compute the full probability distribution of measurement outcomes in the same regime as in the previous section, but for experimental conditions. The measurement time is short compared to the Hamiltonian dynamics of our qubit and the state of the measured system does not vary significantly during this measurement time. For simplicity, in the reminder of this paper we will always consider vanishing cross noises, $S_{QV}^{(i,i)} = 0$, for a set of identical but independent detectors. However, the results can be numerically simulated and extended to any two variable measurement scenario.

To numerically study this limit and longer time intervals in the next Sec. 3.6, let us focus on 3 interesting cases:

- (i) An ideal detection case, where we numerically solve Eq. (3.1) with $\hat{H}_q = \hbar \frac{\Omega}{2} \hat{\sigma}_x$ and parameter values such that the inequality (3.7) becomes an equality. Meaning, all the decoherence is brought by the detectors back action and their rates assume the minimum permitted values, $K = t_a \gamma = 1$.
- (ii) An experimentally relevant case, where we numerically solve Eq. (3.6) with $\hat{H}_q = \hbar \frac{\Omega}{2} \hat{\sigma}_x$, $\gamma_{\downarrow} = (22.5 \mu \text{s})^{-1}$, $\gamma_{\uparrow} = (56 \mu \text{s})^{-1}$ and $\gamma_d = (15.6 \mu \text{s})^{-1}$. The acquisition time comes from the measurement rate $2/t_a \approx (92 \mu \text{s})^{-1}$ as given in [12].
- (iii) Finally, another experimentally relevant case, where we will again solve Eq. (3.6) but with a modified Hamiltonian, in which a rather strong detuning $\Delta \approx 1.7\Omega$ is applied to the qubit as $\hat{H}_q = \hbar \frac{\Omega}{2} \hat{\sigma}_x + \hbar \frac{\Delta}{2} \hat{\sigma}_z$. This value is chosen to maximize $\langle \mathcal{O}_1 \rangle$ for the equilibrium density matrix.

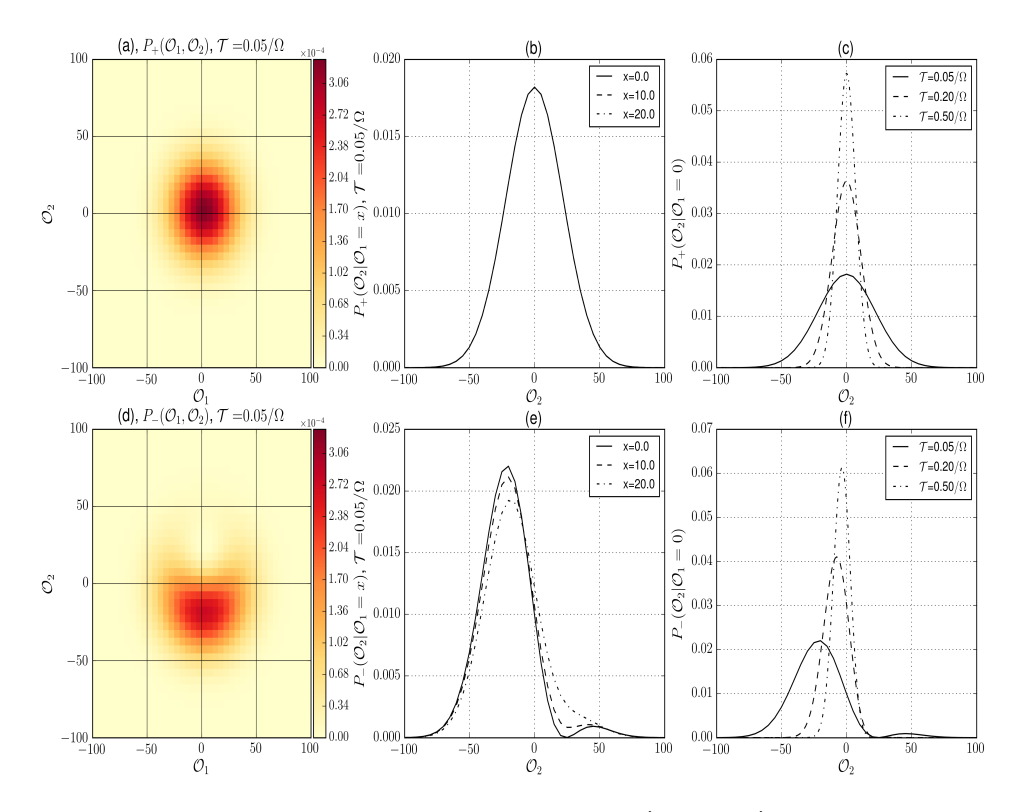


Figure 3.3: Output distributions for the simultaneous measurement of $\hat{\mathcal{O}}_1 = \hat{\sigma}_x$ and $\hat{\mathcal{O}}_2 = \hat{\sigma}_y$. The measurement with ideal detectors (case (i)) for $\mathcal{T} \ll \Omega^{-1}$ or comparable with Ω^{-1} . The qubit is prepared in $|Z^+\rangle$ and post selected at the end of the measurement: In $|Z^+\rangle$ for the first row of figures (plots (a), (b) and (c)); and in $|Z^-\rangle$ for the second row of figures (plots (d), (e) and (f)).

The distributions of the measurements for these three cases are presented in three different figures. Figure 3.3 for the ideal case, and Figures 3.4 and 3.5 for the experimentally relevant scenario without and including a strong qubit detuning respectively.

In these three figures, we plot the joint distribution for different combinations of preparation and post-selection states of the measured qubit. As well as cross sections of this distribution, meaning the distribution of a particular detector output given specific values for the other detector output. The first row of plots, (a), (b) and (c), presents these distributions for a qubit prepared in $|Z^+\rangle$ and post-selected after the measurement in $|Z^+\rangle$; we refer to this as P_+ . The second row of plots, (d), (e) and (f), presents these distributions for a qubit prepared in $|Z^+\rangle$ and post-selected in $|Z^-\rangle$; we refer to this as P_- .

Also, the first column of plots, (a) and (d), are density plots of the joint distribution of measurement outcomes $(P_+(\mathcal{O}_1,\mathcal{O}_2))$ and $P_-(\mathcal{O}_1,\mathcal{O}_2)$ for both measured variables and for the measurement time $\mathcal{T}=0.05\Omega^{-1}$. The second column of plots, (b) and (e), presents different conditioned distributions of the detector output \mathcal{O}_2 given specific values $\mathcal{O}_1=x$ of the other detector output $(P_+(\mathcal{O}_2|\mathcal{O}_1=x))$ and $P_-(\mathcal{O}_2|\mathcal{O}_1=x))$, again for a measure-

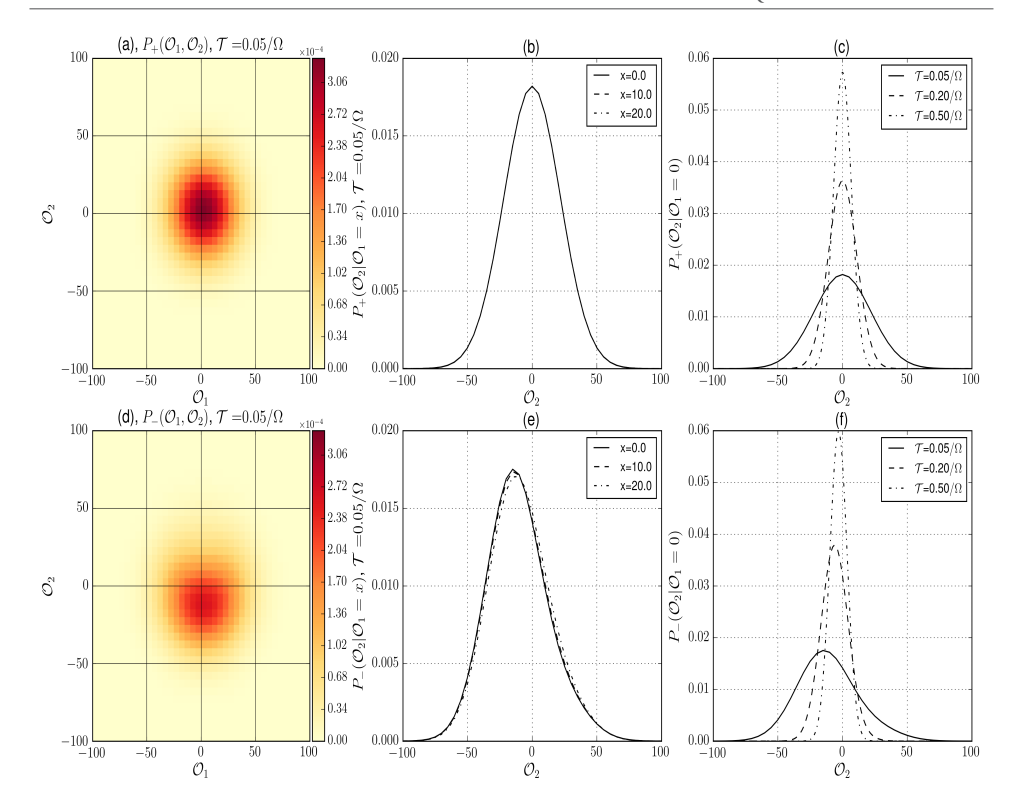


Figure 3.4: The measurement with non-ideal detectors and experimentally relevant parameters, case (ii). The qubit is prepared in $|Z^+\rangle$ and post selected at the end of the measurement: In $|Z^+\rangle$ state for the first row of figures (plots (a), (b) and (c)); and in $|Z^-\rangle$ for the second row of figures (plots (d), (e) and (f)).

ment time $\mathcal{T}=0.05\Omega^{-1}$. Finally, the third column of plots, (c) and (f), presents different conditioned distributions of the detector output \mathcal{O}_2 given a result of $\mathcal{O}_1=0$ of the other detector output $(P_+(\mathcal{O}_2|\mathcal{O}_1=0))$ and $P_-(\mathcal{O}_2|\mathcal{O}_1=0))$ for different measurement times $\mathcal{T}=0.05, 0.2, 0.5\Omega^{-1}$.

At this short measurement times, one expects these distributions to be dully Gaussian spreading over a large range of detector output values. This is seen in the upper row of plots. There is only one particular case, as we have shown previously, where this is not true. When the overlap between the preparation and post-selection states is zero. In second row of plots in Figures 3.3, 3.4 and 3.5, a sudden jump behaviour in the averaged integrated output appears, manifested in these figures as very non-Gaussian distribution shapes. There are small deviations in this numerical results because $\mathcal T$ is finite. The plots show anomalously large values for the average integrated output as big shifts in the distribution peaks, in agreement with the analytical results of the previous section. The agreement is visible if one compares Fig. 3.3 (e) with Fig. 3.1 (c).

As expected, this peculiarity is suppressed as the Hamiltonian dynamics start to be relevant ($\mathcal{T} \sim \Omega^{-1}$) as can be seen in the different curves at increasing time intervals in the third column of plots in Figures 3.3, 3.4 and 3.5. The shape of the distributions be-

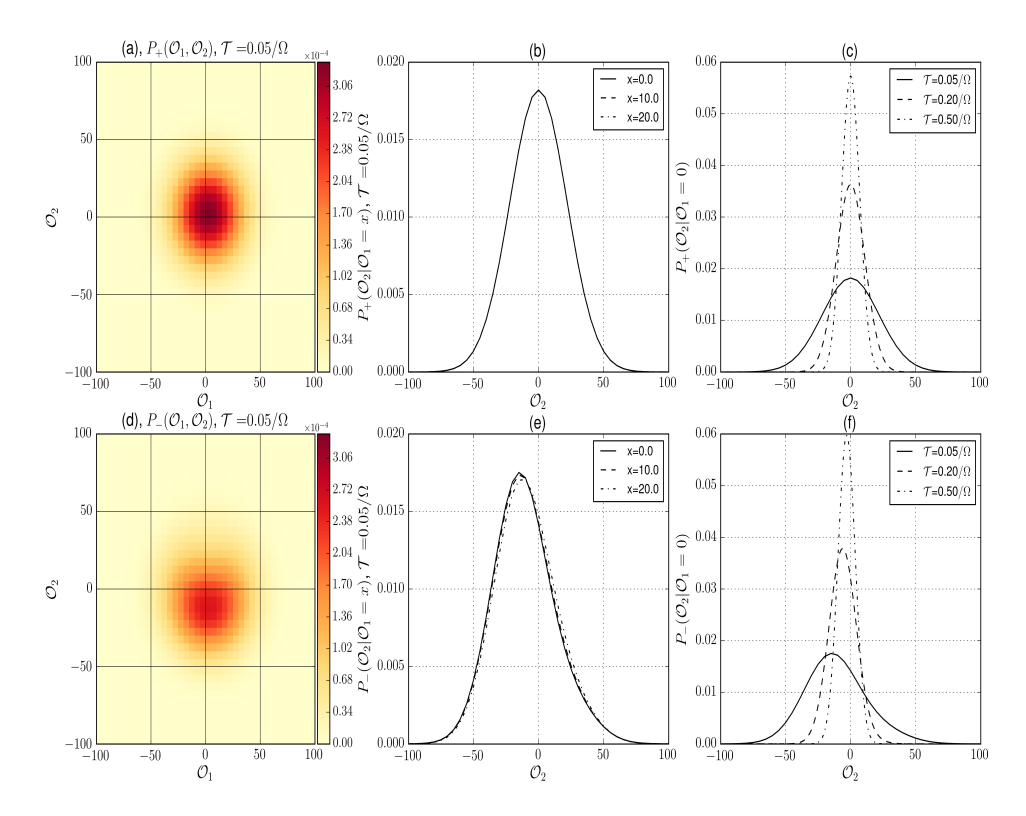


Figure 3.5: The measurement with non-ideal detectors and strong detuning, case (iii). The qubit is prepared in $|Z^+\rangle$ and post selected at the end of the measurement: In $|Z^+\rangle$ for the first row of figures (plots (a), (b) and (c)); and in $|Z^-\rangle$ for the second row of figures (plots (d), (e) and (f)).

comes more Gaussian as the detectors considered are less ideal. This can be seen when comparing the distributions for ideal detectors (Fig. 3.3) and experimentally relevant parameters (Fig. 3.4 and 3.5).

As the measurement time is short compared to the Hamiltonian dynamics, the qubit state changes insignificantly during the measurement. This fact is manifested in the sudden jump behaviour of the P_{-} distributions in the second row of plots, and in the fact that Figures 3.4 and 3.5 are almost the same. At these short measurement times, a difference in the Hamiltonian is not noticeable.

3.6. Numerical results: Longer time scales

In the previous section, we have presented the distributions of CWLM outcomes of the simultaneous measurement of two non-commuting variables in the limit of short measurement times. In this Section, we address the distributions of the CWLM outcomes of the simultaneous measurement of two non-commuting variables at time scales of the order of coherence/relaxation times and t_a .

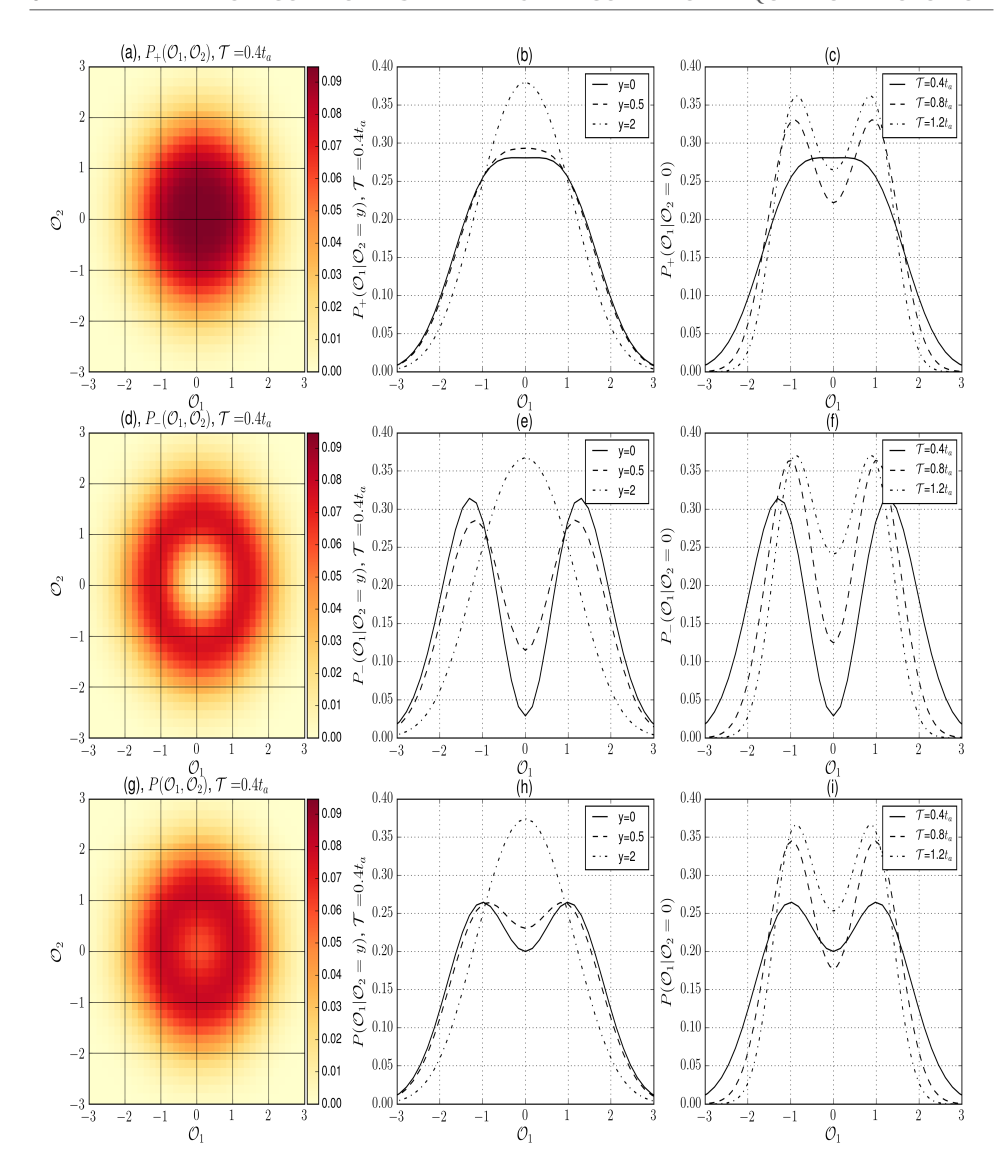


Figure 3.6: Output distributions for the simultaneous measurement of $\hat{\mathcal{O}}_1 = \hat{\sigma}_x$ and $\hat{\mathcal{O}}_2 = \hat{\sigma}_y$. The qubit is prepared in $|Z^+\rangle$ and post selected either in $|Z^+\rangle$ for the first row of figures (plots (a), (b) and (c)); or in $|Z^-\rangle$ for the second row of figures (plots (d), (e) and (f)). There is no post-selection for the last row of figures (plots (g), (h) and (i)). The measurement is performed with ideal detectors and no Hamiltonian dynamics are present during time intervals comparable to the acquisition time of the measurement setup. In this configuration, the peculiarities discussed in Sec. 3.3 are clearly visible in the joint distributions (plots (a), (d) and (g)).

To begin with, let us assume no Hamiltonian and ideal detectors (case (i) with no Hamiltonian). With this, the conditioned distribution of outcomes changes only at the

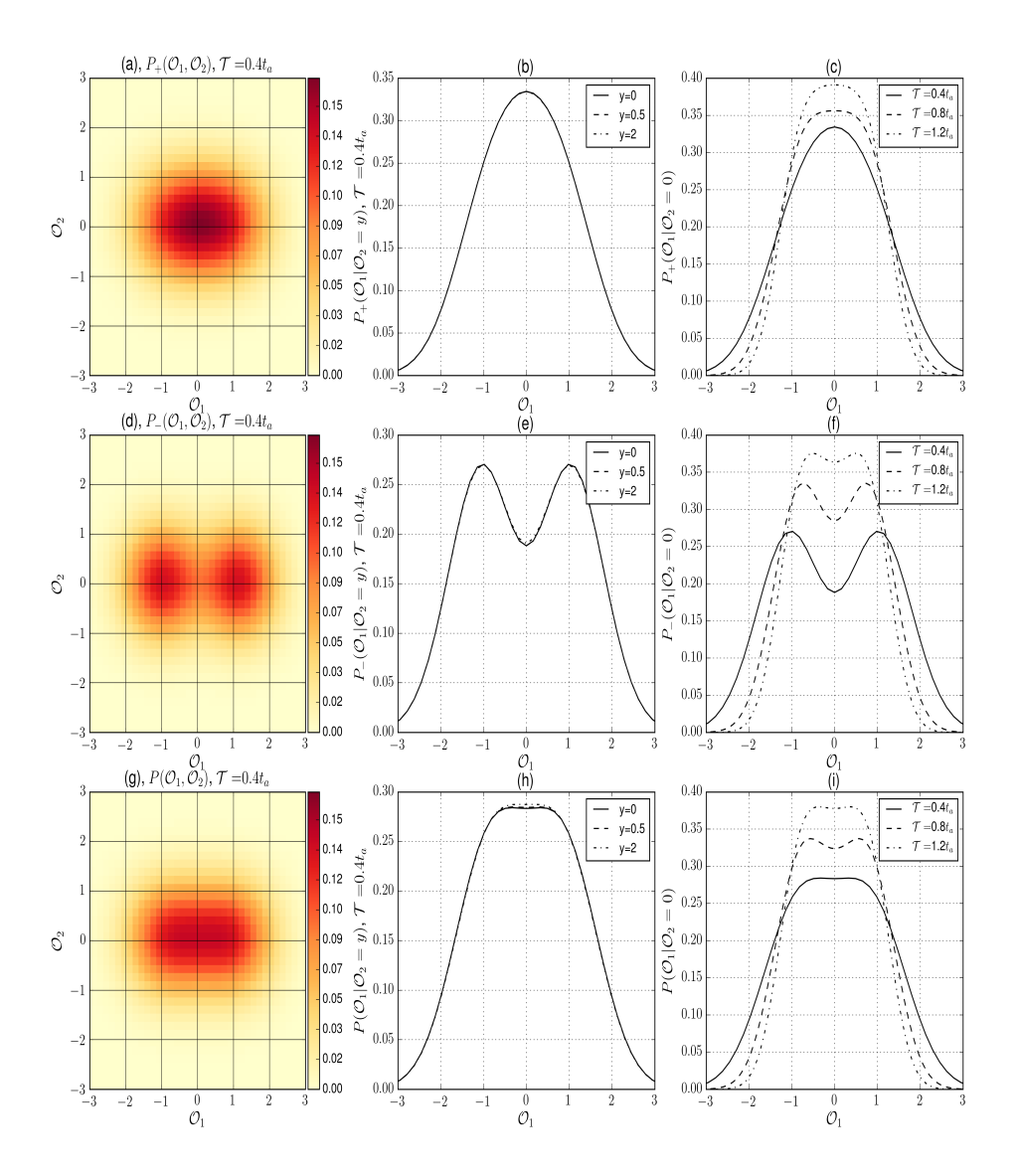


Figure 3.7: Here, the output distributions for a measurement performed with ideal detectors (case (i)) during time intervals comparable to the acquisition time of the measurement setup. The Hamiltonian drastically changes the type of peculiarities seen in the distributions. This can be seen by comparison with Figure 3.6.

time scale $t_a\simeq \gamma^{-1}$, that is much longer than Ω^{-1} , and the dynamics are described by Eq. (3.1) with vanishing $S_{QV}^{(i,i)}$ and \hat{H}_q terms. As discussed in Section 3.3, the pre and post-selection condition leads to peculiarities in

As discussed in Section 3.3, the pre and post-selection condition leads to peculiarities in the joint distribution that are located around the circle $\mathcal{O}_1^2 + \mathcal{O}_2^2 = 1$. These peculiarities should be visible in these conditions, at intermediate measurement times that are longer

than Ω^{-1} but short enough so that they are comparable to $t_a \simeq \gamma^{-1}$.

In fact, this is what we present in Fig. 3.6 when plotting the joint distributions (first column of plots; (a), (d) and (g)). The cross sections ((b), (e) and (h); and (c), (f) and (i)) show the expected half-quantization peculiarities characteristic of a single variable measurement, extensively discussed in [25]. In the last column of plots ((c), (f) and (i)) one could expect the separation of the distribution onto peaks at the limit $\mathcal{T}\gg t_a$. However, this is a signature of a quantum nondemolition measurement, and the fact that we inspect the simultaneous measurement of two non-commuting variables means that the measurement itself will induce rates causing transitions between the qubit states. Thus, not being a nondemolition measurement.

It is worth mentioning that the fact that all these distributions are symmetric under a change $\mathcal{O}_1 \leftrightarrow \mathcal{O}_2$ is due to the choice identical detectors and no Hamiltonian dynamics in any of those variables axes $(\hat{\mathcal{O}}_1 = \hat{\sigma}_x \text{ and } \hat{\mathcal{O}}_2 = \hat{\sigma}_y)$.

To clarify these observations, let us describe precisely the layout both for Fig. 3.6 and Fig. 3.7: The (a) plots show the joint distribution of measurement outcomes $P_+(\mathcal{O}_1,\mathcal{O}_2)$ for a qubit prepared in $|Z^+\rangle$ and post-selected in the same state after the measurement of duration $\mathcal{T}=0.4t_a$. The (d) plots show the joint distribution of measurement outcomes $P_-(\mathcal{O}_1,\mathcal{O}_2)$ for a qubit prepared in $|Z^+\rangle$ and post-selected in the orthogonal state $|Z^-\rangle$ after the measurement of duration $\mathcal{T}=0.4t_a$. The (g) plots show the joint distribution of measurement outcomes $P(\mathcal{O}_1,\mathcal{O}_2)$ for a qubit prepared in $|Z^+\rangle$ unconditioned to any post-selection after the measurement of duration $\mathcal{T}=0.4t_a$. Next, in the second column, the (b) plots present the conditioned distributions $P_+(\mathcal{O}_1|\mathcal{O}_2=y)$ of the first output, given a result $\mathcal{O}_2=y$ for the second output, again for a qubit prepared in $|Z^+\rangle$ and post-selected in the same state after the measurement of duration $\mathcal{T}=0.4t_a$. Respectively, the (e) and (h) plots, show the conditioned distributions $P_-(\mathcal{O}_1|\mathcal{O}_2=y)$ and $P(\mathcal{O}_1|\mathcal{O}_2=y)$. Finally, in the third column, we plot the conditioned distributions $P_+(\mathcal{O}_1|\mathcal{O}_2=y)$ and $P(\mathcal{O}_1|\mathcal{O}_2=0)$ in (c), $P_-(\mathcal{O}_1|\mathcal{O}_2=0)$ in (f), and $P(\mathcal{O}_1|\mathcal{O}_2=0)$ in (i); for different measurement duration $\mathcal{F}=0.4,0.8,1.2t_a$.

In contrast with the figures in the previous section, as the measurement time is big enough so that the qubit state changes appreciably during the measurement, we also plot the unconditioned distributions $P(\mathcal{O}_1,\mathcal{O}_2)$ now being clearly different than the distributions conditioned to a specific pot-selection $P_{\pm}(\mathcal{O}_1,\mathcal{O}_2)$.

Let us incorporate Hamiltonian dynamics to this measurement scenario, focusing now on case (i). If we keep the final state fixed to $|Z^{\pm}\rangle$, the contribution due to the conditioned evolution in these distributions will exhibit fast oscillations as function of \mathcal{T} with a period $2\pi/\Omega$. It is proficient from both theoretical and experimental considerations to quench these rather trivial oscillations. We achieve this by projecting the qubit after the measurement on the states $|\bar{Z}^{\pm}\rangle = e^{-i\hat{H}_q\mathcal{T}}|Z^{\pm}\rangle$ thereby correcting for the trivial qubit dynamics. In practice, such correction can be achieved by applying a short pulse rotating the qubit about x-axis right before the post-selection measurement.

With this, the asymmetry in the Hamiltonian with respect to the measured $\hat{\mathcal{O}}_1$ and $\hat{\mathcal{O}}_2$ variables will break the symmetry in the shape of the distributions. Then, the conditioned distributions for the output \mathcal{O}_2 are just Gaussian functions centered at $\mathcal{O}_2 = 0$ with their spread decreasing over time as $\sim 1/\sqrt{\mathcal{T}}$. Thus giving no information about

the output \mathcal{O}_2 at this time scale. That is why we choose to plot the conditioned distributions for the output \mathcal{O}_1 . This situation is presented in Fig. 3.7. The choice of Hamiltonian now collapses all these peculiarities due to the pre and post-selection conditions in one of the two outputs. This is perfectly visible in the shape of the joint distributions (plots (a), (d) and (g)). Not only that, but the addition of dynamics to the measured qubit results in a clear and strong suppression of the dependence of a given output on the other output outcomes as can be seen in plots (b), (e) and (h). Finally, if one compares the time evolution of these distributions (plots (c), (f) and (i)) for figures 3.6 and 3.7, the addition of dynamics to the measured qubit, results in a less resolved measurement, i.e., less separated peaks for a given measurement time \mathcal{T} .

Although this shows that the interference effect and peculiarities due to conditioned evolution are still visible at longer time scales for an ideal measurement scenario, it is also clear, that those signatures are suppressed by dynamics in the measured qubit. In fact, in an experimental situation, where external sources of decoherence are present, resolving those signatures might become a very challenging task. It is then important to inspect an experimentally relevant parameter regime in these numerical simulations.

To this end, one can inspect experimentally relevant scenarios like cases (ii) and (iii). It is good to note that the quality of the measurement setup in these conditions is far from ideal, $K = t_a \gamma_d \approx 12$, and at longer time scales, the decoherence completely dominates all the measurement dynamics. It is so that the distributions do not show visible characteristics of the conditioned qubit evolution. They appear to be just Gaussian distributions centered at zero value of the outcome variables.

In this case, it is more instructive to inspect the difference of two particular distributions, rather than the distribution itself. With that in mind, in Figures 3.8 and 3.9 we plot different differences of distributions. In Fig. 3.8 we consider case (ii). In Fig. 3.9 we consider case (iii). In doing so, not only we are interested in the phenomena related to conditioned qubit evolution, but also in the difference of simultaneous measurement of several variables from the single variable case.

These two figures are structured with the following layout: The (a) plots, show the difference of the distribution of the first output disregarding the second output and the distribution of the same first output given a specific result y for the second output, $P_+(\mathcal{O}_1) - P_+(\mathcal{O}_1|\mathcal{O}_2 = y)$. The (b) plots, show the same difference divided by its sum, $(P_+(\mathcal{O}_1) - P_+(\mathcal{O}_1|\mathcal{O}_2 = y))/(P_+(\mathcal{O}_1) + P_+(\mathcal{O}_1|\mathcal{O}_2 = y))$. Both for a qubit prepared in $|Z^+\rangle$ state and post-selected in the same state. The (c) plots, show again that difference but for a qubit prepared in $|Z^+\rangle$ and post-selected in $|Z^-\rangle$, i.e., $P_-(\mathcal{O}_1) - P_-(\mathcal{O}_1|\mathcal{O}_2 = y)$. Respectively, (d) show that difference divided by the sum, $(P_-(\mathcal{O}_1) - P_-|\mathcal{O}_1|\mathcal{O}_2 = y))/(P_-(\mathcal{O}_1) + P_-(\mathcal{O}_1|\mathcal{O}_2 = y))$. These differences give an estimation of the correlation between the two outputs in these measurements, or the separability of the joint distribution.

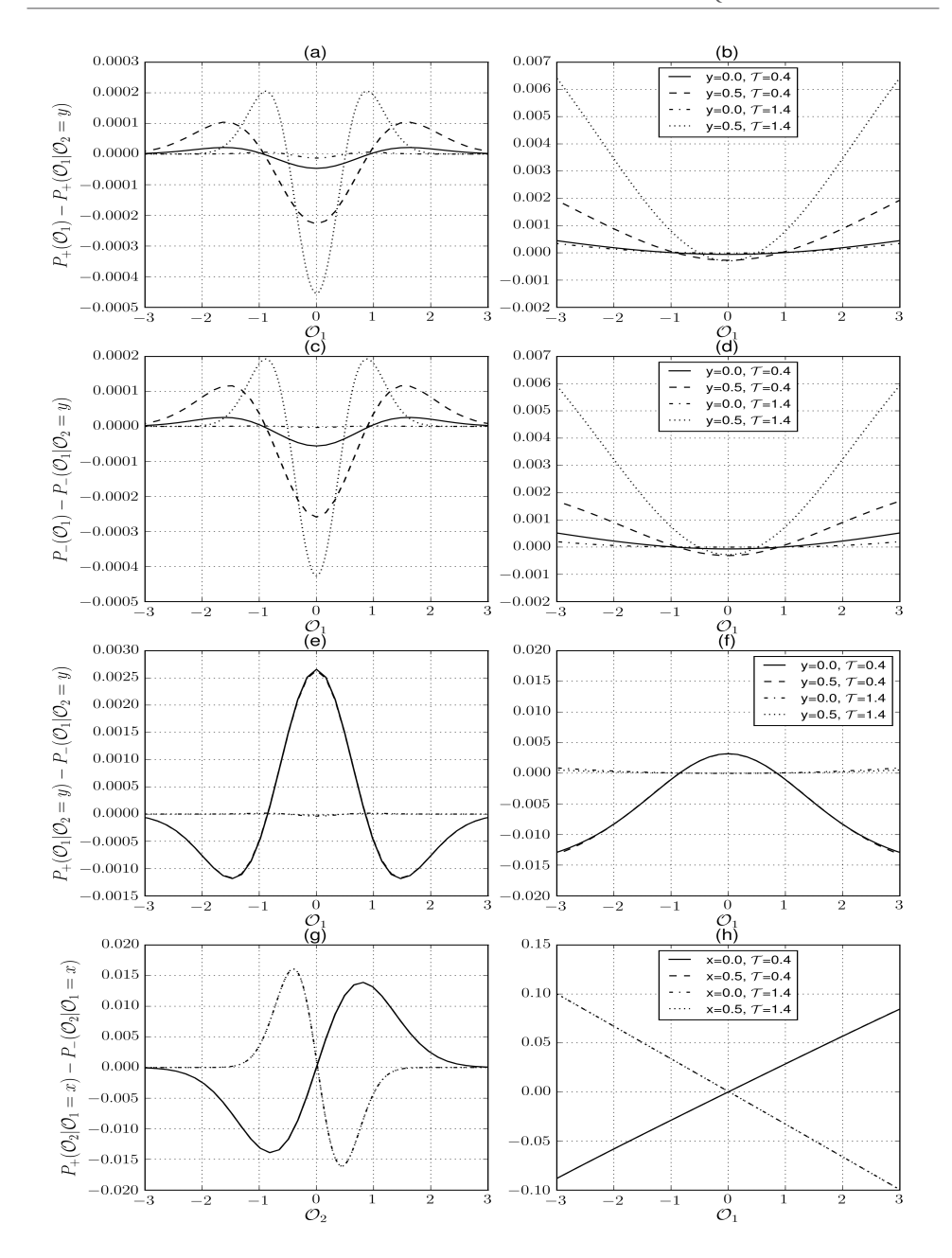


Figure 3.8: Differences of distributions at measurement times of the order of the acquisition time t_a under experimentally relevant measurement conditions, case (ii). The layout is described in detail in Sec. 3.6 in the main text.

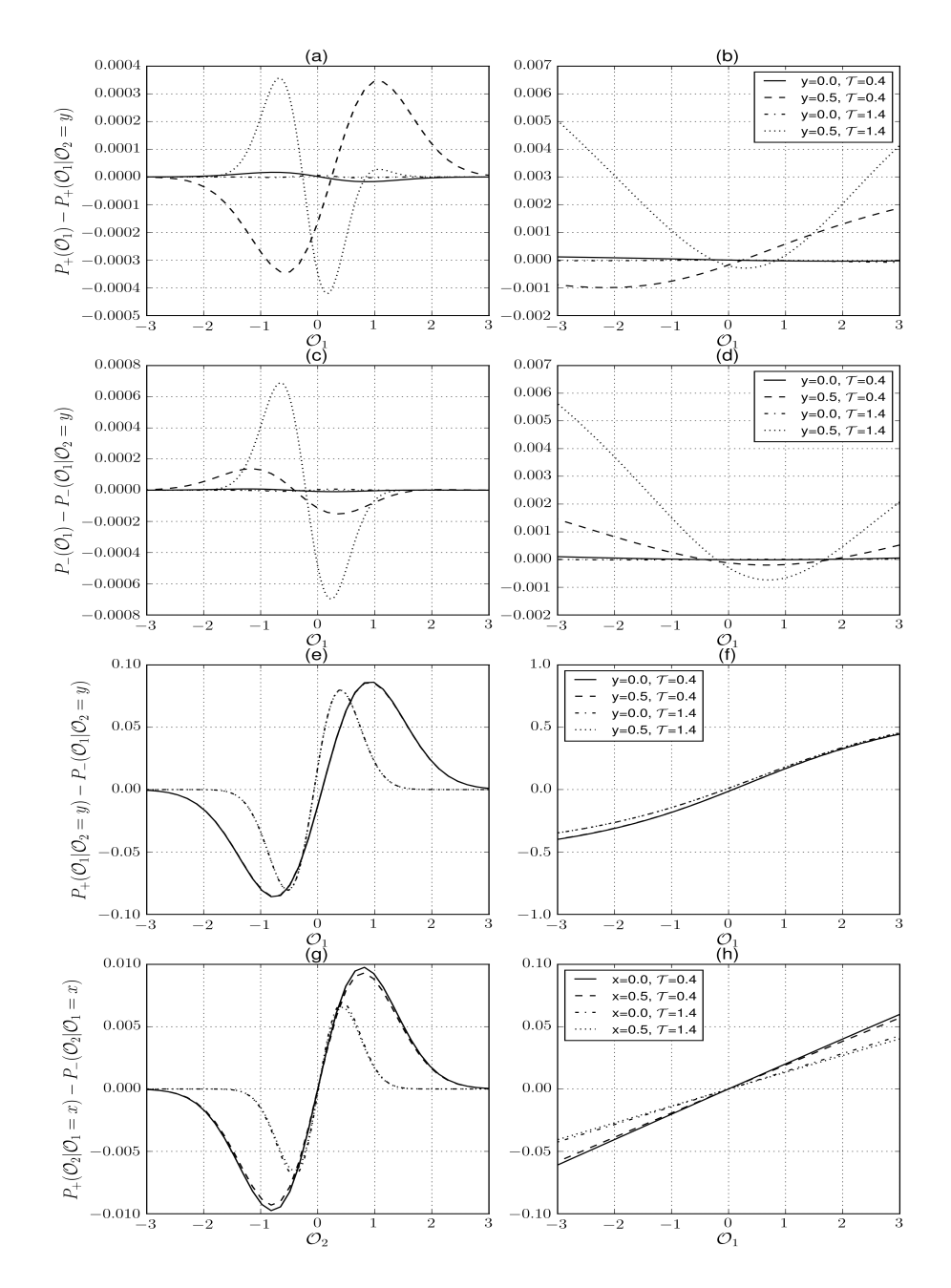


Figure 3.9: Differences of distributions taken at measurement times of the order of the acquisition time t_a and at nonzero detuning, case (iii). The layout is the same as in previous Figure 3.8.

Next, the (e) plots show the difference between the distribution of the first output given a specific result y for the second output for a qubit prepared in $|Z^+\rangle$ and post-

selected in the same state; and the distribution of the first output given a specific result y for the second output for a qubit prepared in $|Z^+\rangle$ and post-selected in $|Z^-\rangle$. That is $P_+(\mathcal{O}_1|\mathcal{O}_2=y)-P_-(\mathcal{O}_1|\mathcal{O}_2=y)$. Again, the (f) plots show this difference divided by their sum, $(P_+(\mathcal{O}_1|\mathcal{O}_2=y)-P_-(\mathcal{O}_1|\mathcal{O}_2=y))/(P_+(\mathcal{O}_1|\mathcal{O}_2=y)+P_-(\mathcal{O}_1|\mathcal{O}_2=y))$. Finally, the (g) plots show the same difference, but for the distributions of the second output given a specific result x for the first output: $P_+(\mathcal{O}_2|\mathcal{O}_1=x)-P_-(\mathcal{O}_2|\mathcal{O}_1=x)$. Respectively (h) show that difference divided by their sum, $(P_+(\mathcal{O}_2|\mathcal{O}_1=x)-P_-(\mathcal{O}_2|\mathcal{O}_1=x))/(P_+(\mathcal{O}_2|\mathcal{O}_1=x)+P_-(\mathcal{O}_2|\mathcal{O}_1=x))$.

The reason for inspecting these last differences is simple, we want to have an estimation for the resolution of any signature that is due to the conditioned evolution of the measured system. Thus, inspecting the difference between the two limiting cases of this conditioned evolution, i.e., same pre and post-selection and orthogonal pre and post-selection; shows how strong these signatures are. Furthermore, these differences divided by their sums, quantify how much these signatures can be resolved by using the output distributions of such measurements. Or in other words, the certainty with which one can distinguish two distributions from each other given a measurement reading: [25]

$$C(\mathcal{O}_i|\mathcal{O}_j = \alpha) = \frac{P_+(\mathcal{O}_i|\mathcal{O}_j = \alpha) - P_-(\mathcal{O}_i|\mathcal{O}_j = \alpha)}{P_+(\mathcal{O}_i|\mathcal{O}_j = \alpha) + P_-(\mathcal{O}_i|\mathcal{O}_j = \alpha)}$$
(3.43)

The values $C = \pm 1$ would imply that the measurement is *certainly* post-selected in $|Z^{\pm}\rangle$.

In this experimental regime at zero detuning, Fig. 3.8, the differences of distributions (a) and (c), reveal that the two outputs are still correlated, and this correlation seems to be bigger for given values of the outputs that are farther away from the origin where the distributions peak at such time scales. Nevertheless, it is very small, as the joint distribution quickly becomes a Gaussian due to decoherence and relaxation. At big values of \mathcal{O}_1 , the difference quickly decreases together with the distributions. In this respect, it is instructive to inspect the difference normalized on the sum of the probability densities. As we see from (b) and (d), this quantity increases with increasing \mathcal{O}_1 , reaches relatively large values at increasing $\mathcal{O}_2 = \gamma$ results due to their low statistical weight, and seems to remain relevant at a small region $\mathcal{O}_1 \sim 0$ even for big times. This region is more relevant because this quantity is not suppressed or increased due to exponentially low probabilities for those values, it is rather a direct measure of the correlation of the two outputs. The signatures of the conditioned evolution are revealed by the differences in (e) and (g). As expected due to the form of the Hamiltonian (on $\hat{\mathcal{O}}_1 = \hat{\sigma}_x$ axis), (e) is very different from (g). In (e), the shape of the difference suggests that the $P_{-}(\mathcal{O}_{1}|\mathcal{O}_{2}=y)$ is pushed on both positive and negative values of \mathcal{O}_1 in comparison with $P_+(\mathcal{O}_1|\mathcal{O}_2=y)$, in agreement with the previous findings. The decoherence and relaxation quickly diminish the difference upon increasing \mathcal{T} . Inspecting the certainty in (f), it saturates with increasing \mathcal{O}_1 , reaches relatively large values at short \mathcal{T} , and fades away upon increasing \mathcal{T} . Note that at short $\mathcal{T} = 0.4t_a$ this relative difference achieves 0.002 at $\mathcal{O}_1 \approx 0$ and can be thus revealed from the statistics of several hundred individual measurements. For the second output \mathcal{O}_2 , the differences in (g) are an order of magnitude bigger than those for the \mathcal{O}_1 distributions in plot (e). Not only that, but the difference does not vanish in the limit

of big \mathcal{T} . Rather, it is concentrated in an increasingly narrow interval of \mathcal{O}_2 conforming to the decreasing width of the distribution. It is worth noting that they also change sign as \mathcal{T} increases. For short times, the shape of $P_-(\mathcal{O}_2|\mathcal{O}_1=x)$ resembles the shape of the distribution at the sudden jump regime (Fig. 3.4), as the time \mathcal{T} increases, the distributions are shifted depending on the post-selected state. This is not the case for the \mathcal{O}_1 output discussed previously because of the chosen Hamiltonian. As to the certainty in (h), it shows a linear behaviour with \mathcal{O}_2 , $C(\mathcal{O}_2|\mathcal{O}_1=x)=\beta\mathcal{O}_2$. The sign of β depends on the sign of the shift in the distributions, and the linear behaviour can be explained in the limit of small shifts. This does not imply that the distributions are different in this limit since they become concentrated with divergent probability density, and the values of \mathcal{O}_2 with high certainty occur with exponentially low probability. This is discussed in detail Section V of [25].

Let us inspect these differences of distributions at nonzero detuning in Fig. 3.9. In this case, there is no reason to expect the $\mathcal{O}_1 \to -\mathcal{O}_1$ symmetry in the distributions, or in turn, the differences. Again the differences showed in (a), (b), (c) and (d); reveal small correlations between the two outputs still in the presence of detuning. These are bigger when the distributions are conditioned with values at bigger distances from the origin. The differences of the probability distributions presented in (e) and (g) seem to be at least one order of magnitude bigger for the distributions of the first output in (e), compared to the zero detuning case in Fig. 3.8. And, for both outputs, the difference does not vanish in the limit of big $\mathcal T$. Rather, it is concentrated in an increasingly narrow interval of $\mathcal{O}_{1,2}$ conforming to the decreasing width of the distribution. This suggests that adding a strong detuning can increase the detection resolution, and reveal these distribution differences from the statistics of fewer individual measurements. However, as mentioned before, the certainties (f) and (g), rather quickly converge when increasing \mathcal{F} to finite and and rather big values in a wide interval of the output $\mathcal{O}_{1,2}$ in question. Again this do not imply that the distributions are fundamentally different in this limit since they become concentrated with divergent probability densities. For the certainty of the second output distributions in (h), a linear behaviour appears due to the small shifts limit of the distributions.

It is worth noting, that although the joint distribution of measurement outcomes effectively becomes a product distribution $P(\mathcal{O}_1,\mathcal{O}_2)\approx P(\mathcal{O}_1)P(\mathcal{O}_2)$, meaning the correlations between the two non-commuting variables are lost rather fast, when increasing \mathcal{F} . The signature of interference due to the conditioned dynamics in the probability distribution can still be revealed from the statistics of several hundred individual measurements in experimental conditions.

3.7. Positivity of the distribution

Here we present the derivation of the inequality (3.4) from the analytical procedure used in Sec. 3.4 to derive the joint distribution of measurement outcomes at short times \mathcal{T} and given a vanishing overlap between preparation and post-selection states, $\langle i|\Psi\rangle=0$. To do so, we focus first on the simple setup considered in the main text. Next, we add different correlations between the two detectors, understand what they add to the pic-

ture and derive a more general restriction.

To start with, note that for any pair of operators \hat{Q}, \hat{V} it is possible to construct a Cauchy-Schwarz inequality of the following form [28]:

$$\left|S_{QQ}(\omega)S_{VV}(\omega) - \left|S_{QV}(\omega)\right|^2 \ge \left|\frac{\hbar}{2}(a_{VQ}(\omega) - a_{QV}(\omega))\right|^2 \left(1 + \Delta \left[\frac{S_{QV}(\omega)}{\frac{\hbar}{2}(a_{VQ}(\omega) - a_{QV}(\omega))}\right]\right)$$
(3.44)

where

$$\Delta[z] = [|1 + z^2| - (1 + |z|^2)]/2. \tag{3.45}$$

In the limit of zero frequency, this reproduces the inequality (3.7).

However, in the case where we have more than one detector or measured variable, i.e., more than one pair of input-output variables \hat{Q}, \hat{V} , there are additional inequalities restricting the correlators between input-output variables pertaining to these different pairs. An easy way to see this is to inspect the distribution we calculated for short time scales, Eq. (3.39). It describes the case of independent detectors without cross noises. Let us find the conditions for it to be positive at all values of $\mathcal{O}_{1,2}$. This condition reads:

$$\gamma \ge \frac{1}{t_{a1}} + \frac{1}{t_{a2}}.\tag{3.46}$$

For us, the inequality can be written as,

$$S_{QQ}^{(1,1)} + S_{QQ}^{(2,2)} \ge \frac{\hbar^2}{4} \left(\frac{\left| a_{VQ}^{(1,1)} \right|^2}{S_{VV}^{(1,1)}} + \frac{\left| a_{VQ}^{(2,2)} \right|^2}{S_{VV}^{(2,2)}} \right). \tag{3.47}$$

We write this assuming the condition of a good amplifier, that is, the direct gain exceeds much the reverse one [28], $a_{VQ}^{(1,1)}\gg a_{QV}^{(1,1)}$. All results presented here can be extended to a more general situation by replacing $a_{VQ}^{(i,i)}$ with the difference $a_{VQ}^{(i,i)}-a_{QV}^{(i,i)}$. This inequality can be constructed as the sum of two inequalities of the form (3.3) for the two sets of input-output variables involved. This fact explicitly shows that this inequality does not add any more restrictions to the correlators than the ones that come from the aforementioned Cauchy-Schwarz inequalities.

Now, let us derive the distribution at short time for a more general case where the cross noises and correlations are present, and then check the condition for positivity once again.

Firstly, for any correlations between output variables, meaning $S_{VV}^{(1,2)} = S_{VV}^{(2,1)} \neq 0$, the distribution (3.39) will change, however, the condition for positivity will not. In particular, adding correlations between output variables modifies it in the following way,

$$P(\mathcal{O}_{1},\mathcal{O}_{2}) = \frac{1}{4\gamma + \mathcal{T}\bar{\Omega}^{2}} \left(4\gamma + \mathcal{T} \left[\left(\Omega_{x} - \frac{4\mathcal{O}_{2}}{t_{a2}} - \frac{2\mathcal{O}_{1}S_{VV}^{(1,2)}}{a_{VQ}^{(2,2)}a_{VQ}^{(1,1)}} \right)^{2} + \left(\Omega_{y} + \frac{4\mathcal{O}_{1}}{t_{a1}} + \frac{2\mathcal{O}_{2}S_{VV}^{(1,2)}}{a_{VQ}^{(2,2)}a_{VQ}^{(1,1)}} \right)^{2} - \frac{4}{\mathcal{T}t_{a2}} - \frac{4}{\mathcal{T}t_{a1}} \right] P_{G}(\mathcal{O}_{1},\mathcal{O}_{2}).$$
(3.48)

The positivity of the distribution is again guaranteed by the same condition (3.47). Let us now introduce cross noises between input-output, i.e., $S_{QV}^{(1,1)}$, $S_{QV}^{(2,2)}$, $S_{QV}^{(1,2)}$, $S_{QV}^{(2,1)} \neq 0$. The distribution of measurement outcomes can then be approximated as

$$\begin{split} P(\mathcal{O}_{1},\mathcal{O}_{2}) &= \frac{1}{4\gamma + \mathcal{F}\bar{\Omega}^{2}} \left[4\gamma + \mathcal{F} \left(\left[\Omega_{x} + \left(\frac{2S_{QV}^{(1,2)}}{a_{V,Q}^{(2,2)}} - 1 \right) \frac{\mathcal{O}_{2}}{\mathcal{F}\sigma_{2}^{2}} + \frac{2S_{QV}^{(1,1)}}{a_{V,Q}^{(1,1)}} \frac{\mathcal{O}_{1}}{\mathcal{F}\sigma_{1}^{2}} \right)^{2} \right. \\ &\quad + \left(\Omega_{y} + \left(1 + \frac{2S_{QV}^{(2,1)}}{a_{V,Q}^{(1,1)}} \frac{\mathcal{O}_{1}}{\mathcal{F}\sigma_{1}^{2}} \right) + \frac{2S_{QV}^{(2,2)}}{a_{V,Q}^{(2,2)}} \frac{\mathcal{O}_{2}}{\mathcal{F}\sigma_{2}^{2}} \right)^{2} \\ &\quad - \left(1 - \frac{2S_{QV}^{(1,2)}}{a_{V,Q}^{(2,2)}} \right)^{2} \frac{1}{\mathcal{F}^{2}\sigma_{2}^{2}} - \left(\frac{2S_{QV}^{(1,1)}}{a_{V,Q}^{(1,1)}} \right)^{2} \frac{1}{\mathcal{F}^{2}\sigma_{1}^{2}} \\ &\quad - \left(1 + \frac{2S_{QV}^{(2,1)}}{a_{V,Q}^{(1,1)}} \right)^{2} \frac{1}{\mathcal{F}^{2}\sigma_{1}^{2}} - \left(\frac{2S_{QV}^{(2,2)}}{a_{V,Q}^{(2,2)}} \right)^{2} \frac{1}{\mathcal{F}^{2}\sigma_{2}^{2}} \right) \left[P_{G}(\mathcal{O}_{1},\mathcal{O}_{2}). \end{split} \tag{3.49}$$

Here, $\sigma_i^2 = t_{ai}/4\mathcal{T}$.

For this distribution to be positive we have the following condition,

$$\gamma - \left(1 - \frac{2S_{QV}^{(1,2)}}{a_{V,Q}^{(2,2)}}\right)^2 \frac{1}{t_{a2}} - \left(\frac{2S_{QV}^{(1,1)}}{a_{V,Q}^{(1,1)}}\right)^2 \frac{1}{t_{a1}} - \left(1 + \frac{2S_{QV}^{(2,1)}}{a_{V,Q}^{(1,1)}}\right)^2 \frac{1}{t_{a1}} - \left(\frac{2S_{QV}^{(2,2)}}{a_{V,Q}^{(2,2)}}\right)^2 \frac{1}{t_{a2}} \ge 0; \quad (3.50)$$

which one can write as

$$\begin{split} S_{QQ}^{(1,1)} + S_{QQ}^{(2,2)} &\geq \frac{\hbar^2}{4} \left[\left(\left(a_{V,Q}^{(2,2)} - 2 S_{QV}^{(1,2)} \right)^2 + \left(2 S_{QV}^{(2,2)} \right)^2 \right) \frac{1}{S_{VV}^{(2,2)}} \\ &\quad + \left(\left(a_{V,Q}^{(1,1)} + 2 S_{QV}^{(2,1)} \right)^2 + \left(2 S_{QV}^{(1,1)} \right)^2 \right) \frac{1}{S_{V,V}^{(1,1)}} \right]. \end{split} \tag{3.51}$$

Conversely, if one takes the initial state to be $|Z^-\rangle$ and the final projection to be $|Z^+\rangle$, then the condition becomes:

$$\begin{split} S_{QQ}^{(1,1)} + S_{QQ}^{(2,2)} &\geq \frac{\hbar^2}{4} \left[\left(\left(a_{V,Q}^{(2,2)} + 2S_{QV}^{(1,2)} \right)^2 + \left(2S_{QV}^{(2,2)} \right)^2 \right) \frac{1}{S_{VV}^{(2,2)}} \\ &\quad + \left(\left(a_{V,Q}^{(1,1)} - 2S_{QV}^{(2,1)} \right)^2 + \left(2S_{QV}^{(1,1)} \right)^2 \right) \frac{1}{S_{V,V}^{(1,1)}} \right]. \end{split} \tag{3.52}$$

The probability distribution of measurement outcomes should remain positive regardless of the initial and final conditions. Thus, both these inequalities (3.51) and (3.52), have to be fulfilled. Taking this into account, one can write the inequality (3.4), where inverse susceptibilities are added back, owing to the possibility of bad amplifiers.

This shows that the existence of cross noises between input-output of different detectors imposes a stronger restriction on the possible values for the set of noises and response functions defining a measurement scenario than the usual Cauchy-Schwarz inequalities considered. It is worth noting that we did not consider non-vanishing responses between input-output of different detectors. The analysis can be extended to this case with even more complex restrictions on the correlators for the positivity of the distribution of measurement outcomes.

3.8. CONCLUSION

In this work, we put forward a proper theoretical formalism based on full counting statistics approach [6, 24] to describe and evaluate the measurement statistics in the course of conditioned quantum evolution. We extend the previous work [25] to the simultaneous measurement of two non-commuting variables. We illustrate this formalism with several examples and prove that the interesting features arising from the conditioned quantum evolution can be seen in the statistics of the measurement outcomes for both short and relatively long measurement intervals. We also reveal the interplay between the two non-commuting variables statistics and the signatures of the conditioned dynamics in the individual and joint distributions.

We describe and investigate two signatures of the conditioned statistics that are related to quantum interference effects. First is the appearance of peculiarities at the circle $\mathcal{O}_1^2 + \mathcal{O}_2^2 = 1$ in the distribution of measurement outcomes, that is revealed by a quasi-distribution of shifts located at the compact support $\mathcal{O}_1^2 + \mathcal{O}_2^2 = 1$, $\mathcal{O}_1^2 + \mathcal{O}_2^2 = 0$ as well as inside the circle $\mathcal{O}_1^2 + \mathcal{O}_2^2 < 1$. This provides a connection with what we termed *half-quantized* measurement values for the single variable measurement case, as the distribution function may display peculiarities, that are either peaks or dips, at half-sums of the quantized values. In the special case of zero overlap between initial and final states and time intervals that are so short as the wave function of the system does not significantly change by either Hamiltonian or dissipative dynamics. We reveal unexpectedly large values of the time-integrated output cumulants for such short intervals, that we termed *sudden jump*. We show that a simultaneous jump in integrated output can be achieved in both measured variables given an appropriate choice of Hamiltonian. This effect is felt in a short time scale γ/Ω^2 where γ^{-1} is the time scale of dissipative dynamics

and Ω^{-1} is the time scale of Hamiltonian dynamics. Additionally our results show that it is possible to achieve bigger saturation values for these anomalously big averages when further conditioning the statistics of one output with the results of other outputs.

Our results show that it is possible to have very detailed theoretical predictions of CWLM distributions. In particular, we show how to use this formalism to account for conditioned quantum evolution and simultaneous non-commuting variable measurements in the paradigm of CWLM. This opens the possibility for investigation and characterization of quantum effects even if the choice of parameters is far from ideal and the effects are small.

The signatures in the distributions that we predict in this paper can be seen in realistic experimental regimes. One of the key elements to experimentally observe this effects is the ability to efficiently record time traces for a weak continuous monitoring of one or rather, several qubit variables, and this has been achieved in several papers [9–15, 18] applying it for the observation of qubit trajectories or real-time feedback. Thus, we believe it is possible to extract these kind of statistics from the existing records of several experiments.

REFERENCES

- [1] M. Nielsen and I. Chuang, *Quantum Computation and Quantum Information* (Cambridge University Press, 2000).
- [2] M. B. Mensky, *The action uncertainty principle in continuous quantum measurements*, Physics Letters A **155**, 229 (1991).
- [3] A. N. Korotkov, *Continuous quantum measurement of a double dot*, Phys. Rev. B **60**, 5737 (1999).
- [4] A. Jordan and M. Buttiker, *Continuous quantum measurement with independent detector cross correlations*, Phys. Rev. Lett. **95**, 220401 (2005).
- [5] K. Jacobs and D. A. Steck, *A straightforward introduction to continuous quantum measurement*, Contemporary Physics **47**, 279 (2006), http://dx.doi.org/10.1080/00107510601101934.
- [6] H. Wei and Y. V. Nazarov, *Statistics of measurement of noncommuting quantum variables: Monitoring and purification of a qubit,* Phys. Rev. B **78**, 045308 (2008).
- [7] A. Chantasri and A. N. Jordan, *Stochastic path-integral formalism for continuous quantum measurement*, Phys. Rev. A **92**, 032125 (2015).
- [8] A. Chantasri, J. Dressel, and A. N. Jordan, *Action principle for continuous quantum measurement*, Phys. Rev. A **88**, 042110 (2013).

- [9] M. Hatridge, S. Shankar, M. Mirrahimi, F. Schackert, K. Geerlings, T. Brecht, K. M. Sliwa, B. Abdo, L. Frunzio, S. M. Girvin, R. J. Schoelkopf, and M. H. Devoret, *Quantum back-action of an individual variable-strength measurement*, Science 339, 178 (2013).
- [10] K. W. Murch, S. J. Weber, C. Macklin, and I. Siddiqi, *Observing single quantum trajectories of a superconducting quantum bit*, Nature **502**, 211 (2013).
- [11] N. Roch, M. E. Schwartz, F. Motzoi, C. Macklin, R. Vijay, A. W. Eddins, A. N. Korotkov, K. B. Whaley, M. Sarovar, and I. Siddiqi, *Observation of measurement-induced entanglement and quantum trajectories of remote superconducting qubits*, Phys. Rev. Lett. 112, 170501 (2014).
- [12] P. Campagne-Ibarcq, L. Bretheau, E. Flurin, A. Auffèves, F. Mallet, and B. Huard, *Observing interferences between past and future quantum states in resonance fluo-rescence*, Phys. Rev. Lett. **112**, 180402 (2014).
- [13] J. P. Groen, D. Ristè, L. Tornberg, J. Cramer, P. C. de Groot, T. Picot, G. Johansson, and L. DiCarlo, *Partial-measurement backaction and nonclassical weak values in a superconducting circuit*, Phys. Rev. Lett. 111, 090506 (2013).
- [14] S. J. Weber, A. Chantasri, J. Dressel, A. N. Jordan, K. W. Murch, and I. Siddiqi, *Mapping the optimal route between two quantum states*, Nature **511**, 570 (2014).
- [15] D. Tan, S. J. Weber, I. Siddiqi, K. Mølmer, and K. W. Murch, *Prediction and retrodiction for a continuously monitored superconducting qubit*, Phys. Rev. Lett. 114, 090403 (2015).
- [16] R. Ruskov, A. N. Korotkov, and K. Mølmer, *Qubit state monitoring by measurement of three complementary observables*, Phys. Rev. Lett. **105**, 100506 (2010).
- [17] L. P. García-Pintos and J. Dressel, *Probing quantumness with joint continuous measurements of noncommuting qubit observables*, Phys. Rev. A **94**, 062119 (2016).
- [18] S. Hacohen-Gourgy, L. S. Martin, E. Flurin, V. V. Ramasesh, K. B. Whaley, and I. Siddiqi, *Quantum dynamics of simultaneously measured non-commuting observables*, Nature **538**, 491 (2016).
- [19] J. Atalaya, S. Hacohen-Gourgy, M. S. Leigh, I. Siddiqi, and A. N. Korotkov, *Correlators in simultaneous measurement of non-commuting qubit observables*, arXiv:1702.08077 [quant-ph] (2017).
- [20] Y. Yamamoto and H. A. Haus, *Preparation, measurement and information capacity of optical quantum states*, Rev. Mod. Phys. **58**, 1001 (1986).
- [21] Y. Aharonov, D. Z. Albert, and L. Vaidman, *How the result of a measurement of a component of the spin of a spin-1/2 particle can turn out to be 100*, Phys. Rev. Lett. **60**, 1351 (1988).

References 75

[22] H. M. Wiseman, *Weak values, quantum trajectories, and the cavity-qed experiment on wave-particle correlation,* Phys. Rev. A **65**, 032111 (2002).

- [23] S. Gammelmark, B. Julsgaard, and K. Mølmer, *Past quantum states of a monitored system*, Phys. Rev. Lett. 111, 160401 (2013).
- [24] Y. V. Nazarov and M. Kindermann, *Full counting statistics of a general quantum me-chanical variable*, The European Physical Journal B Condensed Matter and Complex Systems **35**, 413 (2003).
- [25] A. Franquet and Y. V. Nazarov, *Probability distributions of continuous measurement results for conditioned quantum evolution*, Phys. Rev. B **95**, 085427 (2017).
- [26] Y. V. Nazarov and J. Danon, *Advanced Quantum Mechanics: A practical guide* (Cambridge University Press, 2013).
- [27] H. Wiseman and G. Milburn, *Quantum theory of optical feedback via homodyne detection*, Phys.Rev. Lett. **70**, 548 (1993).
- [28] A. A. Clerk, M. H. Devoret, S. M. Girvin, F. Marquardt, and R. J. Schoelkopf, *Introduction to quantum noise, measurement, and amplification*, Rev. Mod. Phys. **82**, 1155 (2010).

3



STATISTICS OF CONTINUOUS WEAK QUANTUM MEASUREMENT OF AN ARBITRARY QUANTUM SYSTEM WITH MULTIPLE DETECTORS

4.1. Introduction

The concept of quantum measurement is essential for the understanding and interpretation of quantum mechanics, and continuously inspires both theoretical and experimental research [1]. The proper description of the measurement process and setup is essential in the quantum realm. The projective measurement [2], although can be realized experimentally, is not the only way to acquire information about the state of a quantum system. One of the most experimentally relevant situations is the setup and paradigm of continuous weak linear measurement (CWLM) [3-9]. In this setup, a weak coupling between the quantum system and its environment results in continuous entanglement of the system and the environmental degrees of freedom, those include the detector variables. Thereby, the (discrete) quantum information from the measured system is converted to continuous time-dependent detector outputs. At the same time, the environment induces the decoherence and relaxation of the quantum system, which is an inevitable feedback of the measurement process. The measurement results are random incorporating intrinsic noises of the detectors, and their statistics is interesting and important to reveal quantum features of the system measured. Recent experimental advances enable faster and more accurate CWLM and even permit combination of CWLM and projective measurement. [10-14]. This allows to experimentally access the statistics in question and makes it relevant to describe and predict the statistics for arbitrary complex CWLM setups.

There are various approaches to statistics of CWLM. In Ref. [6] an approach based on FCS has been developed and applied for several simple situations, in particular, the qubit purification has been demonstrated. Recently, the same approach has been extended to describe the situation of conditioned measurement where a CWLM ends with a projective measurement. This has been done for a single [15] and two [16] detectors and connection with the theory of weak values [17] has been established. Many authors prefer the so-called Bayesian approach to the description of quantum measurement where one implements a stochastic update of density matrix [4, 13, 18] that does not immediately provide a closed expression for the statistics but permits rather efficient numerical simulations. Recent advances in this direction are presented in [19, 20]. There is still no general scheme unifying the approaches, neither the equivalence between approaches has been shown generally and explicitly. For instance, Ref. [21] basically repeats the numerical calculations of Ref. [6] with a different method. The generalization of the descriptions on an arbitrary number of detectors and arbitrary complex quantum system has not been done yet.

The goal of this article is to establish a general framework for the description of the CWLM in the case of an arbitrary number of detectors and arbitrary quantum system measured. The only important restriction on the applicability of the framework is the assumption that the time correlation of noises and time delays of the susceptibilities take place at a smaller scale than the typical scale of quantum evolution. This results in simple Markovian evolution equations and update schemes. This is also a usual experimental situation.

In the article, we consider three alternative descriptions of the statistics of the measured results employing three different derivation methods and showing their equivalence. First description gives the generating function of the statistics in terms of a solu-

79

4

tion of an evolution equation for a pseudo-density matrix, such equations are common in FCS context [22] Second description is a drift-diffusion equation for a density matrix in the space of integrated detector outputs. Third description involves a stochastic update of the density matrix and summation over random trajectories in the space of integrated outputs. We derive these results with a microscopic method based on FCS approach, a phenomenological method that employs Lindblad construction [23], and, in the context of the update, a method where the detection is modelled with axillary quantum systems. We establish conditions on noises and susceptibilities involved that i. guarantee the unambiguous interpretation of the detector outputs ii. guarantee the positivity of the density matrix. We specify the minimum detection feedback on the quantum system measured.

This does not exhaust all possible approaches and formulations. Various path integral methods [6, 24, 25] are beyond the scope of this article. The potential importance of these methods is their ability to capture the physics beyond Markov approximation, and we believe they are redundant for Markovian setups. We note that the methods described in the article allow for simple non-Markovian extensions in case of delay in classical variables. Similar extensions are plausible for the description of quantum feedback schemes where the feedback does depend on the accumulated value of detector outputs. This will be discussed in detail in future publications.

The paper is organized as follows. In Section 4.2 we provide the full microscopic derivation of the multi-detector measurement and demonstrate that the measurement statistics are completely described by an evolution equation for a pseudo-density matrix. We establish the necessary conditions for the unambiguous interpretation of the measurement results and for the positivity of the density matrix. In Section 4.3, we show the equivalence of this scheme and a drift-diffusion equation for a density matrix that encompasses the integrated detector outputs. In Section 4.4, we reverse-engineer the drift-diffusion equation providing its phenomenological derivation. Thereby we establish the minimum detector feedback on the measured system. At this stage, it is convenient to rescale the outputs and separate the measuring part of the system into independent detectors. This is achieved by a linear transformation diagonalizing the matrix of the detector noises (Section 4.5). In Section 4.6, we turn to another approach introducing a general stochastic discrete update process that is equivalent to the drift-diffusion equation. In Section 4.7 we demonstrate that the process is equivalent to the averaging over stochastic trajectories in the space of the integrated outputs with the trajectoryconditioned density matrix of the system measured. In two subsections of this Section, we specify two concrete realizations of the stochastic update: oscillator and qubit update. We conclude in Section 4.8

4.2. FCS DERIVATION

In this Section, we will derive an equation that determines statistics of time-integrated outputs of a set of detector variables $\hat{V}_i(t)$, Latin index i numbering the detectors. We will follow the approach of [26] in the description of the measurement and extend it to the case of multiple detectors. The key element of the approach is to introduce a pair of extra canonically conjugated variables $\hat{\chi}_i$, \hat{s}_i for each detector. Their operators satisfy the canonical commutation relations $[\hat{\chi}_i, \hat{s}_j] = i\delta_{ij}$, $\hat{s}_i, \hat{\chi}_i$ being analogous to the momen-

tums and coordinates, respectively. The coupling Hamiltonian of these extra variables and the detector variables is postulated to be $H_c = -\hat{\chi}_i \hat{V}_i$ (we assume summation over repeating indices) and there are no other Hamiltonian terms involving $\hat{\chi}_i$, \hat{s}_i . This guarantees that the operators \hat{s} represent an integrated detector output, since by virtue of Heisenberg equations

$$\frac{d\hat{s}_i}{dt} = \hat{V}_i(t). \tag{4.1}$$

To proceed, let us consider the evolution of the density matrix of the detectors in variables $\chi \equiv \{\chi_i\}$ in a time interval (t_1,t_2) . Such representation is especially convenient since $d\hat{\chi}_i/dt = 0$ so that these variables do not change upon the evolution. Following the lines of [26], we obtain the relation between initial and final density matrices of the detectors(\hat{R} here is the initial density matrix of the whole system)

$$\rho_f(\chi^+, \chi^-) = P(\chi^+, \chi^-) \rho_{in}(\chi^+, \chi^-). \tag{4.2}$$

The matrices are thus related by so-called FCS kernel $P(\chi^+, \chi^-)$ that is given by

$$P(\chi^{+}, \chi^{-}) = \operatorname{Tr}_{\text{sys}} \overrightarrow{T} \exp\{-i \int_{t_{1}}^{t_{2}} dt \left[\hat{H}_{\text{sys}} - \chi_{i}^{+} \hat{V}_{i} \right] \} \hat{R} \overleftarrow{T} \exp\{i \int_{t_{1}}^{t_{2}} dt \left[\hat{H}_{\text{sys}} - \chi_{i}^{-} \hat{V}_{i} \right] \}$$
(4.3)

and $\overrightarrow{T}(\overleftarrow{T})$ denotes(inverse) time ordering.

As explained in [26], if the Wigner representation of the density matrix,

$$\rho(\chi, \mathbf{s}) = \int \frac{d\zeta}{2\pi} e^{i\mathbf{s}\cdot\zeta} \rho(\chi + \frac{\zeta}{2}, \chi - \frac{\zeta}{2}), \tag{4.4}$$

can be interpreted as a classical probability distribution $\Pi(\chi,s)$ for the detectors to be at a certain position χ with momentum s, the Wigner representation of the FCS kernel $P(\chi,s)$ can be interpreted as the probability distribution of the shifts in momentum s, that is, as the distribution of integrated detector outputs $\int_{t_1}^{t_2} \hat{V}_i(t) dt$. This does not hold in general. Generally, a Wigner representation cannot be interpreted as a probability distribution, so the same applies to $P(\chi,s)$. In particular, $P(\chi,s)$ does not have to be positive.

There is, however, an important case when the interpretation of the FCS kernel as the probability distribution of integrated detector outputs is indeed applicable. In this particular case, $P(\chi, s)$ does not depend on χ . This implies that $P(\chi^+, \chi^-)$ is a function of the difference of counting fields only, $P(\chi^+, \chi^-) \equiv P(\chi^+ - \chi^-)$. The latter function becomes the generating function of the probability distribution of the detector outputs.

In the following, we specify the model, compute the FCS kernel and reveal the conditions under which it depends on the difference of counting fields only. We argue that these conditions are met for any realistic measurement situation and therefore the FCS can be used for evaluation of the statistics of the integrated detector outputs.

We separate the whole system into a system to be measured and an environment. The system to be measured is a purely quantum system with finite number of degrees of freedom. We measure a set of operators $\hat{\mathcal{O}}_{\alpha}$ in the space of these degrees of freedom labelling them with Greek indices. They are coupled to the environmental degrees of freedom $\hat{\mathcal{Q}}_{\alpha}$, the operators of the corresponding generalized forces,

$$H_c = -\hat{Q}_\alpha \hat{\mathcal{O}}_\alpha \tag{4.5}$$

We will assume that in the absence of coupling the expectation values of the operators $\hat{V}_i, \hat{Q}_\alpha$ are absent, $\langle \hat{V}_i \rangle = 0$, $\langle \hat{Q}_\alpha \rangle = 0$ (if it is not so, we can always redefine the operators adding the constant terms compensating the averages). If the coupling is sufficiently weak, the environment can be regarded as a linear one. The environment provides a reaction proportional to the first power of the operators \mathcal{O}_α . The detector variables \hat{V}_i are also defined as operators in the space of environmental degrees of freedom. The total Hamiltonian thus reads:

$$H_{\text{sys}} = H_{\text{env}} + H_{\text{q}} + H_{\text{c}} \tag{4.6}$$

where $H_{\rm env}$ and $H_{\rm q}$ define the dynamics of the environment and the system to be measured, respectively, and are operators in corresponding spaces. We employ this Hamiltonian to evaluate the FCS kernel (4.3).

The answer would involve the correlators of the time-dependent operators $\hat{V}_i, \hat{Q}_\alpha$. It is instructive to assume that the correlations vanish at a time scale t_c characterizing the environment while the quantum correlations in the system to be measured may persist at much larger scale. Let us separate the time interval (t_1, t_2) into smaller intervals of duration $\mathcal{T} \gg t_c$. The dynamics of environment are independent for different intervals, so that the environmental degrees of freedom can be traced out separately within each interval. The duration \mathcal{T} can be chosen such that the change of the density matrix of the system is small. Tracing out the environmental degrees of freedom in (4.3) till time t, results in a pseudo-density matrix $\tilde{\rho}(t)$ in the space of the system to be measured,

$$\tilde{\rho}(t) = \underset{\text{env}}{\text{Tr}} \overrightarrow{T} \exp\{-i \int_{t_1}^t d\tau \left[\hat{H}_{\mathbf{q}} - \hat{Q}_{\alpha}(\tau) \hat{\mathcal{O}}_{\alpha} - \chi_i^+ \hat{V}_i(\tau) \right] \} \hat{R} \overleftarrow{T} \exp\{i \int_{t_1}^t d\tau \left[\hat{H}_{\mathbf{q}} - \hat{Q}_{\alpha}(\tau) \hat{\mathcal{O}}_{\alpha} - \chi_i^- \hat{V}_i \right] \}$$

$$(4.7)$$

The tracing out the environment in the next smaller interval of duration $\mathcal T$ promotes the pseudo-density matrix as

$$\tilde{\rho}(t+\mathcal{T}) = \tilde{\rho}(t) + \mathcal{T}\left(-i[H_{\rm q},\tilde{\rho}(t)] - \Gamma[\tilde{\rho}(t)]\right) \tag{4.8}$$

where the linear superoperator Γ will be evaluated below. Therefore, the whole FCS kernel can be presented as

$$P(\boldsymbol{\chi}^+, \boldsymbol{\chi}^-) = \text{Tr}[\tilde{\rho}(t_2)] \tag{4.9}$$

where $\tilde{\rho}(t_2)$ is obtained by solving an evolution equation

$$\frac{\partial \tilde{\rho}}{\partial t} = -i[H_{\mathbf{q}}, \tilde{\rho}(t)] - \Gamma[\tilde{\rho}(t)] \tag{4.10}$$

with the initial condition $\tilde{\rho}(t_1) = \rho$, ρ being the true density matrix of the system to be measured at the time moment t_1 .

Let us evaluate the linear superoperator Γ . It is contributed by various second-order terms in operators \hat{V}_i , \hat{Q}_{α} . There are contributions proportional to the second, first, and zero power of χ^{\pm} . Let us consider these three contributions separately.

The second order terms involve the correlators of two \hat{V}_i operators. We denote

$$S_{ij}^{\pm} = \int dt \langle \hat{V}_i(0) \hat{V}_j(t) \Theta(\pm t) \rangle \tag{4.11}$$

and rewrite it as

$$\Gamma[\rho] = \left(\chi_i^+ \chi_j^+ S_{ij}^- + \chi_i^- \chi_j^- S_{ij}^+ - \chi_i^- \chi_j^+ (S_{ij}^- + S_{ij}^+)\right) \rho \tag{4.12}$$

At this point, it is convenient to introduce symmetrized noises S_{ij} and the susceptibilities a_{ij} ,

$$2S_{ij} = S_{ij}^{+} + S_{ij}^{-} + S_{ii}^{-} + S_{ii}^{+}$$
 (4.13)

$$a_{ij} = i(S_{ji}^+ - S_{ij}^-) (4.14)$$

With these more physical quantities, we express the sums of correlators

$$S_{ij}^{\pm} + S_{ji}^{\pm} = S_{ij} \mp i \frac{a_{ij} + a_{ji}}{2}$$
 (4.15)

$$S_{ij}^{-} + S_{ij}^{+} = S_{ij} + i \frac{a_{ij} - a_{ji}}{2}$$
 (4.16)

to obtain

$$\Gamma[\rho] = \frac{1}{2} \left((\chi_i^+ - \chi_i^-)(\chi_j^+ - \chi_j^-) S_{ij} + i(\chi_i^+ + \chi_i^-)(\chi_j^+ - \chi_j^-) a_{ij} \right) \rho \tag{4.17}$$

To make sure that the FCS kernel defines the probability distribution, we need to require $a_{ij} = 0$, no zero-frequency susceptibilities of the detector. We stress that this is the case of most common electrical measurement. The operators \hat{V}_i in this case are associated with currents or voltages in a dissipative electrical circuit. The zero-frequency susceptibilities in this situation would give current and/or voltage response on vector potential and/or charge passed through a point in a circuit, therefore they are zero by virtue of gauge invariance.

Let us evaluate the first-order contribution. In this case, each term involves a single operator $\hat{\mathcal{O}}$ and a correlator of \hat{Q} , and \hat{V} . Adopting the notations (4.11), we represent this term as

$$\Gamma[\rho] = \hat{\mathcal{O}}_{\alpha} \rho \left(\left(S_{\alpha i}^{-} + S_{i \alpha}^{-} \right) \chi_{i}^{+} - \left(S_{i \alpha}^{+} + S_{i \alpha}^{-} \right) \chi_{i}^{-} \right) + \rho \hat{\mathcal{O}}_{\alpha} \left(\left(S_{\alpha i}^{+} + S_{i \alpha}^{+} \right) \chi_{i}^{-} - \left(S_{\alpha i}^{+} + S_{\alpha i}^{-} \right) \chi_{i}^{+} \right)$$
(4.18)

Making use of the relations (4.15), we arrive at

$$\Gamma[\rho] = \hat{\mathcal{O}}_{\alpha} \rho \left(\left(S_{\alpha i} + i \frac{a_{i\alpha}}{2} \right) (\chi_i^+ - \chi_i^-) + i \frac{a_{\alpha i}}{2} (\chi_i^+ + \chi_i^-) \right) + \rho \hat{\mathcal{O}}_{\alpha} \left(\left(S_{\alpha i} - i \frac{a_{i\alpha}}{2} \right) (\chi_i^- - \chi_i^+) - i \frac{a_{\alpha i}}{2} (\chi_i^+ + \chi_i^-) \right) \left(\frac{a_{\alpha i}}{2} (\chi_i^+ + \chi_i^-) \right) \left(\frac{a_{\alpha i}}{2} (\chi_i^+ + \chi_i^-) \right) \left(\frac{a_{\alpha i}}{2} (\chi_i^+ - \chi_i^+) - i \frac{a_{\alpha i}}{2} (\chi_i^+ + \chi_i^-) \right) \left(\frac{a_{\alpha i}}{2} (\chi_i^+ - \chi_i^-) - i \frac{a_{\alpha i}}{2} (\chi_i^+ - \chi_i^-) \right) \left(\frac{a_{\alpha i}}{2} (\chi_i^+ - \chi_i^-) - i \frac{a_{\alpha i}}{2} (\chi_i^+ - \chi_i^-) \right) \left(\frac{a_{\alpha i}}{2} (\chi_i^+ - \chi_i^-) - i \frac{a_{\alpha i}}{2} (\chi_i^+ - \chi_i^-) \right) \left(\frac{a_{\alpha i}}{2} (\chi_i^+ - \chi_i^-) - i \frac{a_{\alpha i}}{2} (\chi_i^+ - \chi_i^-) \right) \left(\frac{a_{\alpha i}}{2} (\chi_i^+ - \chi_i^-) - i \frac{a_{\alpha i}}{2} (\chi_i^+ - \chi_i^-) \right) \left(\frac{a_{\alpha i}}{2} (\chi_i^+ - \chi_i^-) - i \frac{a_{\alpha i}}{2} (\chi_i^+ - \chi_i^-) \right) \left(\frac{a_{\alpha i}}{2} (\chi_i^+ - \chi_i^-) - i \frac{a_{\alpha i}}{2} (\chi_i^+ - \chi_i^-) \right) \left(\frac{a_{\alpha i}}{2} (\chi_i^+ - \chi_i^-) - i \frac{a_{\alpha i}}{2} (\chi_i^+ - \chi_i^-) \right) \left(\frac{a_{\alpha i}}{2} (\chi_i^+ - \chi_i^-) - i \frac{a_{\alpha i}}{2} (\chi_i^+ - \chi_i^-) \right) \left(\frac{a_{\alpha i}}{2} (\chi_i^+ - \chi_i^-) - i \frac{a_{\alpha i}}{2} (\chi_i^+ - \chi_i^-) \right) \left(\frac{a_{\alpha i}}{2} (\chi_i^+ - \chi_i^-) - i \frac{a_{\alpha i}}{2} (\chi_i^+ - \chi_i^-) \right) \left(\frac{a_{\alpha i}}{2} (\chi_i^+ - \chi_i^-) - i \frac{a_{\alpha i}}{2} (\chi_i^+ - \chi_i^-) \right) \left(\frac{a_{\alpha i}}{2} (\chi_i^+ - \chi_i^-) - i \frac{a_{\alpha i}}{2} (\chi_i^+ - \chi_i^-) \right) \left(\frac{a_{\alpha i}}{2} (\chi_i^+ - \chi_i^-) - i \frac{a_{\alpha i}}{2} (\chi_i^+ - \chi_i^-) \right) \left(\frac{a_{\alpha i}}{2} (\chi_i^+ - \chi_i^-) - i \frac{a_{\alpha i}}{2} (\chi_i^+ - \chi_i^-) \right) \left(\frac{a_{\alpha i}}{2} (\chi_i^+ - \chi_i^-) - i \frac{a_{\alpha i}}{2} (\chi_i^+ - \chi_i^-) \right) \left(\frac{a_{\alpha i}}{2} (\chi_i^+ - \chi_i^-) - i \frac{a_{\alpha i}}{2} (\chi_i^+ - \chi_i^-) \right) \left(\frac{a_{\alpha i}}{2} (\chi_i^+ - \chi_i^-) - i \frac{a_{\alpha i}}{2} (\chi_i^+ - \chi_i^-) \right) \left(\frac{a_{\alpha i}}{2} (\chi_i^+ - \chi_i^-) - i \frac{a_{\alpha i}}{2} (\chi_i^+ - \chi_i^-) \right) \left(\frac{a_{\alpha i}}{2} (\chi_i^+ - \chi_i^-) - i \frac{a_{\alpha i}}{2} (\chi_i^+ - \chi_i^-) \right) \left(\frac{a_{\alpha i}}{2} (\chi_i^+ - \chi_i^-) - i \frac{a_{\alpha i}}{2} (\chi_i^+ - \chi_i^-) \right) \left(\frac{a_{\alpha i}}{2} (\chi_i^+ - \chi_i^-) - i \frac{a_{\alpha i}}{2} (\chi_i^+ - \chi_i^-) \right) \left(\frac{a_{\alpha i}}{2} (\chi_i^+ - \chi_i^-) - i \frac{a_{\alpha i}}{2} (\chi_i^+ - \chi_i^-) \right) \left(\frac{a_{\alpha i}}{2} (\chi_i^+ - \chi_i^-) - i \frac{a_{\alpha i}}{2} (\chi_i^+ - \chi_i^-) \right) \left(\frac{a_{\alpha i$$

We see that the terms with the sums of counting fields drop and the correctness of FCS approach is guaranteed provided $a_{\alpha i}=0$, that is, there are no susceptibilities from the detectors to the measured variables. Again this is the case of a common electrical measurement and is guaranteed by gauge invariance. The reverse susceptibilities $a_{i\alpha}$ should be non-zero for the measurement to take place.

The zero-order contribution describes the effect of environment on the dynamics of the measured system. It involves the pairs of the operators \hat{O} , and reads

$$\Gamma[\rho] = S_{\alpha\beta}^{-} \hat{\mathcal{O}}_{\alpha} \hat{\mathcal{O}}_{\beta} \rho + \rho \hat{\mathcal{O}}_{\alpha} \hat{\mathcal{O}}_{\beta} S_{\alpha\beta}^{+} - \hat{\mathcal{O}}_{\alpha} \rho \hat{\mathcal{O}}_{\beta} (S_{\beta\alpha}^{+} + S_{\beta\alpha}^{-})$$
 (4.20)

It is instructive to separate this expression into two parts. The first part is a Lindblad form describing dissipative transitions and decoherence induced by the environment,

$$\Gamma_L[\rho] = \left(\frac{1}{2} \left(\hat{\mathcal{O}}_{\beta} \hat{\mathcal{O}}_{\alpha} \rho + \rho \hat{\mathcal{O}}_{\beta} \hat{\mathcal{O}}_{\alpha}\right) - \hat{\mathcal{O}}_{\alpha} \rho \hat{\mathcal{O}}_{\beta}\right) C_{\beta\alpha} \tag{4.21}$$

where the hermitian matrix $C_{\beta\alpha}$ is defined as

$$C_{\beta\alpha} = (S_{\beta\alpha}^+ + S_{\beta\alpha}^-) = S_{\beta\alpha} + i \frac{a_{\beta\alpha} - a_{\alpha\beta}}{2}.$$
 (4.22)

One can diagonalize the set of Lindblad operators involved. For this, let us present *C* in the diagonal form,

$$C_{\alpha\beta} = \Psi_{\alpha}^{*\gamma} C_{\gamma} \Psi_{\beta}^{\gamma}, \tag{4.23}$$

with γ labelling its eigenvectors and eigenvalues, and introduce an operator set

$$\hat{L}_{\gamma} = \sqrt{C_{\gamma}} \Psi_{\alpha}^{\gamma} \hat{\mathcal{O}}_{\alpha}. \tag{4.24}$$

In these terms, the contribution reads

$$\Gamma_L[\rho] = \frac{1}{2} \left(\hat{L}_{\gamma}^{\dagger} \hat{L}_{\gamma} \rho + \rho \hat{L}_{\gamma}^{\dagger} \hat{L}_{\gamma} \right) - \hat{L}_{\gamma} \rho \hat{L}_{\gamma}^{\dagger}$$

$$(4.25)$$

The second part gives a renormalization of the system Hamiltonian by the coupling to the environment. It reads

$$\Gamma_{H}[\rho] = i[\hat{H}', \rho]; \ \hat{H}' = -\frac{i}{2} (S_{\alpha\beta}^{-} - S_{\alpha\beta}^{+}) \hat{\mathcal{O}}_{\alpha} \hat{\mathcal{O}}_{\beta}$$
 (4.26)

The matrix $i(S_{\alpha\beta}^- - S_{\alpha\beta}^+)/2$ is Hermitian and in general case cannot be expressed in terms of zero-frequency noises and susceptibilities. With a help of a Kramers-Kronig relation, it can be expressed in terms of those at finite frequency,

$$\frac{i}{2}(S_{\alpha\beta}^{-} - S_{\alpha\beta}^{+}) = \int \frac{d\omega}{2\pi\omega} \left(\frac{a_{\beta\alpha}(-\omega) - a_{\alpha\beta}(\omega)}{2} + iS_{\alpha\beta}(\omega) \right) \tag{4.27}$$

If the environment is in the ground state, this matrix can be reduced to the matrix of the zero-frequency susceptibilities, $i(S_{\alpha\beta}^- - S_{\alpha\beta}^+)/2 = a_{ij}$. Since this term can be attributed to the system Hamiltonian, it is not especially interesting for us and we do not discuss it further.

To summarize the results of the derivation of this Section, the distribution of integrated detector outputs P(s) over the time interval (t_1, t_2) is expressed in terms of a pseudo-density matrix $\tilde{\rho}$ that depends on the counting fields χ ,

$$P(\mathbf{s}) = \int \frac{d\boldsymbol{\chi}}{2\pi} e^{i\mathbf{s}\cdot\boldsymbol{\chi}} \operatorname{Tr}[\tilde{\rho}(\boldsymbol{\chi}; t_2)]. \tag{4.28}$$

and satisfies the evolution equation

$$\frac{\partial \tilde{\rho}}{\partial t} = -i[H_{\mathbf{q}}, \tilde{\rho}(t)] - \frac{1}{2} \chi_{i} S_{ij} \chi_{j}
- \left(\hat{\mathcal{O}}_{\alpha} \rho \left(S_{\alpha i} + i \frac{a_{i\alpha}}{2}\right) - \rho \hat{\mathcal{O}}_{\alpha} \left(S_{\alpha a} - i \frac{a_{i\alpha}}{2}\right)\right) \chi_{i}
- \left[\frac{1}{2} \left(\hat{\mathcal{O}}_{\beta} \hat{\mathcal{O}}_{\alpha} \rho + \rho \hat{\mathcal{O}}_{\beta} \hat{\mathcal{O}}_{\alpha}\right) - \hat{\mathcal{O}}_{\alpha} \rho \hat{\mathcal{O}}_{\beta}\right] \left(S_{\beta \alpha} + i \frac{a_{\beta \alpha} - a_{\alpha \beta}}{2}\right)$$
(4.29)

with initial condition $\tilde{\rho}(t_1) = \rho(t_1)$, $\rho(t_1)$ being the density matrix of the system measured.

The noises and susceptibilities involved in this equation are not arbitrary numbers. They should satisfy inequalities that follow from their definition and eventually guarantee that the distribution of the outcomes obtained from the above equation, is positively defined.

Let us consider a matrix \check{C} (Eq. (4.22)) with an index a that takes values of detector and operator indices, $C_{ab} = S_{ab} + i(a_{ba} - a_{ab})/2$. All inequalities required are obtained from the condition that the matrix \check{C} is *positively defined*, that is, for any vector Ψ_a , $\Psi_a^*C_{ab}\Psi_b>0$

If the vector has a single component, the positivity requires rather obvious inequalities $S_{ii} > 0$, $S_{\alpha\alpha} > 0$, diagonal noises are positive. For a two-component vector, in addition to the above conditions, the determinant of the corresponding 2×2 matrix must be positive. For two detectors, this restricts cross-noises since the corresponding susceptibilities are 0, $S_{ii}S_{jj} > S_{ij}^2$. For detector i and operator α , this gives the condition

$$S_{ii}S_{\alpha\alpha} > S_{i\alpha}^2 + a_{i\alpha}^2 \tag{4.30}$$

that is widely discussed in the context of CWLM [1]. Increasingly complex inequalities can be obtained if one considers the vectors with more components [16].

4.3. DRIFT-DIFFUSION EQUATION

There is an alternative way to view this equation. Let us consider a density matrix in system variables and the auxiliary variables s that we have used to represent the integrated detector outputs, $\rho(s_1, s_2)$ where we have made explicit its dependence on the outputs. As a matter of fact, the χ -dependent pseudo-density matrix $\tilde{\rho}$ can be regarded as a Fourier-component of this density matrix for coinciding s_1, s_2 ,

$$\tilde{\rho}(\chi) = \int d\chi e^{i\chi \cdot s} \rho(s, s) \tag{4.31}$$

Performing the inverse Fourier transform, we obtain the following equation for $\rho(s) \equiv \rho(s, s)$ (here, $\partial_i \equiv \partial_{s_i}$)

$$\frac{\partial \tilde{\rho}}{\partial t} = -i[H_{\mathbf{q}}, \tilde{\rho}(t)] + \frac{1}{2} S_{ij} \partial_{i} \partial_{j} \rho
-i \left(\hat{\mathcal{O}}_{\alpha} \partial_{i} \rho \left(S_{\alpha i} + i \frac{a_{i\alpha}}{2} \right) - \partial_{i} \rho \hat{\mathcal{O}}_{\alpha} \left(S_{\alpha a} - i \frac{a_{i\alpha}}{2} \right) \right)
- \left[\frac{1}{2} \left(\hat{\mathcal{O}}_{\beta} \hat{\mathcal{O}}_{\alpha} \rho + \rho \hat{\mathcal{O}}_{\beta} \hat{\mathcal{O}}_{\alpha} \right) - \hat{\mathcal{O}}_{\alpha} \rho \hat{\mathcal{O}}_{\beta} \right] \left(S_{\beta \alpha} + i \frac{a_{\beta \alpha} - a_{\alpha \beta}}{2} \right)$$
(4.32)

This equation is of the drift-diffusion type. In the absence of coupling to the quantum system, it describes a Brownian motion in the multi-dimensional space of integrated outputs. In this case, ρ is just a scalar giving the probability of the integrated outcome s,

$$P_0(s) = \sqrt{\frac{\det[S_{ij}]}{2\pi t}} \exp\left(-\frac{s_i s_j (S^{-1})_{ij}}{2t}\right)$$
(4.33)

In the presence of coupling, the maximum of this distribution drifts with a velocity that is proportional to the measured values of the operators $\hat{\mathcal{O}}_{\alpha}$.

A simple and general solution of the equation (4.32) can be obtained under a rather uninteresting "classical" assumption that all operators $\hat{\mathcal{O}}_{\alpha}$ commute with each other. In this case, the equations for the elements of ρ separate in the basis of the eigenvectors of $\hat{\mathcal{O}}_{\alpha}$.

The time evolution of a diagonal element $\rho\left(\{\mathcal{O}_{\alpha}\},s\right)$ exhibits a simple drift-diffusion behaviour,

$$\rho\left(\{\mathcal{O}_{\alpha}\}, \mathbf{s}\right) = P_0(\mathbf{s} - \mathbf{v}\,t),\tag{4.34}$$

with the velocity $v_k \equiv a_{k\alpha} \mathcal{O}_{\alpha}$ proportional to the eigenvalues.

The non-diagonal elements, in addition to drift, are subject to damping due to decoherence and also exhibit oscillations due to noise correlations $S_{\alpha k}$, and non-symmetric susceptibilities,

$$\rho\left(\{\mathcal{O}_{\alpha}\}, \{\mathcal{O}'_{\alpha}\}, \mathbf{s}\right) = P_0\left(\mathbf{s} - \frac{\mathbf{v} + \mathbf{v}'}{2}t + i(\mathbf{w} - \mathbf{w}')t\right)e^{-\Gamma_d t + i\gamma t}.$$
(4.35)

Here,
$$v_k' = a_{k\alpha}\mathcal{O}_{\alpha}'$$
, $w_k = S_{\alpha k}\mathcal{O}_{\alpha}$, $w_k' = S_{\alpha k}\mathcal{O}_{\alpha}'$, $\Gamma_d = \frac{1}{2}S_{\alpha\beta}(\mathcal{O}_{\alpha} - \mathcal{O}_{\alpha}')(\mathcal{O}_{\beta} - \mathcal{O}_{\beta}')$, $\gamma = \frac{1}{4}a_{\alpha\beta}((\mathcal{O}_{\alpha} + \mathcal{O}_{\alpha}')(\mathcal{O}_{\beta} - \mathcal{O}_{\beta}') - (\mathcal{O}_{\beta} + \mathcal{O}_{\beta}')(\mathcal{O}_{\alpha} - \mathcal{O}_{\alpha}')$.

The solutions become much more involved in the case of non-commuting $\hat{\mathcal{O}}_{\alpha}$.

4.4. LINDBLAD CONSTRUCTION DERIVATION

In this Section, we will 'reverse-engineer' the drift-diffusion equation (4.32) providing its general phenomenological derivation that is mostly based on the positivity of the density matrix utilizing Lindblad construction. This equation is for a density matrix $\hat{\rho}(s_1, s_2)$, where s represents the detector outputs while the rest of the matrix structure is inherited from the measured system. An important additional requirement on the equation is that it does not mix diagonal and non-diagonal components of the matrix this suppressing possible quantum interference of the states with different detector readings.

Let us start with Lindblad construction. Given a set of operators \hat{A}_i and the Hermitian Hamiltonian \hat{H} the positivity of a general density matrix is guaranteed by the following equation (Lindblad construction)

$$\frac{\partial \hat{\rho}}{\partial t} = S_{ij} \left(\hat{A}_i \hat{\rho} \hat{A}_j^{\dagger} - \frac{1}{2} \hat{A}_j^{\dagger} \hat{A}_i \hat{\rho} - \frac{1}{2} \hat{\rho} \hat{A}_j^{\dagger} \hat{A}_i \right) - i \hat{H} \hat{\rho} + i \hat{\rho} \hat{H}$$

$$(4.36)$$

provided S_{ij} is a *positive Hermitian matrix*. At the moment, it is an arbitrary matrix not related to the matrix S_{ij} used in the previous Sections.

Let us specify to the structure $\hat{\rho}(\mathbf{s}_1, \mathbf{s}_2)$. It is convenient to introduce the half-sum and the half-difference of these variables,

$$\mathbf{s}, \mathbf{d} \equiv \frac{\mathbf{s}_1 \pm \mathbf{s}_2}{2}.\tag{4.37}$$

Let us find a Lindblad construction that does not mix diagonal and non-diagonal matrix elements in *s*. As for the operator set, we choose

$$\hat{A}_i = \hat{\chi}_i + \hat{B}_i, \ \hat{\chi}_i \equiv i\partial/\partial s_i$$

This gives three groups of terms.

First group represents the diffusion in the space of detector variables containing the terms quadratic in $\hat{\chi}$.

$$\frac{\partial \hat{\rho}}{\partial t} = S_{ij} \left(\hat{\chi}_i \hat{\rho} \hat{\chi}_j - \frac{1}{2} \hat{\chi}_i \hat{\chi}_j \hat{\rho} - \frac{1}{2} \hat{\chi}_i \hat{\chi}_j \hat{\rho} \right) \tag{4.38}$$

We notice that

$$\langle \mathbf{s}_{1} | \hat{\rho} \hat{\chi}_{i} | \mathbf{s}_{2} \rangle = -i \frac{\partial \hat{\rho}}{\partial s_{2,i}} = -i \frac{1}{2} \left(\frac{\partial}{\partial s_{i}} - \frac{\partial}{\partial d_{i}} \right) \hat{\rho}$$

$$\langle \mathbf{s}_{1} | \hat{\chi}_{i} \hat{\rho} | \mathbf{s}_{2} \rangle = i \frac{\partial \hat{\rho}}{\partial s_{1,i}} = i \frac{1}{2} \left(\frac{\partial}{\partial s_{i}} + \frac{\partial}{\partial d_{i}} \right) \hat{\rho}$$

With this, the equation for density matrix is represented as

$$\frac{\partial \hat{\rho}}{\partial t} = \operatorname{Re}\left[S_{ij}\right] \frac{1}{2} \frac{\partial}{\partial s_i} \frac{\partial}{\partial s_i} \hat{\rho} + i \operatorname{Im}\left[S_{ij}\right] \frac{1}{2} \frac{\partial}{\partial d_i} \frac{\partial}{\partial s_j} \hat{\rho}$$
(4.39)

We have to require here the absence of the terms with the derivatives with respect to **d**. It may seem to require *real* and therefore symmetric matrix *S*.

However, there could be a term in \hat{H} compensating for imaginary part of S. This could happen if this part of the Hamiltonian contains two derivative operators, so let us search for it in the most general form $H = \bar{C}_{ij}\hat{\chi}_i\hat{\chi}_j$ with a Hermitian \bar{C} . This gives the following contribution to the time derivative of the density matrix:

$$\frac{\partial \hat{\rho}}{\partial t} = -i\bar{C}_{ij} \left(\hat{\chi}_i \hat{\chi}_j \hat{\rho} - \hat{\rho} \hat{\chi}_i \hat{\chi}_j \right) = -i \operatorname{Re} \left[\bar{C}_{ij} \right] \frac{\partial}{\partial d_i} \frac{\partial}{\partial s_i} \hat{\rho}. \tag{4.40}$$

This is always symmetric with respect to exchange of i and j, so it cannot compensate the operator in the second term of Eq. 4.39 which is antisymmetric. Therefore S is indeed a symmetric and real matrix.

The second group of terms mixes $\hat{\chi}$ and \hat{B} .

$$\frac{\partial \hat{\rho}}{\partial t} = S_{ij} \left(\hat{\chi}_i \hat{\rho} \hat{B}_j^\dagger + \hat{B}_i \hat{\rho} \hat{\chi}_j - \frac{1}{2} \left(\hat{\chi}_i \hat{B}_j + \hat{B}_i^\dagger \hat{\chi}_j \right) \hat{\rho} - \frac{1}{2} \hat{\rho} \left(\hat{\chi}_i \hat{B}_j + \hat{B}_i^\dagger \hat{\chi}_j \right) \right) \tag{4.41}$$

We collect the terms proportional to the derivatives of s

$$\frac{i}{4}S_{ij}\left(\frac{\partial\hat{\rho}}{\partial s_{i}}\left(3\hat{B}_{j}^{\dagger}+\hat{B}_{j}\right)-\left(3\hat{B}_{j}+\hat{B}_{j}^{\dagger}\right)\frac{\partial\hat{\rho}}{\partial s_{i}}\right)$$

and to the derivatives of d:

$$\frac{i}{4}S_{ij}\left(\frac{\partial\hat{\rho}}{\partial d_{i}}\left(\hat{B}_{j}^{\dagger}-\hat{B}_{j}\right)-\left(\hat{B}_{j}^{\dagger}-\hat{B}_{j}\right)\frac{\partial\hat{\rho}}{\partial d_{i}}\right).$$

We do not like the terms proportional to the derivatives of **d**. Let us try to compensate those by a proper choice of an addition to the Hamiltonian. We seek for it in the form $\hat{H} = -\sum_i \hat{\chi}_i \hat{D}_i$, \hat{D}_i being Hermitian operators. Its contribution to the time derivative of the density matrix reads

$$\frac{\partial \hat{\rho}}{\partial t} = -\frac{1}{4} \left(\hat{D}_i \frac{\partial \hat{\rho}}{\partial s_i} + \frac{\partial \hat{\rho}}{\partial s_i} \hat{D}_i \right) - \frac{1}{4} \left(\hat{D}_i \frac{\partial \hat{\rho}}{\partial d_i} - \frac{\partial \hat{\rho}}{\partial d_i} \hat{D}_i \right) \tag{4.42}$$

To cancel the terms we dislike we need to set

$$\hat{D}_i = i S_{ij} \left(\hat{B}_j - \hat{B}_j^{\dagger} \right)$$

Summing up the terms from the Lindblad form and the Hamiltonian, we obtain

$$\frac{\partial \hat{\rho}}{\partial t} = i \left(\frac{\partial \hat{\rho}}{\partial s_i} \hat{K}_i^{\dagger} - \hat{K}_i \frac{\partial \hat{\rho}}{\partial s_i} \right); \hat{K}_i = S_{ij} \hat{B}_j$$
(4.43)

We can also separate \hat{K}_i into two Hermitian operators, $\hat{K}_i = (\hat{R}_i - i\hat{D}_i)/2$, with this

$$\frac{\partial \hat{\rho}}{\partial t} = \frac{i}{2} \left[\frac{\partial \hat{\rho}}{\partial s_i}, \hat{R} \right] + \frac{1}{2} \left[\frac{\partial \hat{\rho}}{\partial s_i}, \hat{D} \right]_{\perp} \tag{4.44}$$

where, as we will see soon, the first term is associated with the effect of cross-noises between the detector variables and the fields acting on the measured system, while the second term is associated with the susceptibilities.

The third group of terms represents the effect of the measurement on the decoherence and relaxation of the quantum system.

$$\frac{\partial \hat{\rho}}{\partial t} = S_{ij} \left(\hat{B}_i \hat{\rho} \hat{B}_j^{\dagger} - \frac{1}{2} \hat{B}_j^{\dagger} \hat{B}_i \hat{\rho} - \frac{1}{2} \hat{\rho} \hat{B}_j^{\dagger} \hat{A}_i \right) = \hat{B}_i \hat{\rho} \hat{K}_i^{\dagger} - \frac{1}{2} \hat{B}_i \hat{K}_i^{\dagger} \hat{\rho} - \frac{1}{2} \hat{\rho} \hat{B}_i \hat{K}_i^{\dagger}$$
(4.45)

We can bring everything together to a relatively compact form:

$$\frac{\partial \hat{\rho}}{\partial t} = \frac{1}{2} S_{ij} \partial_i \partial_j \hat{\rho} + i \left(\partial_i \hat{\rho} \hat{K}_i^{\dagger} - \hat{K}_i \partial_i \hat{\rho} \right) + \frac{1}{2} \left[\hat{B}_i, \hat{\rho} \hat{K}_i^{\dagger} \right] + \frac{1}{2} \left[\hat{B}_i \hat{\rho}, \hat{K}_i^{\dagger} \right]$$
(4.46)

Let us now compare this with Eq. 4.32 term by term. The comparison of the first group of terms shows that the matrix *S* is nothing but the noise matrix of the detectors. The comparison of the second group gives

$$\hat{D}_{i} = a_{i\alpha}\hat{\mathcal{O}}_{\alpha}, \, \hat{R}_{i} = 2S_{i\alpha}\hat{\mathcal{O}}_{\alpha}, \, \hat{K}_{i} = \left(S_{\alpha i} - i\frac{a_{i\alpha}}{2}\right)\hat{\mathcal{O}}_{\alpha} \tag{4.47}$$

so the operators \hat{R},\hat{D} are indeed associated with the cross-noises and susceptibilities, respectively.

The third group of terms in Eq. 4.46 gives the minimum decoherence and dephasing that is associated with the measurement, or, in other words, to the input noises acting on the detector and corresponding susceptibilities. The contributions can also come from other sources that are not related to the measurement. They can be added to the Lindblad construction (4.36) as a set of operators \mathcal{O}_{α} with a *positively* defined Hermitian matrix. With this, we obtain an important result

$$S_{\alpha\beta} + i \frac{a_{\beta\alpha} - a_{\alpha\beta}}{2} > \left(S_{\alpha i} - i \frac{a_{i\alpha}}{2}\right) (S^{-1})_{ij} \left(S_{j\beta} - i \frac{a_{i\beta}}{2}\right) \tag{4.48}$$

Here, the inequality sign implies that the difference of the matrices on both sides is a positively defined matrix, and the right hand side represents the minimum contribution to the decoherence/dephasing.

Naturally, the same inequality may be derived from the positivity of the matrix \check{C} discussed in the previous sections.

4.5. OUTPUT RESCALING AND SEPARATION

Till this moment, we assume general linear detection working with an arbitrary noise matrix S_{ij} . Since the detection is linear, we can redefine the detector outputs taking arbitrary combinations of those. An orthogonal transformation of the outputs brings the noise matrix to the diagonal form. This separates the detectors, their noises are now independent. The rescaling of the separated outputs brings the diagonal noises to the same value S. It is possible to set S=1. However, this implies the rescaling of the outputs in such a way that all of them have dimension $sec^{1/2}$. We find this rather inconvenient so we prefer to work with a dimensionful S.

Such redefinition of the outputs simplifies the equations to some extent. The resulting equations are obtained by substitution $S_{ij} = S\delta_{ij}$. In particular, Eq. 4.46 takes the form

$$S^{-1}\frac{\partial\hat{\rho}}{\partial t} = \frac{1}{2}\partial_{i}\partial_{i}\hat{\rho} + i(\partial_{i}\hat{\rho}\hat{B}_{i}^{\dagger} - \hat{B}_{i}\partial_{i}\hat{\rho}) + \frac{1}{2}\left[\hat{B}_{i},\hat{\rho}\hat{B}_{i}^{\dagger}\right] + \frac{1}{2}\left[\hat{B}_{i}\hat{\rho},\hat{B}_{i}^{\dagger}\right]$$
(4.49)

4.6. DISCRETE UPDATE

In this Section, we will look at the resulting equations from a different point of view: we will introduce a discrete process, a step-by-step update of the density matrix of the system and detector outputs. As we will see in the next Section, this update can be made stochastic giving stochastic trajectories in the space of integrated detector outputs. The actual $\hat{\rho}(\mathbf{s})$ is then obtained by averaging over different realizations of trajectories. One motivation for considering the stochastic update is that it can be an efficient numerical strategy to solve the drift-diffusion equation. An alternative strategy would involve a discretization of the output space and solving at the resulting multi-dimensional mesh with a lot of nodes. Another motivation is that the stochastic update process can be made to mimic the time-line of an actual experimental run where random outputs of the detectors are quasi-continuously measured.

The stochastic update was considered in [4, 18]. Here, we present its generalization to the general situation of multi-detector measurement of an arbitrary quantum system.

We start by noting that an update that reproduces the drift-diffusion equation can be organized in a variety of ways. We chose a physical but rather general way. We separate the detectors as in the previous section and concentrate on a single detector. We introduce an auxiliary quantum system for this particular detector. At each update step, we first prepare the auxiliary system in an initial state characterized by a certain density matrix \hat{R} . Then we switch on an interaction between the auxiliary system, the system to be measured, and the detector variable χ and let the unitary evolution to take place during a time interval dt.

The idea is to keep dt small so that the change of the system density matrix is small $\propto dt$, and to choose the form of interaction in such a way as to reproduce the contribution of this particular detector into Eq. 4.49. Generalization to many detectors is straightforward: since the contributions of the detectors add, at each update step we run the procedure described for all auxiliary systems representing the detectors. The resulting update does not depend on the order of the procedures with an accuracy $\propto (dt)^2$. The sources of decoherence and relaxation not related to the measurement may be in-

corporated in a similar way with using the auxiliary systems where there is no interaction with the detector variable.

To understand the requirements on the interaction and to make convenient choices is thus enough to concentrate on a single Lindblad operator $\hat{\chi} + \hat{B}$. It is convenient to organize the update in such a way that the interaction with \hat{B} comes first and then the interaction with the detector variable $\hat{\chi}$ takes place. The update of the density matrix is then defined as follows:

$$\hat{\rho}_{new} = \text{Tr}_a \left[\hat{U} \hat{\rho}_{old} \hat{R} \hat{U}^{-1} \right] \tag{4.50}$$

with the unitary evolution operator $\hat{U}=\exp\{-i\hat{V}_\chi\}\exp\{-i\hat{V}_B\}$ and the interaction $\hat{V}_{\chi,B}$ assuming the following form

$$\hat{V}_{\chi} = (Sdt)^{1/2} \hat{\chi} \hat{c} ; \hat{V}_{B} = (Sdt)^{1/2} \left(\hat{B} \hat{b}^{\dagger} + \hat{B}^{\dagger} \hat{b} \right)$$
 (4.51)

and the trace is over the degrees of freedom of the auxiliary system. At the moment, Hermitian \hat{c} and generally non-Hermitian \hat{b} are arbitrary operators in the space of the auxiliary system, with only condition of their zero expectation values $\langle \hat{c} \rangle = 0$, $\langle \hat{b} \rangle = 0$ (Here, $\langle \hat{A} \rangle \equiv \text{Tr}_a \left[\hat{A} \hat{R} \right]$. To derive the evolution equation, we need to expand \hat{U} up to the second order in $(Sdt)^{1/2}$. With this, we obtain

$$S^{-1}\frac{\partial\hat{\rho}}{\partial t} = \frac{1}{2}\langle\hat{c}^{2}\rangle\left[\hat{\chi},\left[\hat{\chi},\hat{\rho}\right]\right] + \frac{1}{2}\langle\hat{b}^{2}\rangle\left[\hat{B}^{\dagger},\left[\hat{B}^{\dagger},\hat{\rho}\right]\right] - \frac{1}{2}\langle\hat{b}^{\dagger}\rangle\left[\hat{B},\left[\hat{B},\hat{\rho}\right]\right] + \frac{1}{2}\langle\hat{b}^{\dagger}\rangle\left[-\frac{1}{2}\hat{B}^{\dagger}\hat{B}\hat{\rho} - \frac{1}{2}\hat{B}^{\dagger}\hat{B}\hat{\rho} + \hat{B}\rho\hat{B}^{\dagger}\right] + \langle\hat{b}^{\dagger}\hat{b}\rangle\left[-\frac{1}{2}\hat{B}\hat{B}^{\dagger}\hat{\rho} - \frac{1}{2}\hat{B}\hat{B}^{\dagger}\hat{\rho} + \hat{B}^{\dagger}\rho\hat{B}\right] - \langle\hat{c}\hat{b}\rangle\hat{B}^{\dagger}\left[\hat{\chi},\hat{\rho}\right] + \langle\hat{b}\hat{c}\rangle\left[\hat{\chi},\hat{\rho}\right]\hat{B}^{\dagger} - \langle\hat{c}\hat{b}^{\dagger}\rangle\hat{B}\left[\hat{\chi},\hat{\rho}\right] + \langle\hat{b}^{\dagger}\hat{c}\rangle\left[\hat{\chi},\hat{\rho}\right]\hat{B}.$$
(4.52)

Comparing this with Eq. 4.49, we recognize we have to require

$$\langle \hat{c}^2 \rangle = \langle \hat{b} \hat{b}^{\dagger} \rangle = \langle \hat{b} \hat{c} \rangle = \langle \hat{c} \hat{b}^{\dagger} \rangle = 1; \ \langle \hat{b}^2 \rangle = \langle \hat{b}^{\dagger 2} \rangle = \langle \hat{c} \hat{b} \rangle = \langle \hat{b}^{\dagger} \hat{c} \rangle = \langle \hat{b}^{\dagger} \hat{b} \rangle = 0. \tag{4.53}$$

Those are the only conditions on the corresponding operators, otherwise they can be chosen in an arbitrary way. We will specify two simple choices below. Yet before this let us present a greater simplification of the method under description. In fact, it is not necessary to deterministically update the whole density matrix that involves the measured system and the detector variables. Equivalently, one can update the system density matrix only while producing at each step a stochastic detector output.

4.7. STOCHASTIC TRAJECTORIES

To see this possibility, let us rewrite Eq. 4.50 in the form that explicates eigenstates of the operator \hat{c} ,

$$\rho_{new} = \sum_{c} \exp\{-i(Sdt)^{1/2} \hat{\chi} \hat{c}\} \mathcal{L}_{c} \rho_{old} \exp\{-i(Sdt)^{1/2} \hat{\chi} \hat{c}\}; \quad (4.54)$$

$$\mathcal{L}_{c}\rho_{old} \equiv \langle c|\exp\{-i(Sdt)^{1/2}\left(\hat{B}\hat{b}^{\dagger} + \hat{B}^{\dagger}\hat{b}\right)\}\hat{\rho}_{old}\hat{R}\exp\{i(Sdt)^{1/2}\left(\hat{B}\hat{b}^{\dagger} + \hat{B}^{\dagger}\hat{b}\right)\}|c\rangle \quad (4.55)$$

If we write in the density matrix the detector variables explicitly $\hat{\rho} \rightarrow \hat{\rho}(s, s')$, and concentrate on diagonal elements, s = s', we see that in the course of the update the s coordinate of any such element is shifted by a value proportional to an eigenvalue of \hat{c} ,

$$\hat{\rho}_{new}(x,x) = \sum_{c} \mathcal{L}_{s} \rho_{old}(x - (Sdt)^{1/2}c, x - (Sdt)^{1/2}c). \tag{4.56}$$

This gives us an idea to regard c as a $random\ variable$. At each update step this variable is generated from the distribution $P(c) = \text{Tr}[(\mathcal{L}_c\hat{r})]$ (the trace here is over the system variables) and contributes to the time-dependent integrated output s(t). The successive updates thus form a $stochastic\ trajectory$ in the space of the outputs, s(t). So we do not have to worry about s-dependence of the density matrix any more since this is certain for a certain trajectory. Instead, we can work with a $stochastic\ density\ matrix\ \hat{r}$ in the system variables that gets a c-dependent update. The actual density matrix $\hat{\rho}(s,s;t)$ is obtained by averaging over all stochastic trajectories that end in the point s. To summarize, the update equations become

$$s_{new} = s_{old} + (Sdt)^{1/2}c;$$
 (4.57)

c is random with the distribution:
$$P(c) = \text{Tr}[(\mathcal{L}_c \hat{r})]$$
 (4.58)

$$\hat{r}_{new} = \frac{\mathcal{L}_c \hat{r}_{old}}{P(c)} \tag{4.59}$$

We remind that for N detectors one has to repeat the update for each detector at each time interval dt, promoting **s** with random **c** in N directions. As mentioned, for the terms of the relevant order (Sdt) the order of these updates does not matter.

In the following two subsections, we describe two concrete examples of the auxiliary systems and corresponding updates.

4.7.1. OSCILLATOR UPDATE

In this case, the possible states of the auxiliary system are those of a harmonic oscillator and the operators \hat{b} , \hat{b}^{\dagger} are conventional annihilation/creation operators of the oscillator. Initially, the oscillator is prepared in the vacuum state, $\hat{R} = |0\rangle\langle 0|$. The operator \hat{c} can be associated with the oscillator coordinate, $\hat{c} = \hat{b} + \hat{b}^{\dagger}$. This choice satisfies the relations (4.53).

Conveniently, the distribution of c is closer to Gaussian in the limit $dt \rightarrow 0$,

$$P(c) \approx |\langle c|0\rangle|^2 = G(c) \equiv (2\pi)^{-1/2} exp(-c^2/2)$$
 (4.60)

It is constructive to specify the full update equation analytically for two cases: no cross-noise, $\hat{B} = -\hat{B}^+ = -\hat{D}/2S$, and no susceptibility, $\hat{B} = \hat{B}^+ = \hat{R}/2S$

For no cross-noise limit, the natural basis is that of eigenfunctions of \hat{D} , that we label with a,b,... The unitary part of the update shifts the wave function of the oscillator in coordinate space by values proportional to D_a . The distribution of c is a composition of shifted Gaussians with weights equal to probabilities to find the system in state a

$$P(c) = r_{aa}G(c - (dt/S)^{1/2}D_a). (4.61)$$

4.8. CONCLUSIONS 91

The density matrix update involves the shifts corresponding both indices,

$$r_{new}^{ab} = r_{old}^{ab} \sqrt{G(c - (dt/S)^{1/2} D_a)G(c - (dt/S)^{1/2} D_b)} / P(c)$$
 (4.62)

For no-susceptibility limit, the relevant basis is of the eigenfunctions of \hat{R} . The unitary part of the update shifts the wave function of the oscillator in momentum space. This does not modify the P(c). The whole update is unitary

$$r_{new}^{ab} = r_{old}^{ab} \exp(ic(dt/S)^{1/2}(R_a - R_b))$$
 (4.63)

yet stochastic owing to the randomness of c. If one knows s(t), the measurement can be "undone" in this situation [8].

4.7.2. QUBIT UPDATE

The simplest auxiliary system is a qubit encompassing two quantum states. The relations (4.53) are satisfied if $\hat{c} = \hat{\sigma}_x$, $\hat{b} = (\sigma_x + i\sigma_y)$ and the initial state is polarized in zdirection (σ -matrices are in the space of the qubit). Two possible random outcomes are therefore $c = \pm 1$.

Let us explicate the update analytically in two limits. For the no cross-noise limit, the unitary part of the update rotates the qubit spin about the y-axis with the angles proportional to the eigenvalues of \hat{D} The probabilities of $c = \pm 1$ outcome read

$$P(c) = \frac{1}{2} \left(1 - \sin((dt/S)^{1/2} D_a) r_{old}^{aa} \right)$$
 (4.64)

and the whole update is expressed as

$$r_{new}^{ab} = r_{old}^{ab} (\cos((dt/S)^{1/2}(D_a - D_b)/2) - c\cos((dt/S)^{1/2}(D_a + D_b)/2)/(2P(c))$$
 (4.65)

In the no susceptibility limit, the probabilities of both outcomes are equal, and the whole update is random and unitary,

$$r_{new}^{ab} = r_{old}^{ab} \exp(ic(dt/S)^{1/2}(R_a - R_b))$$
 (4.66)

The qubit update can be expressed analytically in terms of operators \hat{B} , \hat{B}^+ only, yet the expression is too cumbersome to be instructive.

4.8. CONCLUSIONS

In conclusion, we have established a general framework for the description of a CWLM of an arbitrary quantum system by an arbitrary number of the detectors. We have compared different approaches to the problem and demonstrated their equivalence. The approaches include the full counting statistics (FCS) evolution equation a for pseudodensity matrix (Eq. 4.29), the drift-diffusion equation (Eqs. 4.32, 4.46) for a density matrix in the space of integrated outputs, and discrete stochastic updates (Eq. 4.57). We provide the derivation of the underlying equations from microscopic approach based on full counting statistics method (Section 4.2), a phenomenological approach based on Lindblad construction (Section 4.4), and interaction with auxiliary quantum systems

92 References

representing the detectors (Sections 4.6,4.7). We give the necessary conditions on the phenomenological susceptibilities and noises that guarantee the unambiguous interpretation of the measurement results and the positivity of density matrix.

The applicability of the framework is restricted by a Markov assumption: no delay of susceptibilities and no time correlation of noises at the time scale of quantum dynamics. Different methods are required to treat the effects of delay and time correlations at quantum level. However, the framework can be easily extended to incorporate delays at classical level. It can be also extended to describe various quantum feedback schemes where the quantum system is subject to manipulation, and the decision on the way to manipulate is based on the values of detector outputs. This will be addressed in future work.

REFERENCES

- [1] A. A. Clerk, M. H. Devoret, S. M. Girvin, F. Marquardt, and R. J. Schoelkopf, *Introduction to quantum noise, measurement, and amplification*, Rev. Mod. Phys. **82**, 1155 (2010).
- [2] J. von Neumann, *Mathematische Grundlagen der Quantenmechanik. (German) [Mathematical Foundations of Quantum Mechanics]* (Springer-Verlag, Berlin, Germany / Heidelberg, Germany / London, UK / etc., 1932) reprinted: Dover Publications (1943); Presses Universitaires de France (1947); Madrid, Institute de Matematicas "Jorge Juan" (1949). Translated from German by Robert T. Beyer, Princeton University Press (1955).
- [3] M. B. Mensky, *The action uncertainty principle in continuous quantum measurements*, Physics Letters A **155**, 229 (1991).
- [4] A. N. Korotkov, Continuous quantum measurement of a double dot, Phys. Rev. B **60**, 5737 (1999).
- [5] A. Jordan and M. Buttiker, *Continuous quantum measurement with independent detector cross correlations*, Phys. Rev. Lett. **95**, 220401 (2005).
- [6] H. Wei and Y. V. Nazarov, *Statistics of measurement of noncommuting quantum variables: Monitoring and purification of a qubit,* Phys. Rev. B **78**, 045308 (2008).
- [7] K. Jacobs and D. A. Steck, *A straightforward introduction to continuous quantum measurement*, Contemporary Physics **47**, 279 (2006), http://dx.doi.org/10.1080/00107510601101934.
- [8] A. N. Korotkov and A. N. Jordan, *Undoing a weak quantum measurement of a solid-state qubit*, Phys. Rev. Lett. **97**, 166805 (2006).
- [9] A. Chantasri, J. Dressel, and A. N. Jordan, *Action principle for continuous quantum measurement*, Phys. Rev. A **88**, 042110 (2013).

- [10] M. Hatridge, S. Shankar, M. Mirrahimi, F. Schackert, K. Geerlings, T. Brecht, K. M. Sliwa, B. Abdo, L. Frunzio, S. M. Girvin, R. J. Schoelkopf, and M. H. Devoret, *Quantum back-action of an individual variable-strength measurement*, Science 339, 178 (2013).
- [11] P. Campagne-Ibarcq, L. Bretheau, E. Flurin, A. Auffèves, F. Mallet, and B. Huard, *Observing interferences between past and future quantum states in resonance fluo-rescence*, Phys. Rev. Lett. **112**, 180402 (2014).
- [12] J. P. Groen, D. Ristè, L. Tornberg, J. Cramer, P. C. de Groot, T. Picot, G. Johansson, and L. DiCarlo, *Partial-measurement backaction and nonclassical weak values in a superconducting circuit*, Phys. Rev. Lett. 111, 090506 (2013).
- [13] K. W. Murch, S. J. Weber, C. Macklin, and I. Siddiqi, *Observing single quantum trajectories of a superconducting quantum bit*, Nature **502**, 211 (2013).
- [14] N. Roch, M. E. Schwartz, F. Motzoi, C. Macklin, R. Vijay, A. W. Eddins, A. N. Korotkov, K. B. Whaley, M. Sarovar, and I. Siddiqi, *Observation of measurement-induced en*tanglement and quantum trajectories of remote superconducting qubits, Phys. Rev. Lett. 112, 170501 (2014).
- [15] A. Franquet and Y. V. Nazarov, *Probability distributions of continuous measurement results for conditioned quantum evolution*, Phys. Rev. B **95**, 085427 (2017).
- [16] A. Franquet and Y. V. Nazarov, *Probability distributions of continuous measure-ment results for two non-commuting variables and conditioned quantum evolution*, arXiv:1708.05662 [quant-ph] (2017).
- [17] Y. Aharonov, D. Z. Albert, and L. Vaidman, *How the result of a measurement of a component of the spin of a spin-1/2 particle can turn out to be 100*, Phys. Rev. Lett. **60**, 1351 (1988).
- [18] H. Wiseman and G. Milburn, *Quantum theory of optical feedback via homodyne detection*, Phys.Rev. Lett. **70**, 548 (1993).
- [19] J. Atalaya, S. Hacohen-Gourgy, M. S. Leigh, I. Siddiqi, and A. N. Korotkov, *Multitime correlators in continuous measurement of qubit observables*, Phys. Rev. A **97**, 020104 (2018).
- [20] J. Dressel, A. Chantasri, A. N. Jordan, and A. N. Korotkov, Arrow of time for continuous quantum measurement, Phys. Rev. Lett. 119, 220507 (2017).
- [21] R. Ruskov, A. N. Korotkov, and K. Mølmer, *Qubit state monitoring by measurement of three complementary observables*, Phys. Rev. Lett. **105**, 100506 (2010).
- [22] Y. V. Nazarov and Y. M. Blanter, *Quantum Transport: Introduction to Nanoscience* (Cambridge University Press, 2009).
- [23] G. Lindblad, *On the generators of quantum dynamical semigroups*, Communications in Mathematical Physics **48**, 119 (1976).

94 REFERENCES

[24] M. Mensky, Continuous quantum measurements: Restricted path integrals and master equations, Physics Letters A 196, 159 (1994).

- [25] A. Chantasri and A. N. Jordan, *Stochastic path-integral formalism for continuous quantum measurement*, Phys. Rev. A **92**, 032125 (2015).
- [26] Y. V. Nazarov and M. Kindermann, *Full counting statistics of a general quantum mechanical variable*, The European Physical Journal B Condensed Matter and Complex Systems **35**, 413 (2003).

4

CONDITIONED OUTPUTS,
DISTRIBUTION OF DECISION TIMES
AND MEASUREMENT-BASED
FEEDBACK SCHEME FOR
CONTINUOUS WEAK LINEAR
MEASUREMENT OF A SIMPLE
QUANTUM SYSTEM

5.1. Introduction

The standard description of quantum mechanics introduces projective measurement as an instantaneous non-unitary process by which a quantum system is projected into an eigenstate of a measured observable with a probability given by Born's rule. In reality, the measurements are never instantaneous but occur over some time scale that is determined by the details of the interaction between the measured system and its environment and required to obtain a reliable measurement result. This idea has become one of the basis and principal ingredients in the study of quantum control at the core of quantum computing and communication [1].

A more general and adequate description of the measurement process is provided by the paradigm of continuous weak linear measurement (CWLM) [2–8].

Recent technological advances have made possible to utilize and study CWLM in every detail for a set of quantum device setups. Experiments realize continuous measurement and monitoring of quantum systems, and even provide the information about single quantum trajectories [9–15]. This resulted in a more elaborative and practical understanding of the measurement process in quantum mechanics.

In particular, the experimental realization of interesting phenomena related to the conditioning of a quantum system using measurement and feedback is of relevance to our work [16–20].

In this work, we study the CWLM implementing numerically an iterative simulation procedure that is essentially equivalent to those commonly used [21, 22] but formulated in more transparent and basic terms. This tool permits a deep investigation of the measurement process that is not possible analytically. With this, we can directly simulate individual quantum trajectories from the first principle quantum state evolution and quickly accumulate sufficiently big statistics of these trajectories to compute the distribution of various quantities characterizing the measurement, including the conditioning of the trajectories.

In contrast to usual descriptions of CWLM that are based on a Bloch equation for the density matrix of the measured system , or on stochastic differential equations, the tool gives insight not only into the characteristics of the measured system but also into the generation of a measurement signal in a linear measurement setup. The tool is quite simple. The detector is represented by a qubit. At each step of the simulation, the qubit is first initialized to an equal-weight superposition of two states. Then for a time interval of Δt it is coupled to the system measured. We evaluate the unitary evolution of the system and the qubit on this interval. After that, the qubit is measured projectively. The measurement result counts for the detector output at this time interval, and the density matrix of the system is updated according to the measurement result. We show that this setup accurately reproduces CWLM at proper choice of measurement strength and the duration of the time interval.

Although the tool permits accurate simulation of rather complex quantum systems and measurement setups, in this Article we apply it to the simulation of one of the simplest yet generic situations of CWLM: the non-demolition measurement (see e.g. [23]). The quantum system is a qubit. It is initially prepared in an equal-weight superposition of two quantum states, $(|+\rangle + |-\rangle)/\sqrt{2}$. It is measured in the basis of these two states. As a

5.1. Introduction 97

result of the decoherence induced by the measurements, the superposition is destroyed at certain time scale, and the density matrix of the qubit becomes diagonal. The qubit is in either of the two states. The mean value of the detector output V(t) freezes at one of the two levels corresponding to the states. We normalize the signal such that these levels correspond to $v=\pm 1$. A repetitive measurement would reproduce the same result. Since the detector signal is noisy, it takes a finite time to resolve these two levels of the signal. This acquisition time is of the same order as decoherence time [24]. Owing to simplicity of the system, we can compare some results of the simulation with the analytical results.

We start our study with computing the average value of the detector output. Owing to symmetric initial conditions, this value is always zero. However, we can condition the output at its asymptotic mean value computing $\langle v(t)v(\infty)\rangle$. An intuitive expectation is that this quantity is 0 at t=0 (since the qubit is in an equal-weight superposition) and saturates at 1 if $t\to\infty$. However, we show that the conditioned output does not depend on time. It looks like the qubit "knows" from the very beginning in which of the two states it is and the superposition is indistinguishable from an equal-weight diagonal density matrix. We confirm this counter intuitive result analytically.

In reality, an observer can not instantly decide in which state the qubit is. Let us assume that the observer has full information about the measurement results of the detector qubit and can therefore access the density matrix of the measured qubit along the quantum trajectory at any given moment of time. He monitors the probability to be in one of the states, say, p_+ , and waits till it achieves certain small threshold h. If $p_+ = 1 - h/2$, he decides that the qubit is in '+' state, if $p_+ = h/2$, the qubit must be in the opposite state. This moment we call *decision time*. This time varies from trajectory to trajectory, and we are interested in the distribution of the decision times and its dependence on the threshold h. This quantifies how fast the measurement can bring certain result and helps in planning an actual fast measurement.

We go into details of decision dynamics and consider the situation when the decisions are used for a feedback. As a simple example, we formulate and simulate a feedback scheme that has a purpose to keep the qubit in the equal-weight superposition. The observer accumulates the detector output during a time interval T_f . If the average value of the output exceeds a certain threshold, $|\nu| > I$, he decides the qubit is in the state $\mathrm{sgn}(\nu)$ and applies a correcting unitary transformation that brings the qubit back to the equal-weight superposition. We made detailed simulations of the feedback dynamics and attempt to optimize the average probability to be in the superposition with respect to parameters I, T_f . We compare the results with some analytical predictions.

The structure of the Article is as follows. We explain and present the simulation tool used in Section 5.2 and formulate the general description of the scheme. In subsection 5.2.1 we specify to the case when the detector qubit can be effectively considered as a linear detector that measures another qubit and discuss the conditions for this and the details of numerical implementation.

Further, in Section 5.3 we present the simulation results concerning the average conditioned detector output and the distribution of the decision times.

In Section 5.4, we present and discuss the feedback scheme described. The subsection 5.4.1 elaborates on the scheme on analytical level. We present the simulation results of the feedback dynamics in subsection 5.4.2 and show how optimize the feedback effi-

ciency as a function of two parameters. We conclude in Section 5.5.

5.2. THE SIMULATION TOOL

Our goal is to describe in general a continuous measurement process using a discrete stochastic update approach. We outline a step-by-step stochastic process that will mimic a random time-line of an actual continuous measurement performed in an experimental setup.

Let us consider a general measurement scenario in which a quantum system A is being measured with making use of another quantum system B (the detector). The dynamics of these systems are governed by the corresponding Hamiltonians \hat{H}_A , \hat{H}_B .

For the information transfer from the system measured to the detector, there must be an interaction between those systems, a coupling of a kind between the degrees of freedom of A and B. Thus, the complete dynamics in this simple yet general scenario is governed by a total Hamiltonian:

$$\hat{H} = \hat{H}_A + \hat{H}_B + \hat{H}_C, \tag{5.1}$$

where \hat{H}_c is the coupling Hamiltonian. For a simplest case when the detector is sensitive to a single observable M, the coupling Hamiltonian can be represented as $\hat{H}_c = \hat{M} \otimes \hat{Q}$ where \hat{M} is an operator acting in system A and \hat{Q} is an operator acting in B.

The stochastic update process we construct is supposed to simulate the time-line of an actual experimental run where the random outputs of the detectors in short time intervals are measured and recorded. With this in mind, the coupling at each step persists during a time interval Δt . To simulate a continuous measurement, the Δt should be chosen such that the change of the density matrix of the measured system $\propto \Delta t$ is small. In this limit, the simulation process can be described with a quasi-continuous stochastic differential equation.

At the beginning of the simulation step, the interaction has not been switched on. The measured system and the detector are in a product state $\hat{\rho}_i = \hat{\rho}^A(0) \otimes \hat{\rho}^B(0)$. It is convenient to initialize the detector to the same $\hat{\rho}^B$ at each step. Then the whole density matrix undergoes a unitary evolution determined by \hat{H} . It is convenient to disregard \hat{H}_A and \hat{H}_B for this evolution. One can formally do this, for instance, by applying a unitary transformation that switches to the interaction picture and to disregard subsequently the time dependence of $H_c(t)$ during a short time interval Δt . Alternatively, one can separate the evolution governed by $\hat{H}_A + \hat{H}_B$ and H_c in time, adding an extra simulation step of the same duration where the dynamics is governed by $\hat{H}_A + \hat{H}_B$. This is valid in the limit of small Δt where $\exp\left(i\hat{H}\Delta t\right) \approx \exp\left(i(\hat{H}_A + \hat{H}_B)\Delta t\right) \exp\left(i\hat{H}_c\Delta t\right)$ With this, the whole density matrix in the end of the time interval becomes

$$\hat{\rho}(\Delta t) = e^{-i\Delta t \hat{M} \hat{Q}} \hat{\rho}_i e^{+i\Delta t \hat{M} \hat{Q}}. \tag{5.2}$$

One can use the eigenbasis $|n\rangle$ of the operator \hat{M} , $\hat{M}|n\rangle = M_n|n\rangle$ to rewrite the previous equation

$$\hat{\rho}(\Delta t) = \sum_{n,m} \rho_{n,m}^{A}(0) |n\rangle \langle m| \otimes \hat{K}_{n,m}(\Delta t), \tag{5.3}$$

where $\hat{K}_{n,m}(\Delta t) = e^{-i\Delta t M_n \hat{Q}} \hat{\rho}^B(0) e^{+i\Delta t M_m \hat{Q}}$.

After the time interval, the detector system is projectively measured in the basis $|i\rangle$ that *does not* coincide with the eigenbasis of \hat{Q} . The probability of the outcome i is given by

$$P(i) = \operatorname{Tr}_{A} \langle i | \hat{\rho}(\Delta t) | i \rangle = \sum_{n} \rho_{n,n}^{A}(0) \langle i | \hat{K}_{n,n}(\Delta t) | i \rangle.$$
 (5.4)

Here, Tr_A is a partial trace over the space of the system A Once the detector is projected to the state i, and the result is recorded, the density matrix of the system measured becomes

$$\rho_{new}^{A}(\Delta t) = \frac{\sum_{n,m} \rho_{n,m}^{A}(0) |n\rangle \langle m| \langle i| \hat{K}_{n,m}(\Delta t) |i\rangle}{\sum_{n} \rho_{n,n}^{A}(0) \langle i| \hat{K}_{n,n}(\Delta t) |i\rangle}.$$
(5.5)

This density matrix is taken as the initial one $\hat{\rho}_A$ at the next step of the simulation. The detector is initialized again to $\hat{\rho}^B(0)$ and the step is repeated.

With this procedure, the random outputs of the detector are recorded like eventual readings in an experiment while the measured system undergoes a stochastic update process. The random outputs of the detector can then be combined in a random time-dependent variable V(t) which due to the previous derivation will contain information about the measured system expected values of the operator \hat{M} . As discussed in the following section, this simulates CWLM provided the strength of the interaction at each step $(\hat{M}\Delta t)$ is small.

While any quantum system is in principle suitable to simulate a detector, here we concentrate on a simplest one and consider a qubit.

5.2.1. QUBIT AS A LINEAR DETECTOR

Let us consider a qubit that measures an operator \hat{M} in the space of the system A. In general, this operator may be associated with an effective magnetic field acting on the qubit pseudo-spin. This magnetic field causes precession of the pseudo-spin with the angle directly proportional to this magnetic field. This leads to a straightforward setup of an approximately linear qubit detector. Initially, the qubit pseudo-spin is in x direction. Let the magnetic field rotate it in y direction. This will cause the deviation of the pseudo-spin in z direction that is linear in \hat{M} in the limit of small $\hat{M}\Delta t$.

To quantify, we note that initially the whole system is in a product state $\hat{\rho}(0) = \hat{\rho}^A \otimes |x\rangle \langle x|$ (where $\hat{\sigma}_x |x\rangle = |x\rangle$ is an eigenstate of the Pauli matrix $\hat{\sigma}_x$). At the start of a step, we turn on the coupling Hamiltonian $\hat{H}_c = \hat{M} \otimes \hat{\sigma}_y$ for the duration Δt of the step. By the end of the step, the resulting density matrix in the eigenbasis of the operator \hat{M} reads

$$\hat{\rho}_{n,m}(\Delta t) = \hat{\rho}_{n,m}^{A}(0) \otimes e^{-iM_{n}\hat{\sigma}_{y}\Delta t} |x\rangle \langle x| e^{iM_{m}\hat{\sigma}_{y}\Delta t}$$

$$= \hat{\rho}_{n,m}^{A}(0) \otimes \hat{K}_{n,m}(\Delta t),$$
(5.6)

 M_n being the eigenvalues of \hat{M} .

In the end of the step, the detector qubit is projected onto the $Z(\hat{\sigma}_z)$ basis and a result of ± 1 is recorded, with the probability given by Eq. (5.4),

$$P(\pm) = \frac{1}{2} \sum_{n} \rho_{n,n}^{A}(0) \left(1 \pm \sin(2M_n \Delta t)\right)$$
 (5.7)

We see that $\langle \hat{\sigma}_z \rangle = 2\Delta t \langle \hat{M} \rangle$ in the limit of $\hat{M} \Delta t \to 0$, as one expects from a linear measurement setup.

Finally, the density matrix of the system A is updated depending on the detector reading ± 1 according to Eq. (5.5),

$$\hat{\rho}_{n,m,\pm}^A = P^{-1}(\pm)\rho_{n,m}^A(0)(c_n \pm s_n)(c_m \pm s_m)$$
(5.8a)

$$c_n, s_n \equiv \cos(M_n \Delta t), \sin(M_n \Delta t)$$
 (5.8b)

Naturally, this particular choice of the initial state, the interaction Hamiltonian and the projection basis is somewhat arbitrary. The choice can be modified, as long as the qubit precession retains information about \hat{M} and is detected by a projective measurement.

To simulate the CWLM at a time interval of duration T, the step is repeated $N = T/\Delta t$ times. The resulting data set for the measurement results and the density matrices at each step of the time evolution is referred as a quantum trajectory [9–11, 16]. The averaged quantum evolution is obtained by averaging over the quantum trajectories.

If, in addition to the measurement, the system A is subject to Hamiltonian dynamics with Hamiltonian \hat{H}_A , this can be included by extending each step with a unitary transformation with the corresponding evolution matrix $\exp(-i\hat{H}_A\Delta t)$. The error of such separation of the measurement and the Hamiltonian evolution in time scales as $(\Delta t)^2$ and is therefore negligible in the limit of $\Delta t \to 0$.

For each run, we obtain a set of $\sigma_i=\pm 1$ measurement outcomes that are almost equally distributed and independent provided that the measurement strength $\hat{M}\Delta t$ of each measurement is small. This is in contrast with an output of a linear detector V(t) that is a continuous number defined for continuous time. It has a white noise spectrum $\langle V(t)V(t')\rangle = \delta(t-t')$. The instant output value has an infinite variance so an actual experimental reading gives the output integrated over a time interval \mathcal{T} , $\bar{V}(t)=\mathcal{T}^{-1}\int_t^{t+\mathcal{T}}d\tau V(\tau)$ that has the finite variance $\langle \bar{V}^2\rangle=S/\mathcal{T}$. To simulate the output, we associate

$$\bar{V}(t) = K^{-1} \sum_{i=0}^{K} \sigma_i$$
 (5.9)

where $K = \mathcal{T}/\Delta t$, and summation is over K measurement results in the time interval $(t, t + \mathcal{T})$. The distribution of the sum is normal at $K \gg 1$ so it accurately reproduces the continuous normal-distributed output. Comparing the variances of both sides we conclude that $S = \Delta t$.

We conclude that the qubit can accurately simulate a linear detector provided $\Delta t \ll \mathcal{T} \ll T$ and $M_n \Delta t \ll 1$. To provide more accurate estimations, we assume, for the rest

of the paper, that the system A is also a qubit and $\hat{M} \equiv M \hat{\Sigma}_z$, $\hat{\Sigma}_i$ being the Pauli matrices in the space of the qubit measured. The eigenvalues of \hat{M} are thus $\pm M$. We thus provide the linear detection of z-component of the qubit, $\langle V \rangle = 2M\Delta t \langle \hat{\Sigma}_z \rangle$. For a decisive measurement, the standard deviation of the averaged output signal at the time interval T, $\sqrt{S/T}$, should be smaller than the separation $4M\Delta t$ between the discrete values of the output that correspond to $\langle \hat{\Sigma}_z \rangle = \pm 1$. This gives a typical time scale at which a decisive measurement takes place, $T_c = (M^2 \Delta t)^{-1}$. Since an interesting simulation would encompass a time interval at least of the order of T_c , $N > (M\Delta t)^{-2}$.

A general CWLM is characterized by an inequality [24]

$$S_{out}S_{in} \ge a^2/4 \tag{5.10}$$

where S_{out} , S_{in} are output and input noises, respectively and a is the linear susceptibility of the detector signal to the input. Substituting the parameters of our setup, $S_{out} = \Delta t$, $a = 2M\Delta t$, $S_M = M^2\Delta t$, we conclude that our setup simulates an *ideal* detector. More general CWLM with non-ideal detector can be simulated if we just add an extra white noise signal to the output, this would lead to an expected deterioration of the measurement quality.

5.3. THE SIMPLE MEASUREMENT SETUP: SIMULATION RESULTS

Here, we present the simulation results for a very simple and generic setup. We measure the z-projection of a qubit pseudospin setting it initially to an equal-weight superposition $|x\rangle$. Owing to the symmetry of the initial condition, $\langle \hat{\Sigma}_z \rangle = 0$ at any time. However, at sufficiently long time the superposition is destroyed and the qubit is in one of the states $|+\rangle, |-\rangle$, this is reflected in the measurement output at sufficiently big durations. One can say that a spontaneous symmetry breaking takes place upon the measurement. Owing to the simplicity of the setup, there are simple and known analytical solutions. The average density matrix satisfies an evolution equation

$$\frac{\partial \hat{\rho}}{\partial t} = -\left(\hat{\rho} - \hat{\Sigma}_z \hat{\rho} \hat{\Sigma}_z\right),\tag{5.11}$$

where we measure time in units of T_c . The solution that satisfies the initial condition reads $\hat{\rho}(t) = (1 + e^{-2t}\hat{\Sigma}_x)/2$. One can also evaluate the joint density matrix of the qubit and the measurement outputs. It is convenient for us to use the counting field method [6, 17]. In this method, one considers a time interval $(\tau, \tau + T)$ and solves an evolution equation for the augmented density matrix $\hat{\rho}(\chi)$ in this interval,

$$\frac{\partial \hat{\rho}}{\partial t} = -\frac{\chi^2}{8} \hat{\rho} + i \frac{\chi}{2} (\hat{\Sigma}_z \hat{\rho} + \hat{\rho} \hat{\Sigma}_z) - (\hat{\rho} - \hat{\Sigma}_z \hat{\rho} \hat{\Sigma}_z). \tag{5.12}$$

We normalize the average output in such a way that $v = \pm 1$ for two projections of $\hat{\Sigma}_z$. The joint density matrix $\hat{\rho}(v)$ is then given by

$$\hat{\rho}(\nu) = \frac{T}{2\pi} \int d\chi \hat{\rho}(\chi) e^{-i\chi \nu T}$$
(5.13)

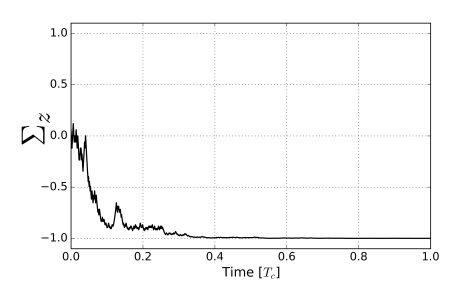
Its trace gives the distribution of the normalized averaged output in this interval.

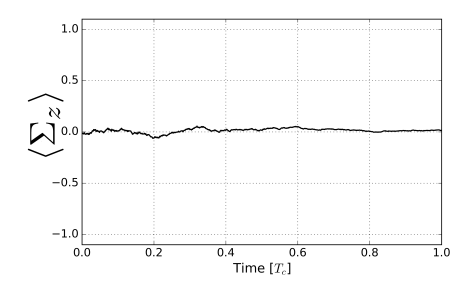
5.3.1. QUANTUM TRAJECTORIES

In Fig. 5.1 we present a typical output of a simulation run. The simulations are performed setting the measurement strength to $M\Delta t=0.03$ and choosing the characteristic time scale $T_c=1$. No Hamiltonian evolution is included. Figure 5.1a shows a single quantum trajectory of the qubit measured during the CWLM. In order to distinguish various averages, we denote $\Sigma_z(t)={\rm Tr}(\hat{\Sigma}_z\rho(t))$ the pseudospin component averaged with the density matrix along a single trajectory, while $\langle \Sigma_z(t) \rangle$ denotes the average over the trajectories at a given moment of time.

We thus plot the $\Sigma_z(t)$. As we see, the projection fluctuates rather wildly, yet approaches ± 1 upon increasing time, so that at sufficiently long time the qubit is projected into either the $|+\rangle$ or the $|-\rangle$ state.

For the plot in Fig. 5.1b, we run the simulation 100 times and average over all the quantum trajectories. As expected, the contributions of the trajectories with opposite final states compensate each other and $\langle \Sigma_z \rangle$ approaches zero with $\simeq 10\%$ deviations.





(a) Single trajectory.

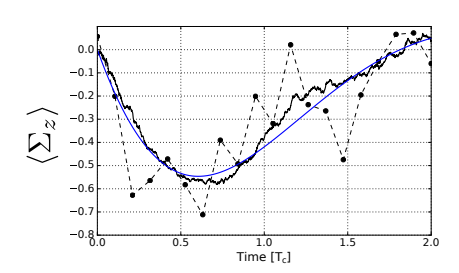
(b) Average of 100 trajectories.

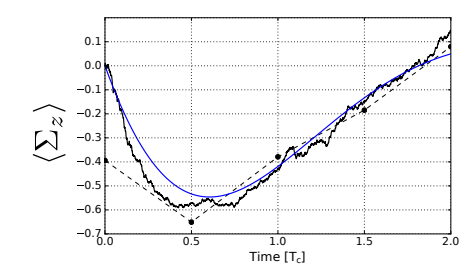
Figure 5.1: Quantum trajectories of the qubit (Σ_z is shown) obtained from the simulation. A single trajectory (Fig. (a)) is rather noisy exhibiting sharp jumps induced by the random measurement at each step. A single trajectory gives an information on the *random* detector outputs. The averaging over 100 trajectories (Fig. (b)) reproduces the result $\Sigma_z = 0$ for the density matrix computed when disregarding the detector outputs.

5.3.2. SIMULATION OF THE DETECTOR SIGNAL

Let us now investigate the detector signal. As described, in our simulation procedure it is obtained by summing up the random results of the projective measurements accumulated during a sampling interval \mathcal{T} . This gives a certain number of detector readings. There is an obvious trade-off between the number of readings and the noise in each reading.

A Hamiltonian $\hat{H}_A = \hbar T_c^{-1} \hat{\sigma}_y$ is added such that the average Σ_z is more "interesting": the Hamiltonian leads to precession of the qubit spin in x-z plane. For this choice, $\langle \Sigma_z \rangle = -2e^{-t}\sin(\sqrt{3}t)/\sqrt{3}$. In Fig. 5.2 we present the average of 100 trajectories and the detector readings for two values of the sampling interval: $\mathcal{F} = 0.1$ (Fig. 5.2a) and $\mathcal{F} = 0.4$ (Fig. 5.2b). We observe that the trajectory average is reasonably close to the analytical prediction $\langle \Sigma_z \rangle (t)$. The same holds for the detector readings. However, the correspondence is worse given the same statistics accumulated. This is related to the trade-off mentioned: the readings at short sampling intervals are too noisy, making the





(a) Average of 100 trajectories with the sampling interval of $\mathcal{T} = 0.1$ for the detector signal. pling interval of $\mathcal{T} = 0.4$ for the detector signal.

Figure 5.2: Averaged qubit trajectories and the corresponding detector signal for different sampling intervals \mathcal{F} . To make the the average detector signal non-zero, we have augmented the dynamics by adding a Hamiltonian $\hat{H}_A = \hbar T_c^{-1} \hat{\sigma}_y$. The duration of the sampling interval \mathcal{F} controls the noise of the detector readings. The plots illustrate how the average over the trajectories and the detector readings approach $\langle \Sigma_z \rangle(t)$ given by the solid line.

interval larger decreases the number of independent detector readings.

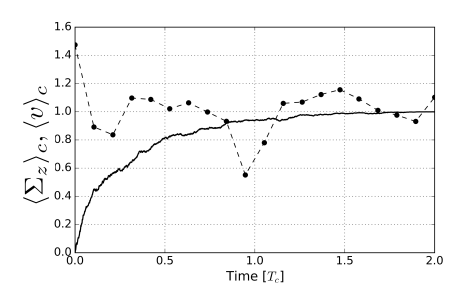
5.3.3. RESULTS FOR CONDITIONED OUTPUT

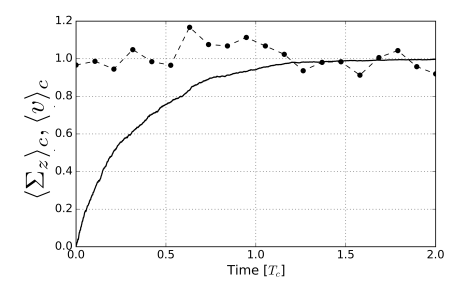
An interesting behaviour of the detector output can be seen in conditioned measurements [17]. For our setup, it is natural to condition the quantum trajectories on their asymptotic values at long times where the corresponding Σ_z sticks to ± 1 . This is equivalent to a post-selection to the states $|+\rangle$ or $|-\rangle$. So we accumulate the statistics of the quantum trajectories and the corresponding detector outputs taking the values of $\Sigma_z(t)$ and v(t) with the sign of $\Sigma_z(\infty)$ (or, equivalently, $v(\infty)$, since the output corresponds to the state at $t \to \infty$). We disregard the Hamiltonian dynamics, $\hat{H}_A = 0$.

In Fig. 5.3 we present these conditional averages of $\Sigma_z(t)$ and v(t), $\langle \Sigma_z(t) \rangle_c$, $\langle v(t) \rangle_c$. In Fig. 5.3a and 5.3b the sampling interval is chosen $\mathcal{T}=0.1$ while in Fig. 5.3c and 5.3d we use $\mathcal{T}=0.4$. We average over 100 post-selected trajectories in Fig. 5.3a and 5.3c , and over 500 post-selected trajectories in Fig. 5.3b and 5.3d.

Let us discuss first the conditioned average of $\Sigma(z)$, $\langle \Sigma_z(t) \rangle_c$. As one may expect, it starts at 0 at t=0 where qubit is in the equal-weight superposition and approaches 1 at the time scale $\simeq T_c$. Collecting statistics of 20000 trajectories, we have shown that with '10⁻² relative accuracy $\langle \Sigma_z(t) \rangle_c = \tanh(f(t))$, f(t) = t(1.15 + 2.8/(1 + 4.2t)).

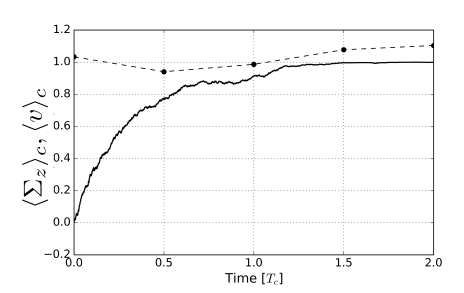
Generally, one may expect that the average detector signal follows $\langle \Sigma_z(t) \rangle_c$. We have seen that this is the case for unconditional averages. Rather surprisingly, it does not. Moreover, the average signal does not depend on time, $\langle \nu(t) \rangle_c = 1$. It looks like the qubit initially is not in a superposition, but just from the beginning is already in one of $|\pm\rangle$ states, and this state does not change during the measurement. The observed conditioned output would be the same as from a classical bit that is randomly put to one of the two states in the beginning.

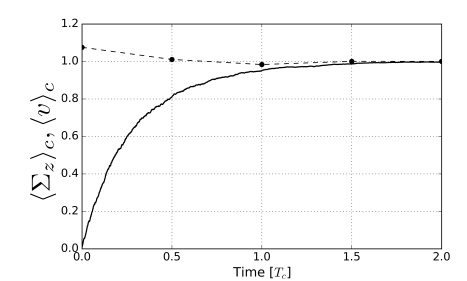




ries. The detector signal is computed with the ries. The detector signal is computed with the sampling interval $\mathcal{T} = 0.1$.

(a) The conditional average over 100 trajecto- (b) The conditional average over 500 trajectosampling interval $\mathcal{T} = 0.1$.





(c) The conditional average over 100 trajecto- (d) The conditional average of 500 trajectories. ries. The detector signal is computed with the The detector signal is computed with the samsampling interval $\mathcal{T} = 0.4$.

pling interval $\mathcal{T} = 0.4$.

Figure 5.3: The average $\langle \Sigma_z(t) \rangle_c$ and the detector signal $\langle v(t) \rangle_c$ conditioned on the final state. The $\langle \Sigma_z(t) \rangle_c$ exhibits an expected behaviour corresponding to transition from the equal-weight superposition at t = 0 where $\Sigma_z = 0$ to the final $|\pm\rangle$ where $\langle \Sigma_z(t) \rangle_C = 1$ at a time scale $\simeq T_C$. Rather counter intuitively, the average output does not follow $\langle \Sigma_z(t) \rangle_C$, and, with numerical accuracy, does not depend on time, $\langle v(t) \rangle_C = 1$. It looks like the qubit "knows" from very beginning that it is in a final state.

It should be possible to confirm such simple result analytically. Indeed, it follows from a straightforward calculation that employs the formalism introduced in [6, 17]. Let us collect detector output during two time intervals: first one of duration t_1 and the second one that follows the first and has the duration t_2 . To find the distribution of two outputs $v_{1,2}$, we need to solve Eq. 5.12 for a time-dependent $\chi(t)$ that takes values $\chi_{1,2}$ in the intervals and is zero otherwise. The distribution is computed from the Fourier transform of $\text{Tr}[\rho(\chi_{1,2}]]$ and reads

$$P(v_1, v_2) = \frac{\sqrt{t_1 t_2}}{\pi} \sum_{+} e^{-2(v_1 \pm 1)^2 t_1} e^{-2(v_2 \pm 1)^2 t_2}$$
(5.14)

It does not depend on the start time moments of the interval but only on their durations. To adjust this general expression to our situation, we take the limit $t_2 \to \infty$ restricting v_2 to ± 1 . The conditional probability then becomes

$$P(\nu_1|\nu_2=1) = \sqrt{\frac{2t_1}{\pi}}e^{-2(\nu_1-1)^2t_1}.$$
 (5.15)

Apparently, $\langle v(t) \rangle_c = 1$ does not depend on time, in agreement with the numerical results.

5.3.4. DECISION TIME DISTRIBUTION

Let us consider a knowledgeable observer who has access to all the results of the projective measurements of the detector. With this, and with the known initial condition he is able to reconstruct the density matrix along an individual quantum trajectory and monitor it in time. Suppose he needs to decide upon the final state of the qubit as soon as possible. He does this by monitoring $\Sigma_z(t)$. Whilst its absolute value reaches a certain threshold $|\Sigma_z| = 1 - h$, he makes the decision based on the sign of Σ_z . We note that the decision may be wrong, and further evolution along the trajectory would bring the qubit to the opposite quantum state. Association $p_{\pm} = (1 \pm \Sigma(z))/2$ suggests that the probability of error is 0.5h, and this is confirmed by our numerical simulations. Thus the decision is well-based in the limit of small h. So-defined decision time is thus a random quantity, its distribution depending on h. This distribution is useful for a less knowledgeable and less devoted observer, who just wishes to quantify a time required for the qubit to come to a certain state with sufficiently high probability.

We have evaluated the distribution numerically at various small threshold values h collecting the statistics of $4 \cdot 10^5$ trajectories. We have made the histograms and fitted their shape. The results are presented in Fig. 5.4.

As expected, the body of the distribution shifts to longer times upon decreasing h, this is accompanied by an increase in the variance. We choose to fit the distribution shape with a rather arbitrary function $ce^{-a/t-bt}$ which is exponentially small at short and long times, a, b being free coefficients and c being fixed by the normalization. The fits are excellent, especially at smaller b. The values of the coefficients a, b for different b are given in the table b.

h	a	b
10^{-1}	0.0820617	4.88529
10^{-2}	0.452684	3.28453
10^{-3}	1.13362240458	2.84497317856
10^{-4}	2.14055480776	2.61165068723
10^{-5}	3.5115442592	2.49436474245
10^{-6}	5.17495025523	2.41115342218
10^{-7}	7.20739094438	2.35187767864
10^{-8}	9.57228930443	2.31735035473

Table 5.1: The fit coefficients for the decision time distribution.

The most probable decision time $t_p \equiv \sqrt{a/b}$ that corresponds to the maximum of the distribution can be fitted well with $t_p = -\ln(2.3h)$. We note that this is rather short time in comparison with the life-time of the superposition. Since $\langle \Sigma_x(t) \rangle = e^{-2t}$, $\langle \Sigma_x(t_p) \rangle \approx$

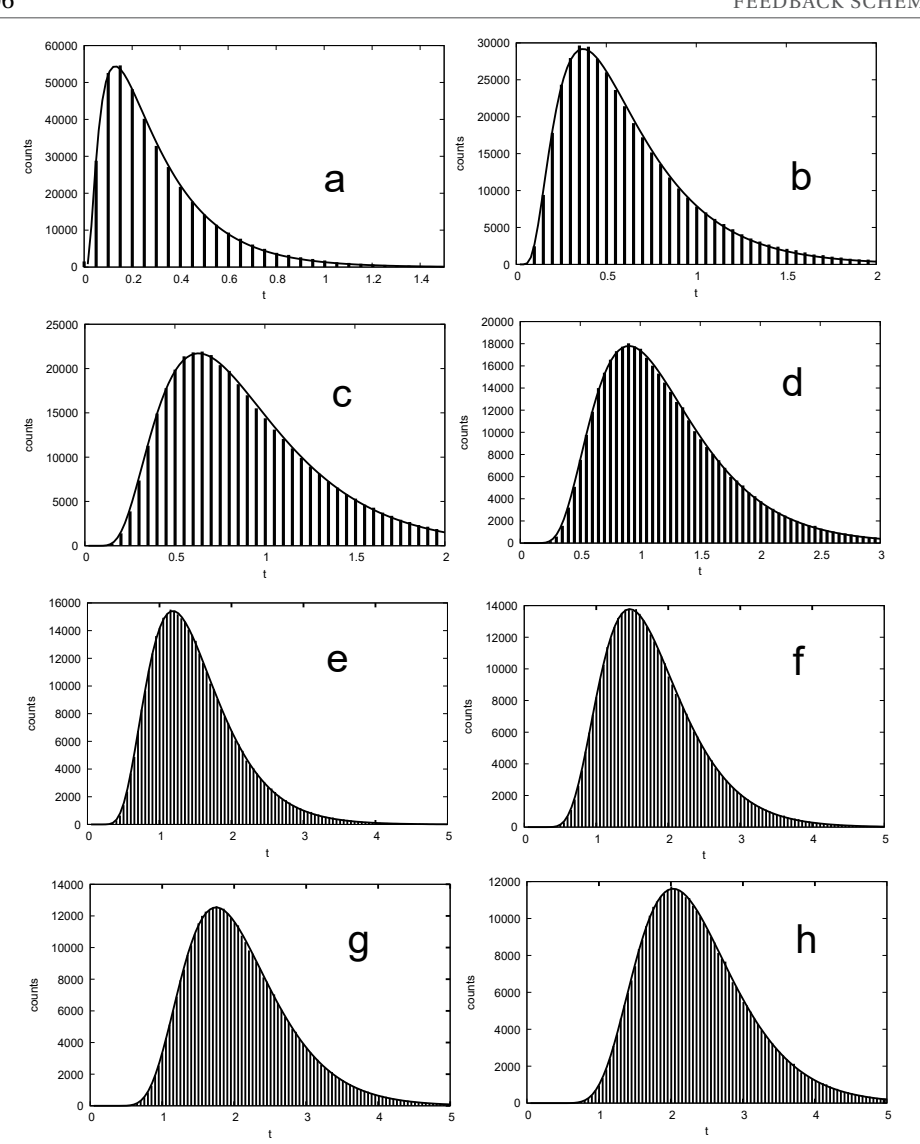


Figure 5.4: Histograms of the decision time at various values of the threshold parameter h. (a) h=0.1, (b) h=0.01, (c) h=0.001, (d) $h=10^{-4}$, (e) $h=10^{-5}$,(f) $h=10^{-6}$,(g) $h=10^{-7}$, (h) $h=10^{-8}$. The body of the distribution shifts to longer times upon decreasing h and the variance decreases slightly. The fit is made with an exponential function of the form $ce^{-a/t-bt}$, a,b being free parameters and c being set by the normalization. The fits are plotted with solid lines.

 $(2.3h)^{1/4} \gg h$, although a naive expectation would be $\langle \Sigma_x(t_p) \rangle \simeq h$. The distribution has a prominent exponential tail at $t \to \infty$. The corresponding coefficient b can be neatly fitted with $b = 2.0 - 6/\ln h$ thus approaching 2 at small thresholds. This is probably the manifestation of the superposition life-time. We note that although the variance

5

 $\approx 0.25 \sqrt{a/b^3} \approx t_p/8$ grows with decreasing h, the relative variance $\approx (8t_p)^{-1}$ actually decreases resulting in a concentrated distribution. This permits an accurate quantification of the expected decision time for small h and corresponding error probability h/2.

5.4. RESULTS ON THE FEEDBACK SCHEME

One can think of further technological developments whereby the information collected during the CWLM is used to manipulate the measured system. Modern qubit implementations make it realistic. Here we consider a simple example of such feedback scheme.

The measurement destroys the superposition and brings the qubit to a certain final state. The detector shows what state is reached. Let us note that the state can be "corrected": the qubit can be brought back to the initial superposition by a unitary manipulation, rotation about Y axis. The rotation angle, however, does depend on the state reached. General rotation by angle α is given by a unitary matrix $\hat{U}(\alpha) = \cos \alpha + i \Sigma_y \sin \alpha$. We see that $|\pm\rangle$ state is corrected by $\hat{U}(\pm \pi/4)$.

Let us devise a simple feedback scheme with a goal to keep the qubit in the equal-weight superposition while being measured. It works as follows. We collect the detector output during a time interval T_f . We use the reading v to decide which rotation we apply. The simplest decision scheme utilizes a reaction threshold I: no correcting manipulation takes place if |v| < I, otherwise the rotation $\hat{U}(\operatorname{sgn}(v)\pi/4)$ is applied. Alternatively, the rotation angle is

$$\alpha(\nu) = \operatorname{sgn}(\nu)\Theta(|\nu| > I)\frac{\pi}{4}.$$
 (5.16)

Then the feedback cycle is repeated again and again: the collection of the output at a time interval T_f is followed by a correcting rotation.

If the collection time $T_f\gg T_c$, the correction to the superposition will be exact if I<1. However, the superposition will be destroyed at the time scale of T_c and will persist for only a small fraction of the cycle. In the opposite limit $T_f\ll T_c$ the superposition will not be destroyed during the cycle. However, the output collected at such small time interval will exhibit large fluctuations and will hardly reflect the state measured. This will make the correction very inefficient. As a criterion for a good feedback, we take the average value of $\Sigma_x(t)$ integrated over the whole cycle, $\bar{\Sigma_x} \equiv T_f^{-1} \int_0^{T_f} dt \langle \Sigma_x(t) \rangle$. This value will depend on T_f and I, and we will find the optimal values of these parameters.

5.4.1. ANALYTICS

Owing to the simplicity of the scheme, we can find analytical expressions for $\bar{\Sigma}_x$. We note that the solution for the density matrix must be periodic in time with the period T_f . Let $\hat{\rho}_a$ be the density matrix of the qubit right after the correction. It evolves on the time interval T_f to the joint density matrix $\hat{\rho}(v)$ of the qubit and output. This can be found by solving Eq. 5.12 with the initial condition $\hat{\rho}_a$. Applying the output-dependent correction to the joint density matrix, we return to $\hat{\rho}_a$,

$$\hat{\rho_a} = \int d\nu \hat{U}(\alpha(\nu))\hat{\rho}(\nu)\hat{U}(\alpha(\nu))^{-1}$$
(5.17)

This forms a closed self-consistency equation for $\hat{\rho_a}$ to solve. In our situation, owing to symmetry, we can seek for $\hat{\rho}_a$ in the form $\hat{\rho}_a = (1 + \rho_x \hat{\Sigma}_x)/2$. The joint density matrix

where $G(v) \equiv (2T_f/\pi)^{1/2} \exp(-2T_f v^2)$, $G_{\pm}(v) = G(v \mp 1)$.

The self-consistency equation reads

$$\rho_x = A + B\rho_x \tag{5.19}$$

$$A \equiv \int d\nu \frac{G_+ - G_-}{2} \sin(2\alpha(\nu)) \tag{5.20}$$

$$= \frac{1}{2} (erf((I+1)\sqrt{2T_f}) - erf((I-1)\sqrt{2T_f}))$$
 (5.21)

$$B \equiv \int dv e^{-2T_f} \int G\cos(2\alpha(v)) = e^{-2T_f} \operatorname{erf}(I\sqrt{2T_f})$$
 (5.22)

The time-averaged *x*-projection is computed as

$$\bar{\Sigma}_x = \rho_x \frac{1 - e^{2T_f}}{2T_f} = \frac{A}{1 - B} \frac{1 - e^{2T_f}}{2T_f}$$
 (5.23)

In Fig. 5.5 we plot $\bar{\Sigma}_x$ versus I for a set of T_f . The curves reach maximum at some intermediate value of I. More detailed optimization shows that the maximum value of $\bar{\Sigma}_x = 0.661$ is achieved at I = 0.88, $T_f = 0.21$. The average value of spin immediately after the correction is higher, $\langle \Sigma_x \rangle_a = 0.81$ for the optimal settings. We see from the plot that close values of $\bar{\Sigma}_z$ are achieved in a rather wide window of I and T_f . This is a rather large value given the primitive feedback scheme in use. More elaborated feedback schemes may improve this even further.

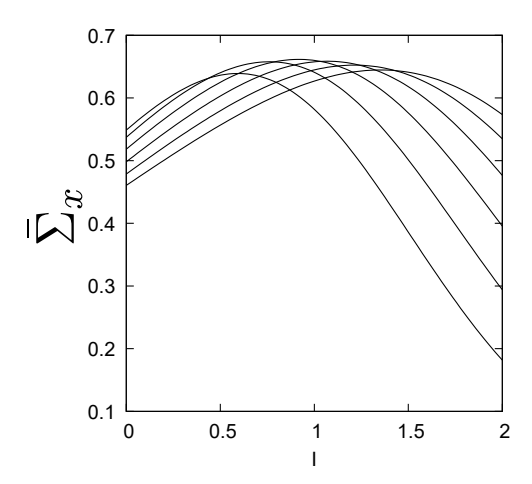


Figure 5.5: The efficiency $\bar{\Sigma}_X$ versus the reaction threshold I for a set of collection times T_f . The T_f takes the values 1/3, 1/4, 1/5, 1/6, 1/7, 1/8 from the lower to the upper curve at I=2, respectively. The curves come in opposite order at I=0. The plot shows that the efficiency close to 2/3 can be achieved in a wide region of I and T_f .

5.4.2. Numerical results

We investigate the feedback scheme numerically with the tool described. The simulation proceeds by time intervals of duration T_f . The detector output is collected during the interval, and the correcting rotation about y axis is applied depending on the resulting output in accordance with Eq. 5.16. We always start with the equal-weight superposition at t=0 and collect the quantum trajectories along with the detector readings. Some time is required for the simulation to achieve a steady state where the averages are periodic. We have found that in the range of T_f explored this time is of the order of 5-7 cycles irrespective of the cycle duration.

We explore and illustrate numerically the effect of the reaction threshold I and the collection time T_f on the performance of the feedback scheme and find numerically the optimal settings I, T_f that maximize this performance.

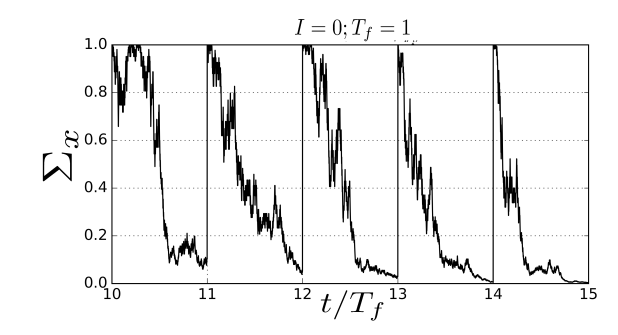
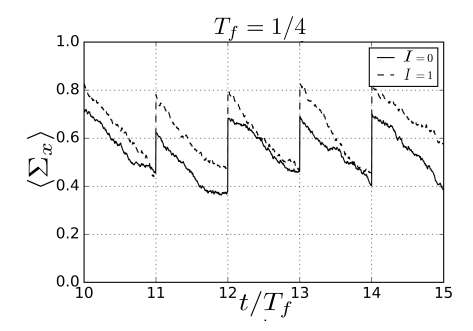


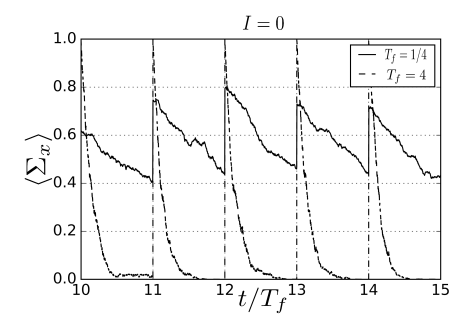
Figure 5.6: A single quantum trajectory $\Sigma_X(t)$ of the qubit subject to the feedback. The collection time is set to a rather large value $T_f = 1$, I = 0. At these settings, the superposition is strongly suppressed within the collection time. This provides an accurate measurement and efficient correction to the target superposition state.

Figure 5.6 gives an example of a single quantum trajectory. We plot $\langle \Sigma \rangle_x$ versus time for 5 collection interval. The collection time is set to a rather large value $T_f = 1$. The superposition is essentially suppressed during this time so the measurement of the final state is accurate and the resulting correction is accurate. We see the $\langle \Sigma \rangle_x$ coming back to ≈ 1 any time after the correction. We also see strong and fast fluctuations of $\langle \Sigma \rangle_x$ in time.

To suppress these fluctuations, we plot in the subsequent figures the averages over 50 quantum trajectories. To illustrate the effect of the parameters I and T_f on the dynamics of the qubit under feedback, we present in Fig. 5.7 such averages for different parameter values. In Figure 5.7a we set $T_f = 1/4$ and compare the results for I = 0 (solid) and I = 1 (dashed). One can see the improved performance in the latter case: the qubit is closer to the target equal-weight superposition. At this choice of I, no correction is applied if the collected output |v| < 1 and its reduced value does not indicate a certain z-projection. At these settings, this happens in approximately 1/3 of the cases. Apparently, the rule "it is better to do nothing than to do wrong" works here well.

In Fig. 5.7b we set I=0 and plot the average $\langle \Sigma_x(t) \rangle$ for two collection times: $T_f=1/4$ (solid curve) and $T_f=4$ (dashed). For the long collection time, we observe almost complete decay of the superposition and accurate correction to the target superposition at each feedback cycle. For the shorter correction time, the correction at each cycle is by





(a) The average of $\langle \Sigma_x(t) \rangle$ over 50 trajectories (b) The average $\langle \hat{\Sigma}_x(t) \rangle$ over 50 trajectories for something wrong.

for $T_f = 0.25$ and two values of the reaction I = 0 and two values of T_f , $T_f = 4$ (dashed) threshold, I = 0 (solid) and I = 1 (dashed). and $T_f = 1/4$ (solid). Long collection time im-For the latter setting, the correction is not approves the efficiency of the correction but does plied for small values of the collected output not keep the superposition. $T_f = 0.25$ is close v. Apparently, this improves the feedback per- to optimal settings providing a good trade-off formance. It is better to do nothing than to do between the superposition decay and the variance of the output collected.

Figure 5.7: The effects of the parameters I and T_f on the feedback performance illustrated with numerical simulations.

far less accurate, but the superposition does not decay much and is big in average.

We explore the feedback efficiency $\bar{\Sigma}_x$ in a wide range of I, T_f . We present the results in Fig. 5.8 where each point corresponds to averaging over 500 quantum trajectories during 100 collection time intervals. Apart from the remaining noise, these numerical data are in agreement with the results of the analytical calculation presented in Fig.5.5. Each data set at fixed T_f exhibit a maximum in efficiency at some intermediate value of I. The exact optimization settings are difficult to see since the similar efficiency close to 2/3 is reached in a wide region of the parameters. We employ the numerical iterative optimization procedure that bring us to the values $\bar{\Sigma}_x = 0.66$ at I = 0.9, $T_f = 0.2$ that is close to the settings obtained from numerical analysis. This proves that the simulation tool in use can be efficiently implemented for the analysis of more sophisticated and efficient feedback schemes that are too complicated to be treated analytically.

The efficiency of the feedback scheme can be definitely improved, for instance, by choosing the rotation angle $\alpha(v)$ in a more flexible way and taking into account the detector outcomes from the previous collection intervals.

5.5. CONCLUSION

In this paper, we explore the peculiarities of a continuous weak linear measurement in a simple but generic setup. We develop an efficient numerical simulation tool that generates single quantum trajectories along with the corresponding detector signal. We study References 111

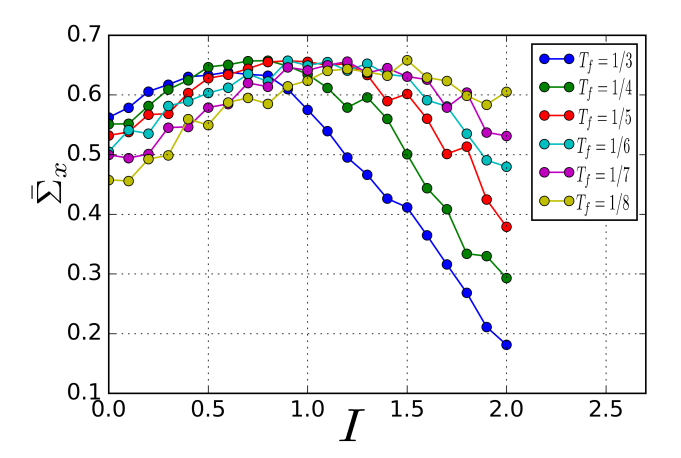


Figure 5.8: The feedback efficiency $\bar{\Sigma}_X$ in a wide region of the reaction thresholds I and collection times T_f . Each data point is computed by averaging of 500 quantum trajectories over time interval of 100 T_f . An efficiency \simeq 0.6 is observed in a wide parameter range.

the statistics of the trajectories and outputs with and without post-selection.

We prove numerically that the detector output conditioned on the final state does not depend on time and does not follow the average $\Sigma_z(t)$. Seemingly this implies that the measured qubit "knows" from very beginning of the measurement in which final state it is. To investigate this further, we study the statistics of the decision times. We have found an accurate fit for corresponding distribution and revealed that the decision time is commonly much shorter than the life-time of the superposition. This simple description gives insight into the interplay of the measured system and the detector system from a quantum point of view. It describes the translation of discrete quantum information to a continuous classical signal.

While similar methods have been successfully used to study such measurement scenarios [9–11, 16], our method allows not only to describe the measured system dynamics but also the detector system signal. How this signal is constructed and in which circumstances can correspond to a real integrated signal of an experimental run.

We have also presented and investigated a simple feedback scheme where the measurement results are used to keep the qubit in the initial superposition state despite being measured. Despite the simplicity, the feedback scheme can be tuned to provide rather high efficiency $\bar{\Sigma}_x = 0.66$. The feedback can be further improved and sophisticated.

The results obtained are relevant in the context of experimental situations where continuous weak linear measurement is used and for the design of interesting quantum feedback schemes and measuring protocols.

REFERENCES

[1] M. Nielsen and I. Chuang, *Quantum Computation and Quantum Information* (Cambridge University Press, 2000).

- [2] M. B. Mensky, *The action uncertainty principle in continuous quantum measurements*, Physics Letters A **155**, 229 (1991).
- [3] A. N. Korotkov, *Continuous quantum measurement of a double dot*, Phys. Rev. B **60**, 5737 (1999).
- [4] A. Jordan and M. Buttiker, *Continuous quantum measurement with independent detector cross correlations*, Phys. Rev. Lett. **95**, 220401 (2005).
- [5] K. Jacobs and D. A. Steck, *A straightforward introduction to continuous quantum measurement*, Contemporary Physics **47**, 279 (2006), http://dx.doi.org/10.1080/00107510601101934.
- [6] H. Wei and Y. V. Nazarov, *Statistics of measurement of noncommuting quantum variables: Monitoring and purification of a qubit*, Phys. Rev. B **78**, 045308 (2008).
- [7] A. Chantasri and A. N. Jordan, *Stochastic path-integral formalism for continuous quantum measurement*, Phys. Rev. A **92**, 032125 (2015).
- [8] A. Chantasri, J. Dressel, and A. N. Jordan, *Action principle for continuous quantum measurement*, Phys. Rev. A **88**, 042110 (2013).
- [9] M. Hatridge, S. Shankar, M. Mirrahimi, F. Schackert, K. Geerlings, T. Brecht, K. M. Sliwa, B. Abdo, L. Frunzio, S. M. Girvin, R. J. Schoelkopf, and M. H. Devoret, *Quantum back-action of an individual variable-strength measurement*, Science 339, 178 (2013).
- [10] K. W. Murch, S. J. Weber, C. Macklin, and I. Siddiqi, *Observing single quantum trajectories of a superconducting quantum bit*, Nature **502**, 211 (2013).
- [11] N. Roch, M. E. Schwartz, F. Motzoi, C. Macklin, R. Vijay, A. W. Eddins, A. N. Korotkov, K. B. Whaley, M. Sarovar, and I. Siddiqi, *Observation of measurement-induced en*tanglement and quantum trajectories of remote superconducting qubits, Phys. Rev. Lett. 112, 170501 (2014).
- [12] P. Campagne-Ibarcq, L. Bretheau, E. Flurin, A. Auffèves, F. Mallet, and B. Huard, *Observing interferences between past and future quantum states in resonance fluo-rescence*, Phys. Rev. Lett. **112**, 180402 (2014).
- [13] J. P. Groen, D. Ristè, L. Tornberg, J. Cramer, P. C. de Groot, T. Picot, G. Johansson, and L. DiCarlo, *Partial-measurement backaction and nonclassical weak values in a superconducting circuit*, Phys. Rev. Lett. 111, 090506 (2013).
- [14] S. J. Weber, A. Chantasri, J. Dressel, A. N. Jordan, K. W. Murch, and I. Siddiqi, *Mapping the optimal route between two quantum states*, Nature **511**, 570 (2014).
- [15] D. Tan, S. J. Weber, I. Siddiqi, K. Mølmer, and K. W. Murch, *Prediction and retrodiction for a continuously monitored superconducting qubit*, Phys. Rev. Lett. 114, 090403 (2015).

REFERENCES 113

[16] H. M. Wiseman, Weak values, quantum trajectories, and the cavity-qed experiment on wave-particle correlation, Phys. Rev. A 65, 032111 (2002).

- [17] A. Franquet and Y. V. Nazarov, *Probability distributions of continuous measurement results for conditioned quantum evolution*, Phys. Rev. B **95**, 085427 (2017).
- [18] A. Franquet and Y. V. Nazarov, *Probability distributions of continuous measure-ment results for two non-commuting variables and conditioned quantum evolution*, arXiv:1708.05662 [quant-ph] (2017).
- [19] R. Vijay, C. Macklin, D. H. Slichter, S. J. Weber, K. W. Murch, R. Naik, A. N. Korotkov, and I. Siddiqi, *Stabilizing rabi oscillations in a superconducting qubit using quantum feedback*, Nature **490**, 77 (2012).
- [20] G. de Lange, D. Ristè, M. J. Tiggelman, C. Eichler, L. Tornberg, G. Johansson, A. Wall-raff, R. N. Schouten, and L. DiCarlo, *Reversing quantum trajectories with analog feedback*, Phys. Rev. Lett. 112, 080501 (2014).
- [21] E. Greplova, K. Mølmer, and C. K. Andersen, *Quantum teleportation with continuous measurements*, Phys. Rev. A **94**, 042334 (2016).
- [22] M. W. Jack and M. J. Collett, *Continuous measurement and non-markovian quantum trajectories*, Phys. Rev. A **61**, 062106 (2000).
- [23] T. C. Ralph, S. D. Bartlett, J. L. O'Brien, G. J. Pryde, and H. M. Wiseman, *Quantum nondemolition measurements for quantum information*, Phys. Rev. A **73**, 012113 (2006).
- [24] A. A. Clerk, M. H. Devoret, S. M. Girvin, F. Marquardt, and R. J. Schoelkopf, *Introduction to quantum noise, measurement, and amplification*, Rev. Mod. Phys. **82**, 1155 (2010).



CURRICULUM VITÆ

Albert Franquet González

29-05-1990 Born in Barcelona, Spain.

EDUCATION

2006 Primary and Secundary Education

Ramon Fuster, Cerdanyola del Vallès (1996-2006)

2008 Batxillerat - High School

Frederic Mistral-Tècnic Eulàlia, Barcelona (2006–2008)

2008–2012 BSc. in Physics

Universitat Autònoma de Barcelona

Thesis: Entanglement Percolation with Graph States

Promotor: Prof. dr. J. Calsamiglia

2012–2013 MSc. in Photonics

Uninversitat Politècnica de Catalunya

Thesis: Preparation of entangled Dicke states using atomic

ensembles

Promotor: Prof. dr. D. E. Chang

2013–2018 PhD. in Physics

Delft University of Technology, Delft Netherlands

Thesis: Statistics of continuous weak linear measurement

Promotor: Prof. dr. Y. V. Nazarov



LIST OF PUBLICATIONS

- 4. **A. Franquet**, Y. V. Nazarov, *Probability distributions of continuous measurement results for conditioned quantum evolution*, Phys. Rev. B **95**, 085427 (2017).
- 3. **A. Franquet**, Y. V. Nazarov, *Probability distributions of continuous measurement results for two non-commuting variables and conditioned quantum evolution*, arXiv:1708.05662 [quant-ph]. Submitted to Phys. Rev. B, in peer review (2017).
- 2. **A. Franquet**, Hongduo Wei, Y. V. Nazarov, *Statistics of continuous weak quantum measure-ment of an arbitrary quantum system with multiple detectors*, arXiv:1804.07639 [quant-ph]. Submitted to Phys. Rev. B, in peer review (2018).
- A. Franquet, N. C. Kruse, B. Vervliet, Y. V. Nazarov, Simulating continuous weak linear measurement of a quantum system and measurement based feedback., arXiv:1808.00836 [quant-ph]. Submitted to Quantum Measurements and Quantum Metrology, in peer review (2018).